Synthesis and Characterization of Microporous Coordination Polymers as Adsorbents for CO_2 Capture

by

Austin Cornell Kizzie

A dissertation submitted in partial fulfillment
of the requirements for the degree of
Doctor of Philosophy
(Chemistry)
in The University of Michigan
2012

Doctoral Committee:

Professor Adam J. Matzger, Chair
Professor Mark M. Meyerhoff
Professor Phillip E. Savage
Assistant Professor Bart M. Bartlett

Acknowledgements

I thank God for the opportunity that I have been given to further my education through dissertation research, and the ability to achieve my goal of attaining the Ph.D. I am grateful for the support of my parents, Audrey Kizzie, and Carlton Kizzie, who early on during my childhood stressed the importance of obtaining a good education. I also thank my sister Cameo for her support. In addition, I am thankful for the support and well-wishes from my extended family, and friends. I give a special "thank you" to my buddy Joshua Davis, for his genuine friendship and support.

I thank my advisor Professor Adam Matzger for his guidance and support throughout my graduate research, and my dissertation committee members for their thoughtful guidance. I thank Dr. Antek Wong-Foy for his willingness to entertain wildly random questions with insightful discussion, his knowledgeable advice, and his persistent efforts in the maintenance of critical laboratory instrumentation so often taken for granted. Also, I thank Steve Parus and Jim Durka in the Electronics Shop for their technical assistance.

I thank all of my colleagues in the Matzger group for their advice, support and well-wishes. "Thank you!" to the group members whose dissertations line the wall of the computer room, as these were especially helpful in assembling my own, :-) . I am thankful for having the opportunity to work with Dr. Jennifer Schnobrich, whose advice and helpful discussions were very much appreciated. I am especially thankful for being able to work with Dr. Kyongmoo-Koh. As an exceptionally talented researcher, and a powerfully effective communicator, he has undoubtedly left a positive and indelible impact on the group members fortunate enough to have worked with him. For me, his generous offering of time, genuine advice, and knowledgeable discussions (on topics ranging from science to politics!) were very much enjoyed, and are sorely missed.

Table of Contents

List of Figures

List of Tables

Abstract

The accumulation of CO_2 in the Earth's atmosphere is an important environmental issue, and coal-fired power plants are significant contributors to anthropogenic CO_2 emissions. The capture of CO_2 from these facilities via amine-scrubbing has been well-investigated, but deemed to be too costly for widespread deployment. An adsorption-based process that relies on microporous coordination polymers (MCPs) may offer an efficient route to CO_2 capture. In particular, MCPs of the M/DOBDC series (DOBDC = 2,5-dioxido-1,4-benzenedicarboxylate; M = Zn, Ni, Co, and Mg) have previously been shown to exhibit exceptional CO_2 uptake at low partial pressures under static conditions; the best performer, Mg/DOBDC, exhibits a CO_2 uptake of 23 wt% at 0.1 atm and 25 °C, superior to the 12 wt% uptake of zeolite 13X, a benchmark candidate for CO_2 capture, under similar conditions.

In this dissertation, the performance of the M/DOBDC materials was examined under flow conditions with mixtures of N_2/CO_2 and $N_2/CO_2/H_2O$ as surrogates for flue gas; after hydration and subsequent thermal regeneration Co/DOBDC retained 85% of the pristine CO_2 capacity while Mg/DOBDC, retained only 15% of the pristine capacity. These data indicated that improving material stability in the presence of H_2O was a critical issue to confront in designing new MCPs for CO_2-capture, and two approaches were explored to confront this problem.

The first approach entailed enhancing the CO_2 uptake of a H_2O-stable MCP, MIL-100(Al), via post-synthetic modification with proximal amines, namely those in tris(2-aminoethyl)amine (tren). This yielded a new MCP, tren@MIL-100(Al), which exhibited an initial CO_2 capacity of 9 wt% under dry conditions; the capacity diminished after several cycles. When fully hydrated, tren@MIL-100(Al) had a CO_2 capacity of 4 wt%, an improvement over M/DOBDC materials, which displayed no capacity under this condition.

A second approach involved the synthesis of an MCP based on the acetylacetonylate coordination functionality, which is known to generate H_2O-stable metal complexes. Simple geometric design principles were executed, wherein a ditopic linker bearing acetylacetonylate units was combined with Al^{3+} to yield a new MCP, Al/BAB. The material represents successful deployment of acetylacetonylate as a coordination functionality in MCPs, thus opening a new subset of these materials.

Chapter 1

Introduction

1.1 Anthropogenic CO_2 Emission, and Strategies for its Reduction

Atmospheric CO_2 originating from human activities, primarily the combustion of fossil fuels, has received much attention in recent decades as a 'greenhouse' gas and a contributor to climate change.[1] Rapid and large-scale combustion of fossil fuels began during the Industrial Revolution, and since then, atmospheric CO_2 concentration has dramatically increased from an estimated 280 ppmv in the year 1750,[2] to 393 ppmv in early 2012.[3] Additionally, emissions are expected to continue increasing due to persistently strong consumption of fossil fuels in global economies. In response, efforts have been mounting to develop approaches to reduce anthropogenic CO_2 emissions. One approach to accomplish this goal is to reduce consumption of fossil fuels and gradually replace them with energy derived from solar, wind, geothermal and hydroelectric systems, or fuels such as hydrogen, which do not rely upon energy released by the oxidation of carbon-based fuels. Although the contribution from these alternative energy sources is expected to grow, critical barriers inhibiting their adoption include high capital costs and lack of infrastructure.[4] A second approach is to capture CO_2 at the sources of production and sequester it in geological reservoirs. In particular, coal-fired power stations have been identified as the largest point-source emitters of CO_2, and therefore have been the focus of emission reduction systems.[5]

Schemes for reducing CO_2 emissions from coal-fired power plants are divided into three broad categories, which include: (1) pre-combustion processes; (2) in-situ CO_2 capture processes and (3) post-combustion CO_2 capture processes. Pre-combustion processes involve the preparation of a feed stream of fuel that is rich in CO_2, or feed stream that results in combustion exhaust that is rich with CO_2. The advantage is that the high concentration of CO_2 facilitates its separation. For example, in the gasification

process a gaseous stream rich in CO_2 and H_2 is generated via steam reformation of coal and subsequent water gas-shift reaction; CO_2 is removed and the H_2 is burned in air. A second pre-combustion process is the oxy-firing process, wherein O_2 is separated from air and utilized directly as the combustion gas, thus generating an exhaust stream of ~ 90 vol% CO_2.[5] In-situ processes involve capturing CO_2 as it is produced in the boiler unit. An example is a process studied by Hughes et al. that utilizes CaO as a sorbent that reacts with CO_2 to form $CaCO_3$; subsequent calcination of the carbonate releases the CO_2.[6] A key drawback to these processes is that they would require extensive modification of existing power stations, or construction of entirely new stations in order to be implemented. Also, in the case of building new power stations, a concomitant decommissioning of present stations is needed in order to achieve a net reduction in CO_2-emissions. Thus post-combustion CO_2 capture, illustrated in Figure 1.1 is an attractive approach since the necessary facilities could be retro-fitted to power plants currently in operation, in principle, with no modification to upstream process units.

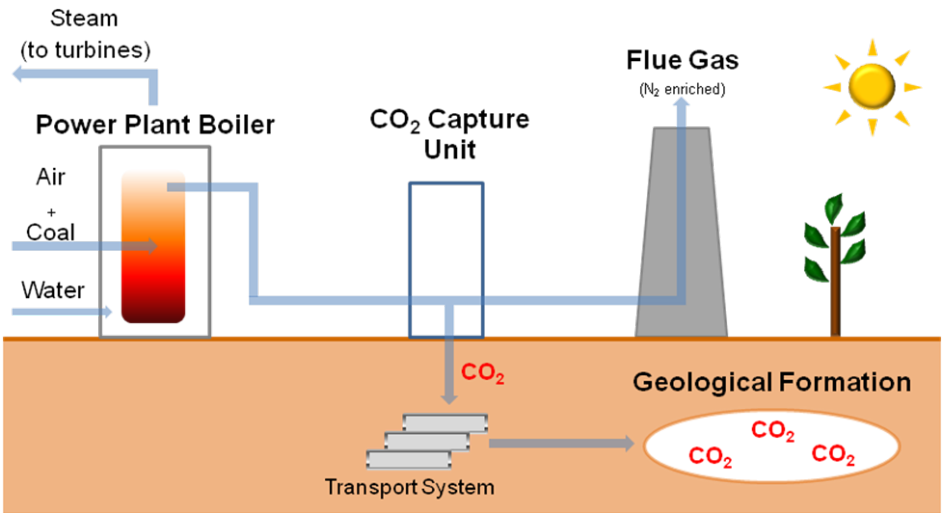

Figure 1.1. Simple flow scheme for a post-combustion CO_2 capture and sequestration system.

A principal goal of post-combustion CO_2 capture is the separation of CO_2 from power plant combustion exhaust gas, commonly referred to as flue gas, which is composed of N_2 (~ 75 vol%) , CO_2 (~ 16 vol%) , H_2O (3 ~ 5 vol%), SO_x, NO_x and other minor components.[7] Among the most studied post-combustion capture processes has been the amine scrubbing process, which has been deployed in the removal of CO_2 from gas mixtures such as natural gas.[8,9] The removal of CO_2 is performed by introducing the gas into an absorber unit, where it is placed in intimate contact with an aqueous solution that contains a primary or secondary alkylamine (aqueous solutions of 20 ~ 30 wt% monoethanolamine, or MEA, are currently regarded as the benchmark amine systems) which reversibly reacts with CO_2 to form a solution of the corresponding alkylammonium carbamate salt; the mechanism[10-13] is depicted in Figure 1.2.

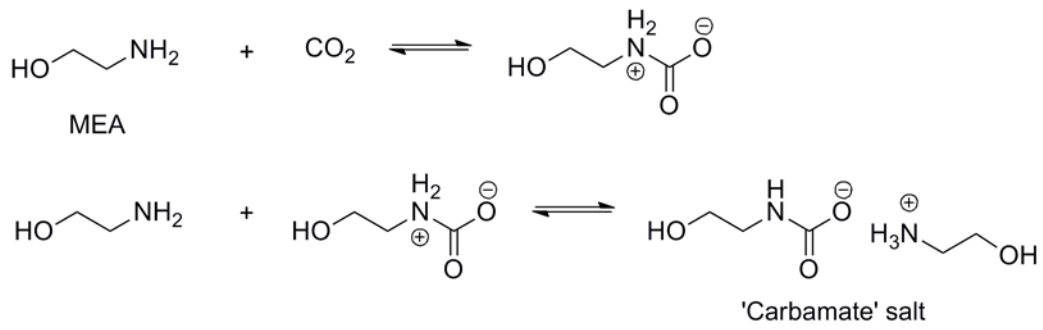

Figure 1.2. Chemical reaction between monoethanolamine and CO_2.

The CO_2 is released by heating the solution to 100 ~ 120 °C,[9] thus pushing the equilibrium back to the starting amine. Although amine scrubbing has been noted for its high selectivity for CO_2, a critical drawback is the relatively high parasitic energy demand, primarily due to the regeneration of the amine solution, which is estimated to be around 20 - 30% of a typical power station's energy output.[9] As a result of capital costs, and high energy consumption, utilization of the MEA process is expected to raise electricity prices by 50% or higher.[14,15]

An alternative approach to capturing CO_2 from flue gas, is an adsorption-based system that relies on packed columns of a solid, highly porous material. Adsorbents

capable of capturing CO_2 by physical adsorption (physisorbents) could be advantageous because CO_2 can be reversibly adsorb and desorb at near-ambient conditions, thus significantly reducing energy costs. Adsorbents designed to trap CO_2 chemically (chemisorbents) may also be advantageous, with regards to the reduction of equipment costs. Liquid-based systems such as the MEA process require bubble trays or packed beds[8,9] to create surface area for mass transport of CO_2. The need for these is eliminated with porous adsorbents because of their high intrinsic internal surface area. A brief overview of adsorption fundamentals, and the characterization methods that are utilized to ascertain the performance of potential CO_2 capture adsorbents, are discussed in the following section.

1.2 Adsorption-Based Metrics for Assessing CO_2 Capture Performance

Adsorption is the phenomenon in which atoms or molecules in a fluid (termed the adsorbate) bind to the surface of a solid material (adsorbent). If the nature of the adsorbate–adsorbent interaction is purely physical, the process is termed physisorption. This type of adsorption arises as a result of weak, attractive, non-covalent interactions, such as van der Waals and Columbic forces, between the adsorbate and the adsorbent surface.[16] If the adsorbate-adsorbent interaction results in the formation of chemical bonding between the two species, then the process is termed chemisorption.

Industrially relevant adsorbent materials typically exhibit a high proportion of free internal volume defined by pores. The size of a pore is typically assessed by its diameter or characteristic dimension (d), and is classified into one of three regimes: macropores (d > 500 Å), mesopores (500 Å > d > 20 Å), and micropores (d < 20 Å).[17] Pore size dictates the maximum dimensions of species than can reside within the material; this property has been extensively exploited via molecular sieving, where a mixture of two or more species is separated by introducing an adsorbent that allows smaller species to reside in its pores while rejecting species that are too big. Pore size also influences the relative strength of physisorptive interaction. As shown in Figure 1.3, diagrams[17] showing the interaction potential (denoted as 'energy') as a function of adsorbate distance from the pore surface, are provided for the case of an adsorbate in the aforementioned pore regimes. In the case

of a macroporous physisorbent, as an adsorbate approaches the pore surface the interaction potential decreases to a minimum, before sharply rising. In the case of a mesoporous physisorbent, two potential minima are shown, representing increased proximity of the adsorbent pore walls. However, in the case of microporous physisorbents, the potential minima overlap, resulting in a stronger physical interaction. This enhanced physical interaction is a desirable attribute for gas separation applications such as CO_2 capture.

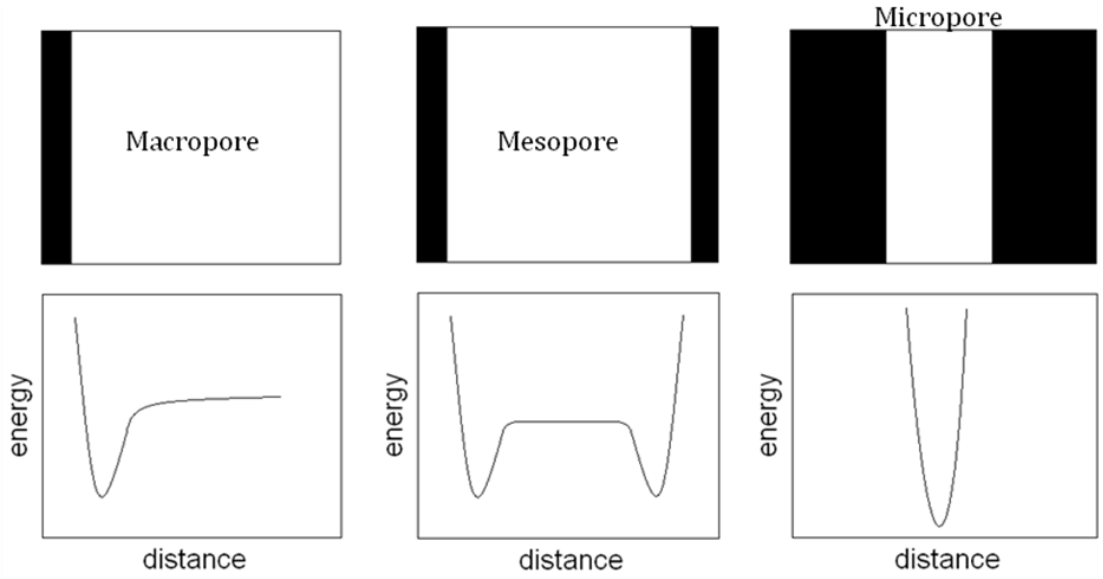

Figure 1.3. Energy potential diagrams shown for a macropore, mesopore, and mircopore.

An important metric of performance is the quantity, or uptake, of adsorbate on the surface of the material. The uptake is a function of temperature, and pressure (in the case of gases) or concentration (in the case of mixtures). The function relating uptake at constant temperature and varying pressure/concentration is referred to as an isotherm, which is typically expressed as a graph that shows adsorbate uptake plotted against pressure/concentration. The specific surface area (commonly referred to as simply 'surface area', and typically expressed in units of m^2/g) of an adsorbent can be determined by applying adsorption models to a pure gas sorption isotherm (N_2 at 77K is the IUPAC standard)[17] of the adsorbent of interest. The Langmuir model and Brunauer-Emmett-Teller (BET) model, are most commonly used for determining surface areas from gas

sorption isotherms. Detailed discussions of these models are presented elsewhere,[17] but the BET model is more widely used because it accounts for multilayer adsorption, and has been demonstrated to be applicable to multiple classes of materials;[18-20] the Langmuir model assumes only monolayer coverage, and can only be correctly applied to materials with exceptionally small pores.[19]

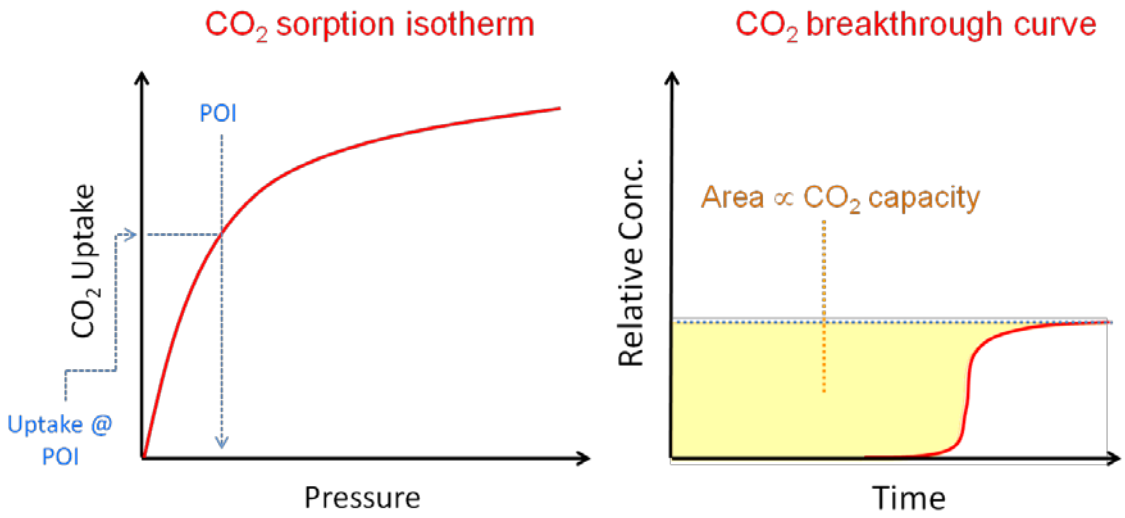

Figure 1.4. Graphical representation of obtaining CO_2 uptake at a point-of-interest (POI) from a sorption isotherm, and CO_2 capacity from a breakthrough curve.

Gas sorption isotherms can be useful for identifying candidate materials for CO_2 capture. The uptake of CO_2 at some point-of-interest (as shown in Figure 1.4), which is typically a pressure that corresponds to the partial pressure of CO_2 in flue gas (0.1 atm to 0.17 atm), is used as a metric of performance. These pressures correspond to the concentration of CO_2 in flue gas at, or near, ambient pressure. Materials with relatively high CO_2 uptakes at the point-of-interest have the potential to serve as CO_2 capture adsorbents.

Another approach to assessing CO_2 capture performance is to generate a gas mixture that serves as a surrogate for real flue gas, and to introduce the mixture into a column packed with a candidate sorbent. A simple surrogate for flue gas would be a dry or humid mixture of N_2 and CO_2 in a 5/1 ratio. When a gas mixture is in contact with an adsorbent, the relative strength of the van der Waals interactions between the gases and

the adsorbent determines the relative surface coverage for each species. Species with higher polarizabilities and quadrupole moments are typically more strongly retained.[16] In the case of a N_2/CO_2 mixture, CO_2 is selectively retained because it has a polarizability of 3.02×10^{-40} $C^2 \cdot m^2/J$ and a quadrupole moment of -13.71×10^{-40} $C \cdot m^2$ which are larger in magnitude than those of N_2, which has a polarizability of 0.78×10^{-40} $C^2 \cdot m^2/J$ and a quadrupole moment of -4.91×10^{-40} $C \cdot m^2$.[16] When the material capacity for a particular gas is reached, the ability of the bed to achieve further separation is exhausted, and the composition of the column effluent becomes identical to that of the feed. The time-dependent concentration profile of a gas in the column effluent is referred to as a breakthrough curve. The capacity that the material exhibits for the gas can be calculated by integrating the curve front (graphically represented in Figure 1.4) and subtracting the amount of gas that occupies the void volume in the system and in the sample. The CO_2 capacity determined from a gas breakthrough experiment is yet another metric that when compared amongst candidate adsorbents, can be used to identify optimal materials for CO_2 capture.

1.3 Classes of Adsorbents Studied for CO_2 Capture

Candidate adsorbents for CO_2 capture should exhibit the following general characteristics: Relatively high adsorption capacity for CO_2, sustained performance in the presence of flue gas components, and facile regeneration. Some of the most well-studied candidates for CO_2 capture are traditional adsorbents such as activated carbons and zeolites. Amine-modified silicas have also been extensively investigated, and there is also growing interest in the application of microporous coordination polymers (MCPs) for CO_2 capture. General considerations such as structural features and advantages/drawbacks of these materials are highlighted in the preceding sections, with more in-depth reviews cited accordingly.

1.3.1 Activated Carbons

Activated carbons, which are porous materials derived from highly carbonaceous feed-stocks (e.g., coal, wood, etc.) are attractive due to their relatively low cost and excellent stability. Their porosity is derived from the inefficient packing of rigid planes of carbon locked in highly disordered assemblies.[21] Owing to their relatively high surface areas, activated carbons exhibit significant CO_2 uptakes at high pressures; however, the consensus is that CO_2 uptakes in the low partial pressure regime (typically 1 ~ 3 wt% CO_2 at 0.1 ~ 0.l7 atm and 25 °C) are too low for these materials to be viable candidates for CO_2 capture.[22-24] This can be attributed to the low polarity of the pore surface of activated carbons,[16] resulting in weak affinity for CO_2 molecules and low CO_2 uptake under conditions relevant for CO_2 capture.

1.3.2 Zeolites

Zeolites are materials comprised of aluminosilicate frameworks built-up from corner-sharing SiO_4 and AlO_4 tetrahedra; given the net negative charge of the AlO_4 units, charge-balancing cations are present, which can be exchanged to tune properties such as pore size, acidity and catalytic performance.[25-27] Due to the presence of these ionic species, the zeolite pore surface is relatively polar resulting in strong physisorptive interactions with guest molecules such as CO_2, and consequently high capacities for CO_2 at low pressures. For example, the zeolite NaX (13X molecular sieve), shown in Figure 1.5, regarded as a benchmark adsorbent for CO_2 capture, has an uptake of about 12 wt% CO_2 at 0.1 atm and temperatures at or near 25 °C.[28,29] However, the highly polar pore surface also possesses high affinity for H_2O, a combustion product present in flue gas, which severely diminishes CO_2 uptake.[30,31] In addition, removal of H_2O typically requires heating these materials to relatively high temperatures (~300 °C); this would lead to a significant parasitic energy draw during the regeneration of the material. These considerations severely limit the prospective of utilizing these materials for CO_2 capture.

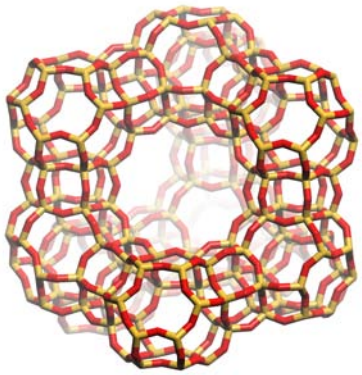

Figure 1.5. Structure of the faujasite framework for zeolite NaX. Yellow tetrahedral vertices represent Al or Si atoms; red vertices represent O atoms.

1.3.3 Amine-Modified Silicas

Amine-modified mesoporous silicas have garnered much attention as potential adsorbents for CO_2 capture. The unmodified silicas are noted for their large pore sizes (20 Å ~ 100 Å),[25] which are tuned via the judicious selection of organic surfactants that serve as templates during synthesis, and surface hydroxyls which can be utilized for chemical modification. Surface-grafting of primary or secondary amines onto silicas has been investigated as an approach to generating solid sorbents tailored for CO_2 capture. Grafting is typically accomplished via condensation of small chain aminoalkylsiloxanes with surface hydroxyl groups, thus covalently anchoring the amine to the pore surface. Amines can also be physically incorporated into silicas via wet-impregnation, which involves immersing the desired silica in a solution of an oligomeric or polymeric amine such as polyethyleneimine (PEI). As a result of the van der Waals interactions between the pore surface and the amine, it becomes physically bound within the adsorbent.

Amine modified silicas exhibit significantly higher CO_2 uptakes when compared to their unmodified analogs, and unlike zeolites, humidity has been reported in some cases to improve performance. These enhancements are often claimed to be the result of CO_2 reacting with surface amines to generate carbamates under dry conditions,[32,33] and carbonates[33,34] or bicarbonates under humid conditions.[33,34] There is however,

disagreement in the literature regarding the spectral assignment of the bands for these species, and the reproducibility of the data.[22]

A potential drawback to the utilization of amine-grafted silicas is the potential hydrolysis of the siloxane linkages, facilitated by either acidic conditions (such as those found in flue gas), or by the amine itself,[35] thus potentially reducing performance. Likewise, the performance of silicas with physically bound amine may diminish over time due to leaching or redistribution within the material during usage.

1.3.4 Microporous Coordination Polymers

Microporous coordination polymers (MCPs) are a subclass of coordination polymers that consist of multi-topic organic ligands (linkers) that bind with metal atoms or metal atom clusters to form porous structures. These materials grew out of early work pioneered by Robson and co-workers,[36-39] who demonstrated that coordination polymers with logically pre-conceived structures could be generated via judicious selection of the linker-metal combination. Early materials possessed highly ordered structures that exhibited exceptional porosity as evidenced by X-ray diffraction; as a result, these materials were intensely studied as potential complements to zeolites,[38] with the organic linker allowing for a higher degree of structural tunability and pore surface functionalization, than could be achieved with traditional adsorbents such as zeolites and activated carbons. However, early materials suffered from structural collapse, and generally did not exhibit porosity by gas sorption. This changed in the late 1990s with reports from Kitagawa,[40] Williams,[41] and Yaghi[42] of coordination polymers that were structurally stable enough to exhibit porosity as evidenced by gas sorption. Although exhibition of porosity by gas sorption is a characteristic that is dependent upon the unique structural features of individual materials, the combination of moieties with high rigidity (such as an aryl ring) and multiple functional groups that can bind to metals (or coordinating functionalities; commonly carboxylates) serves as a general design principle for guiding the synthesis of new linkers that are amenable to yielding porosity in coordination polymers.

In the time since the aforementioned early works, interest in the field has significantly grown, and numerous terms have been generated to denote this class of materials, the most popular of these terms being metal-organic framework (MOFs); other terms include porous coordination polymers (PCPs), porous coordination networks (PCNs), and microporous coordination polymers (MCPs), the term which will be utilized in throughout this dissertation. MCPs have been studied for a variety of applications such as high-pressure storage of gases,[43-51] liquid phase separations[52-55] and gas phase separations such as CO_2 capture.[22-24,56] Studies that examine MCPs as potential adsorbents for CO_2 capture will be highlighted in Chapter 2.

1.4 Organization of Dissertation

The work presented in this dissertation centers on assessing the performance of MCPs as potential adsorbents for CO_2 capture and investigating possible strategies for improving performance. Chapter 2 covers work that examines the effect of humidity on the performance of MCPs of the M/DOBDC series (M = Zn, Ni, Co, and Mg; DOBDC = 2,5-dioxido-1,4-benzenedicarboxylate), which are regarded as the best candidate MCPs for CO_2 capture. Sensitivity to moisture has long been known to be a critical issue that could inhibit the utilization of MCPs for applications involving humidity process streams such as flue gas. Quantification of the effect of humidity in the M/DOBDC series, achievable by comparing the performance of pristine materials versus that of post-regenerated materials, is an important task in the process of down-selecting candidate materials that could potentially serve as CO_2 capture adsorbents. It will be shown that stability in the presence of moisture is still a critical issue that may encumber future utilization.

In Chapter 3, an effort towards generating MCPs that exhibit both superior stability and superior CO_2 capture performance will be presented. A synthetic strategy commonly referred to as post-synthetic modification, wherein pre-fabricated MCPs are treated with modifiers to generate new materials, will be discussed in the context of CO_2 capture. Utilization of this approach will be shown as an effective means of generating MCPs with enhanced CO_2 capture performance.

Chapter 4 will outline an effort toward generating MCPs from linkers bearing β-diketonate functionalities. Monotopic ligands of this class, particularly acetylacetonate, are known to bind to a single trivalent metal atom to form octahedral complexes featuring exceptional stability. As a result of the low contribution of the metal's mass to the total mass of the complex, these complexes could serve as lightweight units for assembly of highly porous MCPs. In the context of CO_2 capture, reduction in scaffold weight is important because performance is typically measured in gravimetric units (g CO_2/g sorbent). Progress toward this goal and remaining challenges will be discussed.

The last section, Chapter 5, will offer a summary, and outlook on future directions that could be explored in the development of MCPs for CO_2 capture.

1.5 References

(1) Ritter, S. K. In *Chemical and Engineering News*; American Chemical Society: 2009; Vol. 87, p 11-21.

(2) Canadell, J. G.; Quéré, C. L.; Raupach, M. R.; Field, C. B.; Buitenhuis, E. T.; Ciais, P.; Conway, T. J.; Gillett, N. P.; Houghton, R. A.; Marland, G. *Proc. Natl. Acad. Sci. U.S.A* **2007**, *104*, 18866-18870.

(3) National Oceanic and Atmospheric Administration Earth System Research Laboratory: Global Monitoring Division. http://www.esrl.noaa.gov/gmd/ccgg/trends/global.html (Apr. 12, 2012)

(4) Neuhoff, K. *Oxford Rev. Econ. Pol.* **2005**, *21*, 88-110.

(5) Yang, H.; Xu, Z.; Fan, M.; Gupta, R.; Slimane, R. B.; Bland, A. E.; Wright, I. *J. Environ. Sci.* **2008**, *20*, 14-27.

(6) Hughes, R. W.; Lu, D. Y.; Anthony, E. J.; Macchi, A. *Fuel Process. Technol.* **2005**, *86*, 1523-1531.

(7) Granite, E. J.; Pennline, H. W. *Ind. Eng. Chem. Res.* **2002**, *41*, 5470-5476.

(8) Dow Chemical. Gas Sweetning. http://msdssearch.dow.com/PublishedLiteratureDOWCOM/dh_0039/0901b803800391f8.pdf?filepath=gastreating/pdfs/noreg/170-01395.pdf&fromPage=GetDoc

(9) Rochelle, G. T. *Science* **2009**, *325*, 1652-1654.

(10) Danckwerts, P. V. *Chem. Eng. Sci.* **1979**, *34*, 443-446.

(11) Laddha, S. S.; Danckwerts, P. V. *Chem. Eng. Sci.* **1981**, *36*, 479-482.

(12) Versteeg, G. F.; van Swaaij, W. P. M. *Chem. Eng. Sci.* **1988**, *43*, 573-585.

(13) Xie, H.-B.; Zhou, Y.; Zhang, Y.; Johnson, J. K. *J. Phys. Chem. A* **2011**, *114*, 11844-11852.

(14) Davison, J. *Energy* **2007**, *32*, 1163-1176.

(15) Rao, A. B.; Rubin, E. S. *Environ. Sci. Tech.* **2002**, *36*, 4467-4475.

(16) Sherman, J. D.; Yon, C. M. In *Kirk-Othmer Encyclopedia of Chemical Technology*; John Wiley & Sons, Inc.: 2000.

(17) Lowell, S. *Characterization of Porous Solids and Powders: Surface Area, Pore size, and Density*; Kluwer Academic Publishers: Dordrecht ; Boston, 2004.

(18) Bae, Y.-S.; Yazaydin, A. Ö.; Snurr, R. Q. *Langmuir* **2010**, *26*, 5475-5483.

(19) Düren, T.; Millange, F.; Férey, G.; Walton, K. S.; Snurr, R. Q. **2007**, *111*, 15350-15356.

(20) Walton, K. S.; Snurr, R. Q. *J. Am. Chem. Soc.* **2007**, *129*, 8552-8556.

(21) Baker, F. S.; Miller, C. E.; Repik, A. J.; Tolles, E. D. In *Kirk-Othmer Encyclopedia of Chemical Technology*; John Wiley & Sons, Inc.: 2000.

(22) Choi, S.; Drese, J. H.; Jones, C. W. *ChemSusChem* **2009**, *2*, 796-854.

(23) Samanta, A.; Zhao, A.; Shimizu, G. K. H.; Sarkar, P.; Gupta, R. *Ind. Eng. Che. Res.* **2011**, *51*, 1438-1463.

(24) Sayari, A.; Belmabkhout, Y.; Serna-Guerrero, R. *Chem. Eng. J.* **2011**, *171*, 760-774.

(25) Wright, P. A.; Royal Society of, C. *Microporous framework solids*; RSC Publishing: Cambridge, 2008.

(26) Čejka, J.; Kubička, D. In *Kirk-Othmer Encyclopedia of Chemical Technology*; John Wiley & Sons, Inc.: 2000.

(27) Kresge, C. T.; Dhingra, S. S. In *Kirk-Othmer Encyclopedia of Chemical Technology*; John Wiley & Sons, Inc.: 2000.

(28) Walton, K. S.; Abney, M. B.; Douglas LeVan, M. *Microporous Mesoporous Mater.* **2006**, *91*, 78-84.

(29) Harlick, P. J. E.; Tezel, F. H. *Microporous Mesoporous Mater.* **2004**, *76*, 71-79.

(30) Brandani, F.; Ruthven, D. M. *Ind. Eng. Chem. Res.* **2004**, *43*, 8339-8344.

(31) Belmabkhout, Y.; Sayari, A. *Energy Fuels* **2010**, *24*, 5273-5280.

(32) Leal, O.; Bolívar, C.; Ovalles, C.; García, J. J.; Espidel, Y. *Inorg. Chim. Acta* **1995**, *240*, 183-189.

(33) Chang, A. C. C.; Chuang, S. S. C.; Gray, M.; Soong, Y. *Energy Fuels* **2003**, *17*, 468-473.

(34) Khatri, R. A.; Chuang, S. S. C.; Soong, Y.; Gray, M. *Energy Fuels* **2006**, *20*, 1514-1520.

(35) Asenath Smith, E.; Chen, W. *Langmuir* **2008**, *24*, 12405-12409.

(36) Abrahams, B. F.; Hoskins, B. F.; Robson, R. *J. Am. Chem. Soc.* **1991**, *113*, 3606-3607.

(37) Hoskins, B. F.; Robson, R. *J. Am. Chem. Soc.* **1989**, *111*, 5962-5964.

(38) Hoskins, B. F.; Robson, R. *J. Am. Chem. Soc.* **1990**, *112*, 1546-1554.

(39) Robson, R. *Dalton Trans.* **2008**, 5113-5131.

(40) Kondo, M.; Yoshitomi, T.; Matsuzaka, H.; Kitagawa, S.; Seki, K. *Angew. Chem. Int. Ed.* **1997**, *36*, 1725-1727.

(41) Chui, S. S.-Y.; Lo, S. M.-F.; Charmant, J. P. H.; Orpen, A. G.; Williams, I. D. *Science* **1999**, *283*, 1148-1150.

(42) Li, H.; Eddaoudi, M.; O'Keeffe, M.; Yaghi, O. M. *Nature* **1999**, *402*, 276-279.

(43) Dincă, M.; Long, J. R. *Angew. Chem. Int. Ed.* **2008**, *47*, 6766-6779.

(44) Hu, Y. H.; Zhang, L. *Adv. Mater.* **2010**, *22*, E117-E130.

(45) Lin, X.; Jia, J.; Hubberstey, P.; Schröder, M.; Champness, N. R. *CrystEngComm* **2007**, *9*, 438-448.

(46) Murray, L. J.; Dincă, M.; Long, J. R. *Chem. Soc. Rev.* **2009**, *38*, 1294-1314.

(47) Collins, D. J.; Zhou, H.-C. *J. Mater. Chem.* **2007**, *17*, 3154-3160.

(48) Eddaoudi, M.; Kim, J.; Rosi, N.; Vodak, D.; Wachter, J.; O'Keeffe, M.; Yaghi, O. M. *Science* **2002**, *295*, 469-472.

(49) Ma, S.; Sun, D.; Simmons, J. M.; Collier, C. D.; Yuan, D.; Zhou, H.-C. *J. Am. Chem. Soc.* **2007**, *130*, 1012-1016.

(50) Ma, S.; Zhou, H.-C. *Chem. Comm.* **2010**, *46*, 44-53.

(51) Millward, A. R.; Yaghi, O. M. *J. Am. Chem. Soc.* **2005**, *127*, 17998-17999.

(52) Cychosz, K. A.; Wong-Foy, A. G.; Matzger, A. J. *J. Am. Chem. Soc.* **2008**, *130*, 6938-6939.

(53) Cychosz, K. A.; Wong-Foy, A. G.; Matzger, A. J. *J. Am. Chem. Soc.* **2009**, *131*, 14538-14543.

(54) Cychosz, K. A.; Ahmad, R.; Matzger, A. J. *Chem. Sci.* **2010**, *1*, 293-302.

(55) Cychosz, K. A.; Matzger, A. J. *Langmuir* **2010**, *26*, 17198-17202.

(56) D'Alessandro, D. M.; Smit, B.; Long, J. R. *Angew. Chem. Int. Ed.* **2010**, *49*, 6058-6082.

Chapter 2

Effect of Humidity on the Performance of Microporous Coordination Polymers as Adsorbents for CO_2 Capture

Published in *Langmuir* **2011**, *27*, 6368-6373

2.1 Introduction

After the first reports of coordination polymers that exhibited porosity by gas sorption,[1-4] numerous applications were proposed for their potential usage. MCPs were initially touted as potential adsorbents for the high pressure storage of gases. Yaghi et al. examined CO_2 uptakes within a group of MCPs, and showed that materials with the highest surface areas exhibited superior uptakes at high pressures.[5] However, surface area was not an important factor when examining uptake in the low pressure region. In this regime, gas uptake is correlated to interaction strength between the adsorbent and the gas. Unique structural features referred to as coordinatively unsaturated metal centers are present in some MCPs, and have been shown to exhibit relatively strong interactions with adsorbates such as H_2[6-8] and CO_2.[6] The interaction between coordinatively unsaturated metal centers and guest species residing in the pores, can either be physisorptive in character, where the exposed metal cations polarize the adsorbates, or in some cases chemisorptive, where adsorbates with one or more lone pairs of electrons coordinate to the metal site. With regards the interaction strength, well-defined ranges in heats of adsorption cannot be established to clearly differentiate the two phenomena. However, physisorptive interactions are generally weaker (5 ~ 40 kJ/mol), while chemisorptive interactions can be much stronger (40 ~ 800 kJ/mol).[9]

Matzger and co-workers[10] postulated that MCPs with a relatively high density of open metal sites might serve as good adsorbents for capturing CO_2, and demonstrated that MCPs of the M/DOBDC series (where M = Zn,[8,11,12] Ni,[13] Co,[14] Mg[10,15,16] and DOBDC =

2,5-dioxido-1,4-benzenedicarboxylate) exhibit exceptionally high CO_2 uptakes at low partial pressure, near room temperature. The CO_2 sorption isotherms for these materials were fully reversible at 22 °C, indicating physical adsorption of CO_2 within the pores. As shown in Figure 2.1, compounds of the M/DOBDC series are synthesized under solvothermal conditions to yield crystalline materials featuring hexagonal pores. Upon solvent exchange and subsequent activation, the guest species are removed resulting in pores that are approximately 15 Å in diameter. Mg/DOBDC was shown to exhibit an uptake of nearly 25 wt% at 0.1 atm and 22 °C, surpassing the performance of 13X molecular sieves under similar conditions (12 wt% at 0.1 atm and 25 °C).[17] In comparison to other MCPs, members of the M/DOBDC series have been shown to have superior CO_2 uptakes.[18]

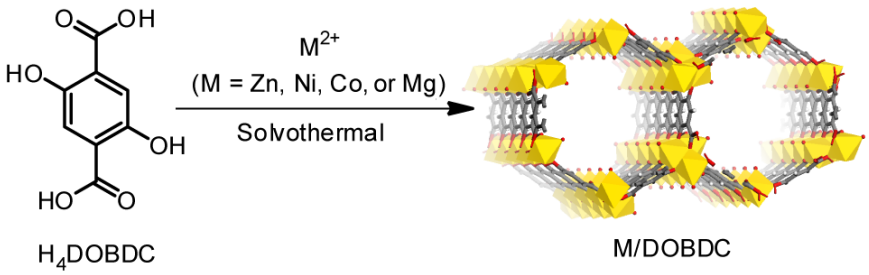

Figure 2.1. Synthesis and structure of M/DOBDC materials.

The effect of H_2O, which is an ever-present component of flue gas, on CO_2 capacities has been examined under static conditions for Ni/DOBDC[19] and HKUST-1,[19-21] but prior to the work presented here, its impact on performance had not been ascertained across multiple members of the M/DOBDC series. Here, the performance of Zn, Ni, Co and Mg/DOBDC materials was evaluated under flow-through conditions by determining the CO_2 capacities from N_2/CO_2breakthrough curves and then comparing the capacities with CO_2 uptakes obtained from static sorption measurements. The effect of humidity was investigated by passing a gaseous mixture of $N_2/CO_2/H_2O$ through the materials until breakthrough was observed for each component, followed by regenerating samples thermally, and then comparing the post-regeneration CO_2 capacities with those of pristine samples.

2.2 CO_2 Capture Performance under Dry Conditions

Although a complex milieu depending on the material in the feed and scrubbing regimen, flue gas emitted from coal-fired power plants is primarily composed of N_2, CO_2, and H_2O.[22] Initial experiments were conducted with dry surrogate flue gas (5/1 N_2/CO_2, hereafter referred to as SFG) in order to compare material capacity for CO_2 under flow conditions with CO_2 uptakes under static conditions. Samples of M/DOBDC materials were packed into columns, purged with Ar, then subjected to a mixture of 5/1 N_2/CO_2, and then purged again with Ar. Column effluent was continuously monitored by mass spectrometry. N_2/CO_2 breakthrough curves for Zn/DOBDC, Ni/DOBDC, Co/DOBDC and Mg/DOBDC are shown in Figure 2.2 through Figure 2.5. Each material exhibited selective retention of CO_2 as evidenced by the initial 'roll-up' in N_2 concentration, followed by CO_2 breakthrough. Roll-up occurs when an adsorbate is displaced by another component with a higher affinity for the adsorbent, resulting in the effluent concentration of the weakly adsorbed gas, which in this case is N_2, surpassing its concentration in the feed.[23] However, when the amount of CO_2 captured reaches the adsorbent capacity, no additional CO_2 is retained and the effluent composition becomes identical to the feed composition. In all cases, this is clearly shown by the simultaneous decline in N_2 response with CO_2 breakthrough.

CO_2 flow-through capacities for each material were determined from respective CO_2 breakthrough curves, averaged over three runs, and compared with static CO_2 uptakes determined at P = 0.167 atm (corresponding to 5/1 N_2/CO_2 at 1 atm in flow-through experiments) and T = 25 °C. CO_2 sorption isotherms obtained for M/DOBDC materials synthesized in this work (Figure 2.6) were consistent with those previously reported[10] indicating reproducible material quality. A virial-type isotherm[24] was fit to the experimental CO_2 isotherms measured at 25 °C and the resulting fitting constants were used to calculate the static CO_2 uptakes of M/DOBDC materials at P = 0.167 atm. Flow-through CO_2 capacities of 6.9 wt%, 12.0 wt%, 13.9 wt%, and 22.6 wt% were obtained for Zn/DOBDC, Ni/DOBDC, Co/DOBDC and Mg/DOBDC, respectively. These values are quite comparable to CO_2 uptakes obtained under static conditions, as shown in Figure 2.7, indicating a minimal role for nitrogen as an interfering adsorbate. Previous gas

breakthrough studies involving the resolution of CO_2 from N_2/CO_2 or CH_4/CO_2 mixtures with Ni/DOBDC,[15] Zn/DOBDC,[25] and Mg/DOBDC[15,25] have also demonstrated that these materials have relatively high capacities for CO_2, although direct comparisons cannot made between these data and the capacities reported here, because the feed gas compositions are not identical.

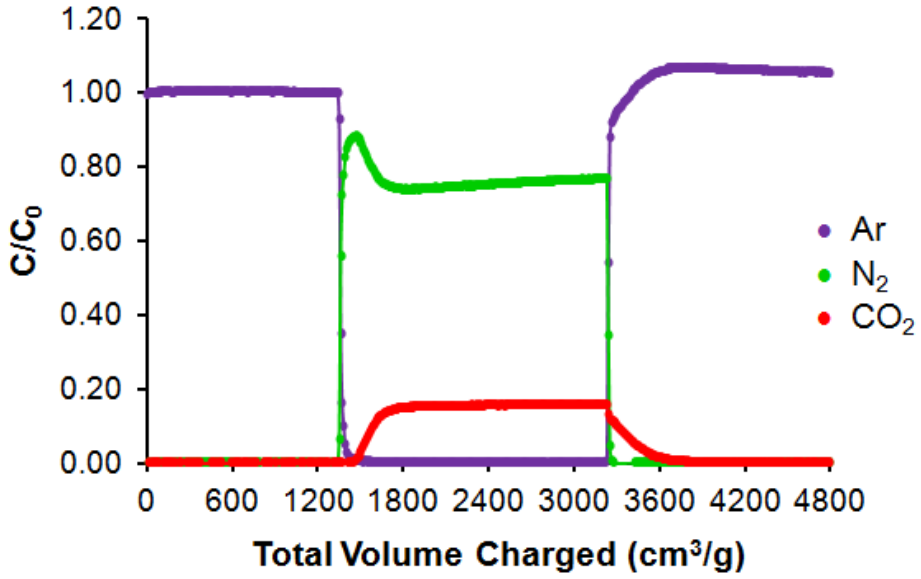

Figure 2.2. N_2/CO_2 breakthrough curves in a column of Zn/DOBDC treated with surrogate flue gas.

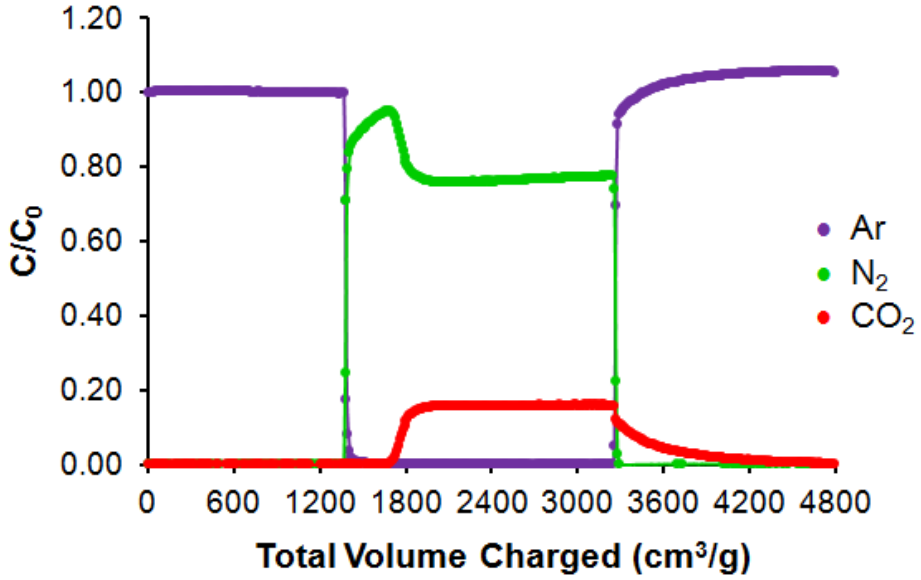

Figure 2.3. N_2/CO_2 breakthrough curves in a column of Ni/DOBDC treated with surrogate flue gas.

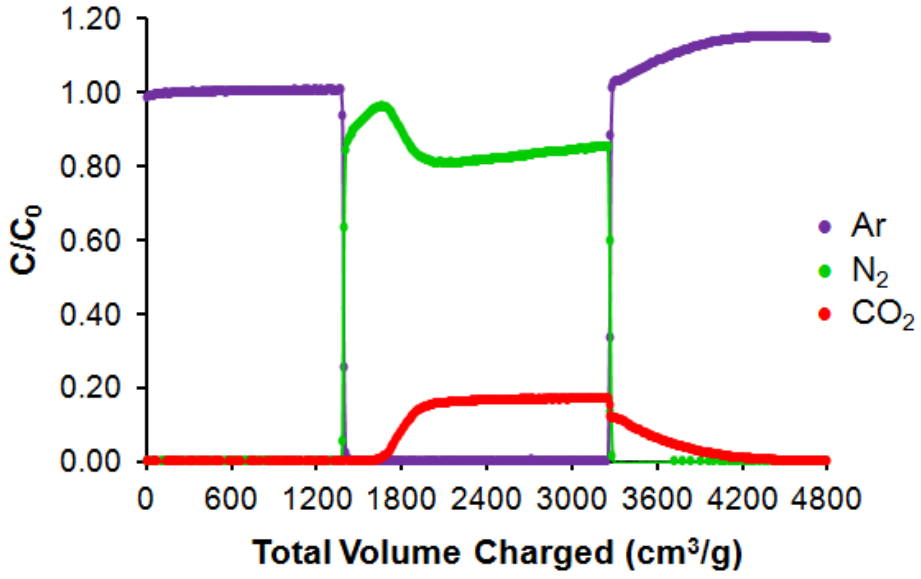

Figure 2.4. N_2/CO_2 breakthrough curves in a column of Co/DOBDC treated with surrogate flue gas.

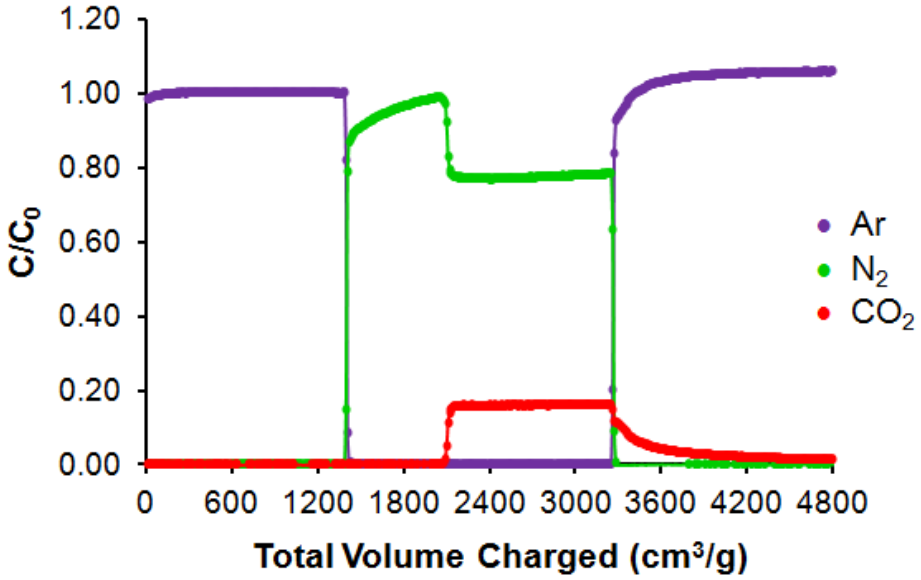

Figure 2.5. N_2/CO_2 breakthrough curves in a column of Mg/DOBDC treated with surrogate flue gas.

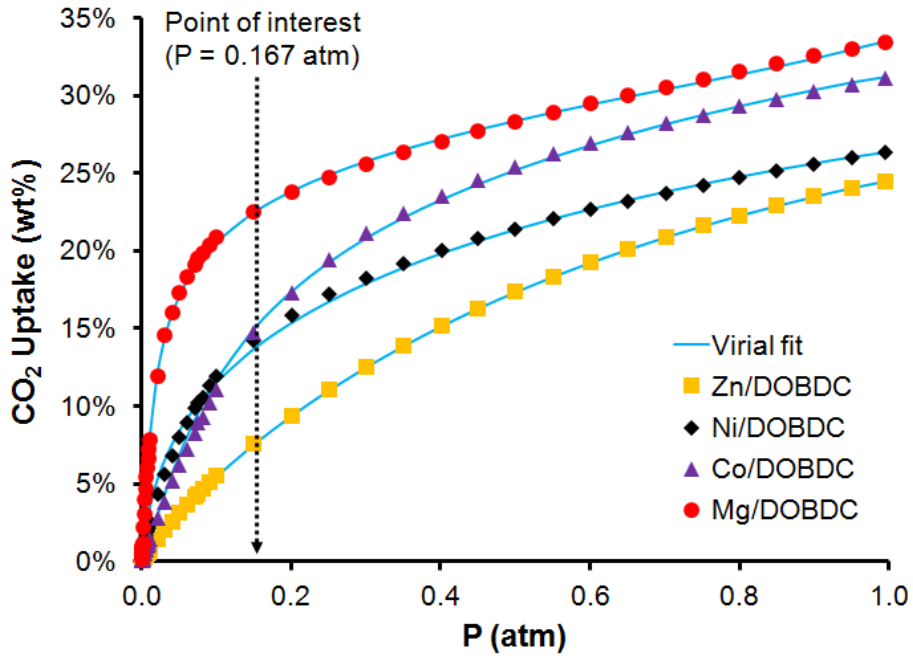

Figure 2.6. CO_2 sorption isotherms of M/DOBDC materials at 25 °C (points), and overlaid with virial-type isotherms (blue lines) fit to the experimental data.

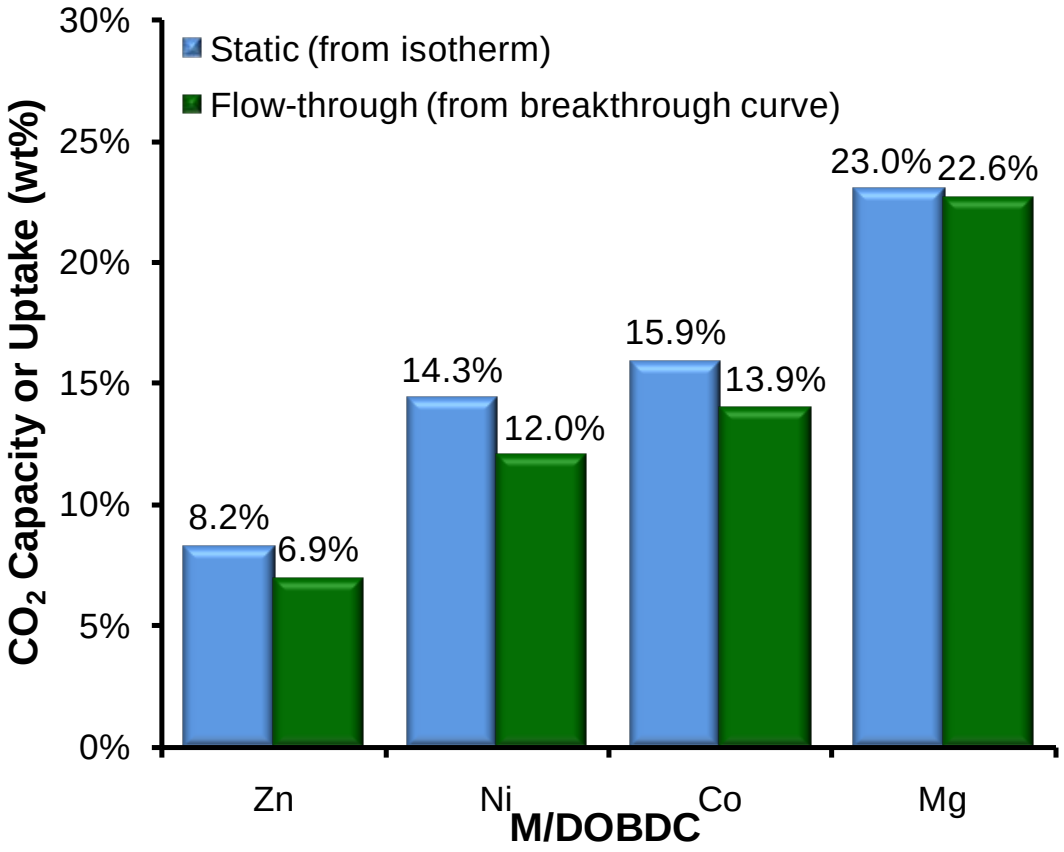

Figure 2.7. Comparison between static CO_2 uptakes at P = 0.167 atm calculated using parameters obtained from the virial-type isotherm fit to CO_2 sorption isotherms measured at 25 °C, with flow-through CO_2 capacities determined from CO_2 breakthrough curves; breakthrough experiments were performed at room temperature.

2.3 CO_2 Capture Performance under Humid Conditions

At the outset of the humidity study, we sought to determine if a humidity threshold existed for which Mg/DOBDC could be fully regenerated without significant loss in the flow-through CO_2 capacity. To investigate this, Mg/DOBDC samples were treated with humidified SFG at relative humidities (RH's) of 9%, 35% and 70%. Humidification was achieved by directing dry N_2 gas through a bubbler filled with saturated aqueous NaCl,[26] and mixing the humidified N_2 stream with CO_2 to achieve 5/1 N_2/CO_2 with 70% RH. Ar was used as a diluent to achieve humidities at 35% and 9%. $N_2/CO_2/H_2O$ breakthrough curves in columns of Mg/DOBDC at 70%, 35%, and 9% RH's are shown in Figure 2.8.

In all cases, H_2O was selectively retained versus N_2 and CO_2, while CO_2 selectivity was retained versus N_2; such results are perfectly in line with expectations based on adsorbate boiling points and therefore the capacities are the notable quantity. Flow-through CO_2 capacities were determined from the CO_2 breakthrough curves, and were found to be consistent with those determined from dry SFG. After H_2O breakthrough, the samples were thermally regenerated at 150 °C under a stream of Ar. Samples were then treated with dry SFG in order to evaluate the post-regeneration material performance. For each humidity, three samples were subjected to the aforementioned protocol, and the CO_2 capacities of the regenerated materials were averaged. As shown in Figure 2.9, the CO_2 capacity of Mg/DOBDC in 5/1 N_2/CO_2 is drastically reduced after hydration at 70% RH and regeneration. CO_2 capacities for samples exposed to 35% RH and 9% RH were also significantly diminished relative to the pristine material. This observation contrasts with a previous report where the authors claim that sorption capacity of Mg/DOBDC (Mg-MOF-74) is not diminished by H_2O vapor.[25] Mg/DOBDC is clearly not a suitable adsorbent for repetitive CO_2 capture from humid flue gas, since the performance drastically degrades after a single regeneration treatment.

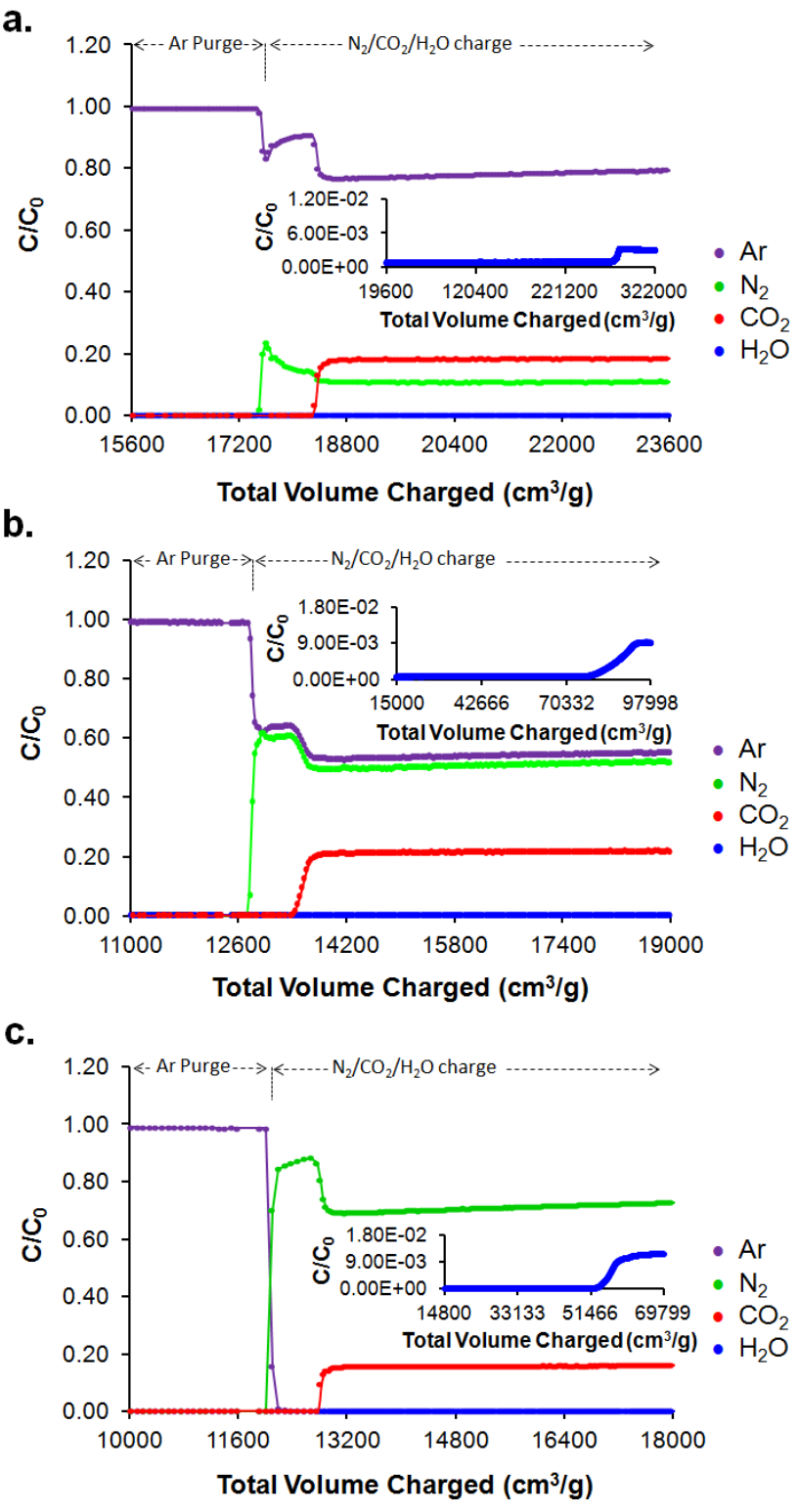

Figure 2.8. $N_2/CO_2/H_2O$ breakthrough curves in columns of Mg/DOBDC at (a) 70% RH, (b) 35% RH, and (c) 9%.

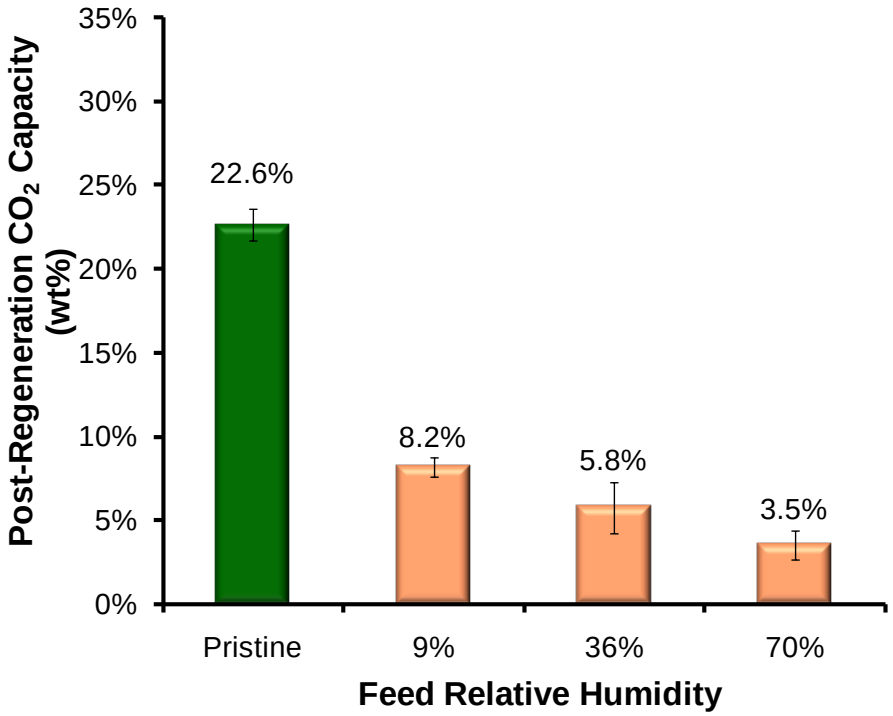

Figure 2.9. Comparison between CO_2 capacities of pristine Mg/DOBDC, and regenerated Mg/DOBDC samples after hydration at 70% RH, 36% RH, and 9% RH. Bars represent one unit of standard deviation above and below the mean.

The effect of humidity on the CO_2 flow-through capacities of other M/DOBDC materials at 70% RH was also investigated. The materials were subjected to $N_2/CO_2/H_2O$ breakthrough, and CO_2 capacities of the regenerated materials were obtained from dry SFG and compared with those of the pristine materials. As shown in Figure 2.10, the flow-through CO_2 capacity for regenerated Zn/DOBDC is almost completely lost, yet Ni/DOBDC and Co/DOBDC still exhibit relatively high capacities for CO_2 when compared with the pristine materials. In fact, the capacity of the regenerated Co/DOBDC sample is about 90% of the pristine material.

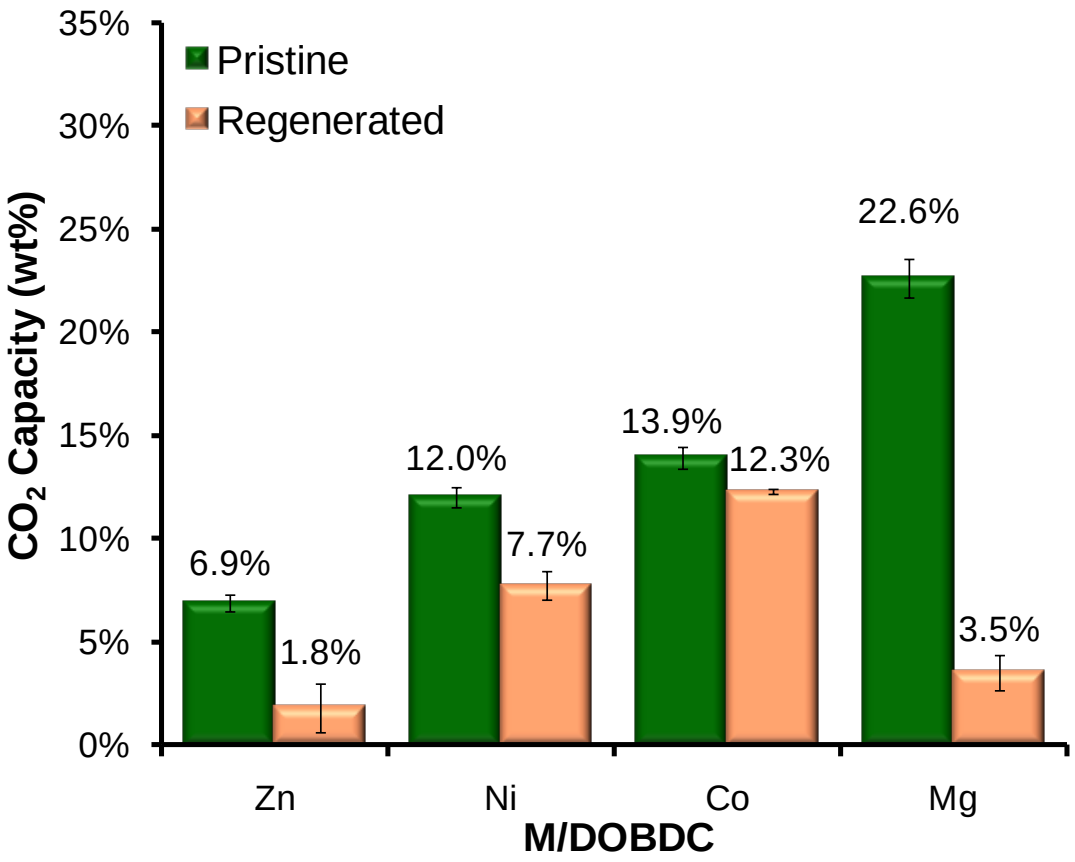

Figure 2.10. Comparison between CO_2 capacities of pristine M/DOBDC, and regenerated M/DOBDC samples after hydration at 70% RH. Bars represent one unit of standard deviation above and below the mean.

2.4 Effect of Cyclical Usage on Co/DOBDC Performance

The performance of Co/DOBDC was further investigated by determining the effect of cyclical H_2O exposure on CO_2 capacity at 70% RH. A sample of Co/DOBDC was taken through three hydration/thermal regeneration cycles by the aforementioned protocol. The material retained the ability to resolve CO_2 from SFG (Figure 2.11), and exhibited a capacity of 7.4 wt% CO_2, or 53% of the pristine capacity.

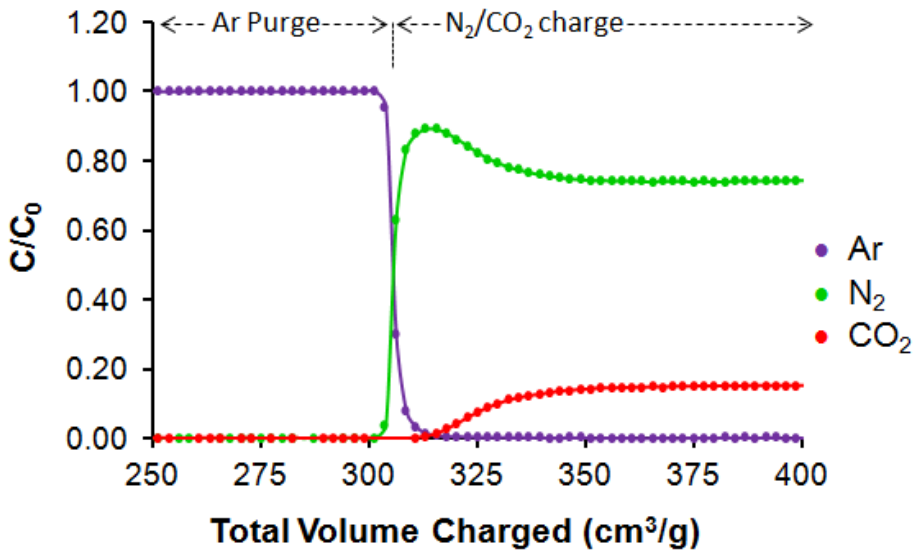

Figure 2.11. 5/1 N_2/CO_2 breakthrough curves collected from Co/DOBDC after three hydration/regeneration cycles.

The effect of cyclical exposure of Co/DOBDC to humid SFG at 70% RH was also examined. A sample of the material was treated with SFG at 70% RH, and then purged with Ar after a fixed period of $N_2/CO_2/H_2O$ exposure; in a single cycle, 1820 cm^3/g of humid SFG was introduced into the sample, followed by Ar purge of 3640 cm^3/g to remove CO_2. As shown in Figure 2.12, after 20 cycles Co/DOBDC looses nearly all capacity for CO_2. The hydrated sample was stored for two weeks at room temperature under Ar then regenerated at 150 °C under Ar flow, and displayed a post-regeneration CO_2 capacity of 7.7 wt% CO_2. Although these experiments do not represent optimized process conditions (wherein material performance would be maximized by limiting the

period of $N_2/CO_2/H_2O$ exposure to the gradually diminishing CO_2 breakthrough time), they demonstrate that even after extended exposure to humid environments, Co/DOBDC still exhibits the ability to capture CO_2 after regeneration.

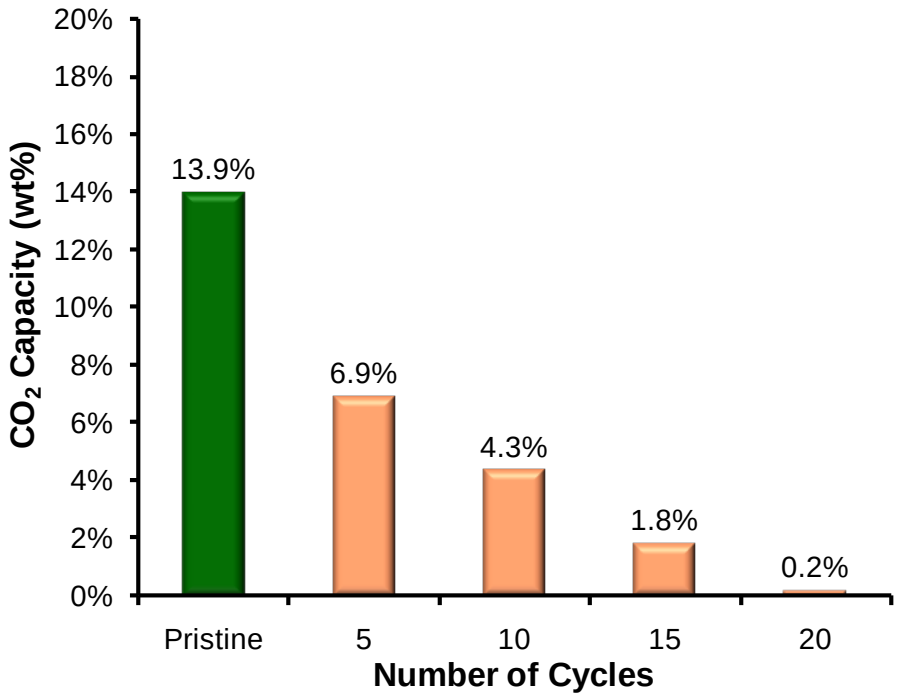

Figure 2.12. CO_2 capacity of Co/DOBDC after humidity exposure/Ar purge cycles.

In an attempt to understand why Co/DOBDC exhibited superior capacity retention in comparison to other members of the M/DOBDC series, hypotheses were put forth and thermophysical data associated with these hypotheses were examined against the percentage of capacity retention. One hypothesis was that H_2O should be more readily removed from smaller metal cations (ionic radius is measure of size), given that coordination sites associated with smaller cations are more sterically hindered. A separate conjecture examined the aqueous solubilities of metal chloride salts, which relates to the covalency of the metal-anion bond; greater aqueous solubility would represent higher ionic character, translating to higher propensity of the analogous MCP to be detrimentally impacted by H_2O, while lower aqueous solubility is indicative of a stronger covalency in

the metal-anion bond thereby reducing the propensity for H_2O to detrimentally impact the structure. However, no correlations were observed when the aforementioned thermophysical data were plotted against the percentage of capacity retention after hydration and thermal regeneration. Interestingly, the comparatively high tolerance of Co/DOBDC to humid conditions is in stark contrast to the behavior of another Co MCP, MOF-5(Co), which is reported by Martens and co-workers to be extremely sensitive to moisture.[27]

2.5 Post-regeneration Material Analysis

Powder X-ray diffraction patterns (Figure 2.13) collected from samples that were regenerated after hydration were generally consistent with that of the pristine materials, cautioning that PXRD is not a good diagnostic for materials quality with regards to *sorption performance*; this has been corroborated in a study[28] reported shortly after publication of the work presented here. In order to determine if residual H_2O remained on regenerated samples of the material, IR spectra of pristine, hydrated, and regenerated samples were obtained for Mg/DOBDC and Co/DOBDC. The IR spectra for Co/DOBDC materials are shown for the region between 4000 cm^{-1} and 1800 cm^{-1} (Figure 2.14), and the region between 1800 cm^{-1} and 450 cm^{-1} (Figure 2.15); peaks shifts of 2 ~ 4 cm^{-1} are observed upon hydration, but generally to return to within 1 cm^{-1} of the pristine peaks, indicating minimal change in the material structure, facile removal of H_2O. However IR spectra of Mg/DOBDC for the same regions (4000 cm^{-1} to 1800 cm^{-1} shown in Figure 2.16, 1800 cm^{-1} to 450 cm^{-1} shown in Figure 2.17) reveal 2 ~ 4 cm^{-1} shifts in peaks from the pristine and thermally regenerated materials, with a broad band at ~3430 cm^{-1} present in the regenerated material, corresponding to residual H_2O, based on the presence of this band in the hydrated sample, and thus suggesting strong retention of H_2O in Mg/DOBDC.

To investigate the porosity of the regenerated materials, BET surface areas were obtained from N_2 sorption isotherms of the regenerated samples and compared to those of the pristine materials. As shown in Figure 2.18, the surface area for both Co/DOBDC and Mg/DOBDC are diminished relative to the pristine materials, but the regenerated

Mg/DOBDC material is more severely impacted. In the case of Co/DOBDC, it is conceivable that capacity loss is due to collapse at, or near, the pore entrances. This phenomenon would block off access to the interior space within the 1D dimensional pores thus reducing the apparent surface area, while the bulk material structure is retained; this is supported by the data, as evidenced by the significant reduction in surface area, coupled with the lack of structural change observed by PXRD and IR. In the case of Mg/DOBDC, capacity loss is attributable to strong retention of H_2O, possibly also coupled with pore entrance collapse.

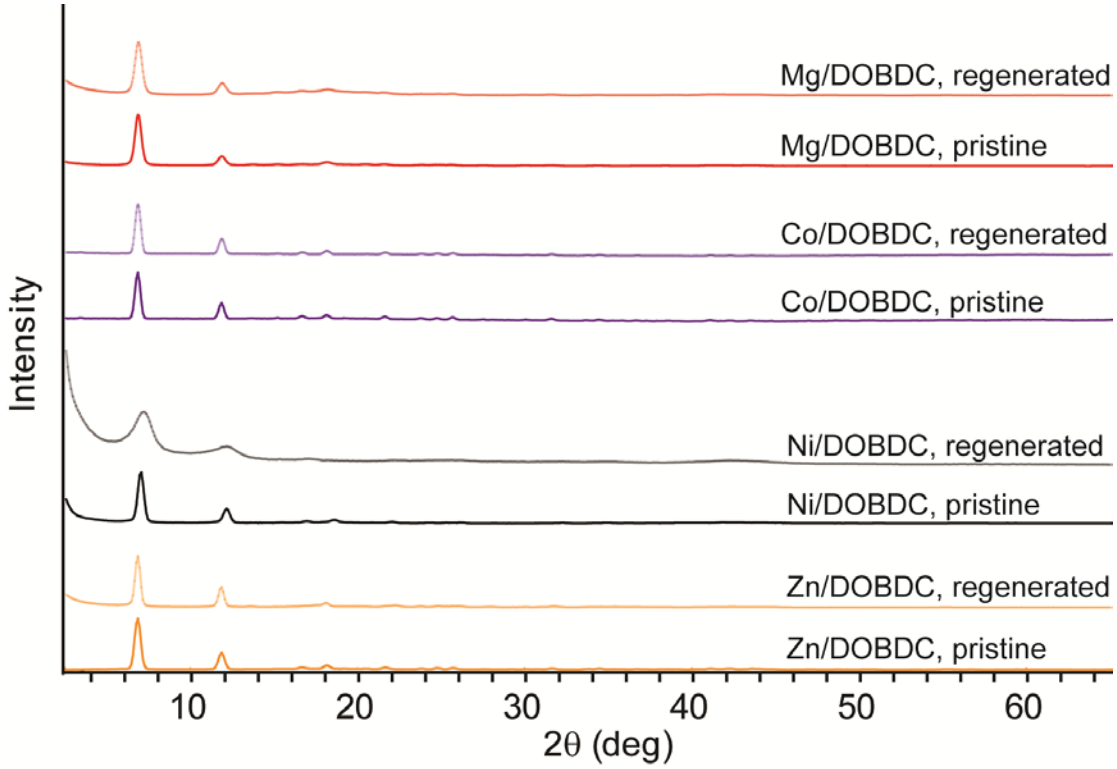

Figure 2.13. Overlay of powder X-ray diffraction patterns of activated (pristine) M/DOBDC materials, and M/DOBDC samples regenerated after hydration at 70% RH.

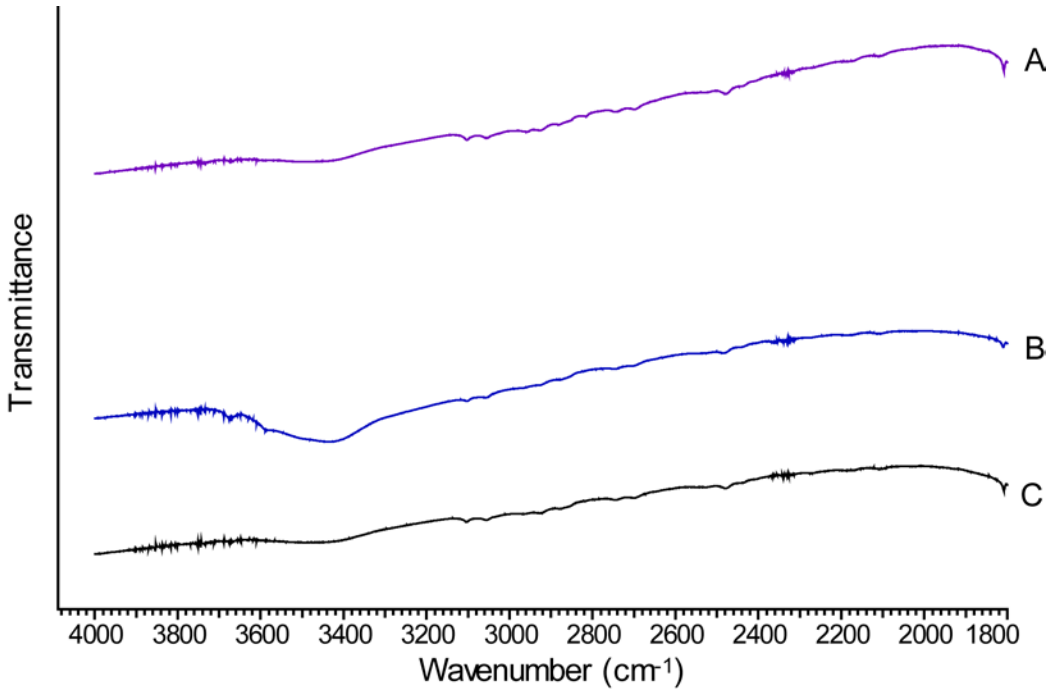

Figure 2.14. Overlay of IR spectra of: a) pristine, b) hydrated, and c) regenerated Co/DODBC.

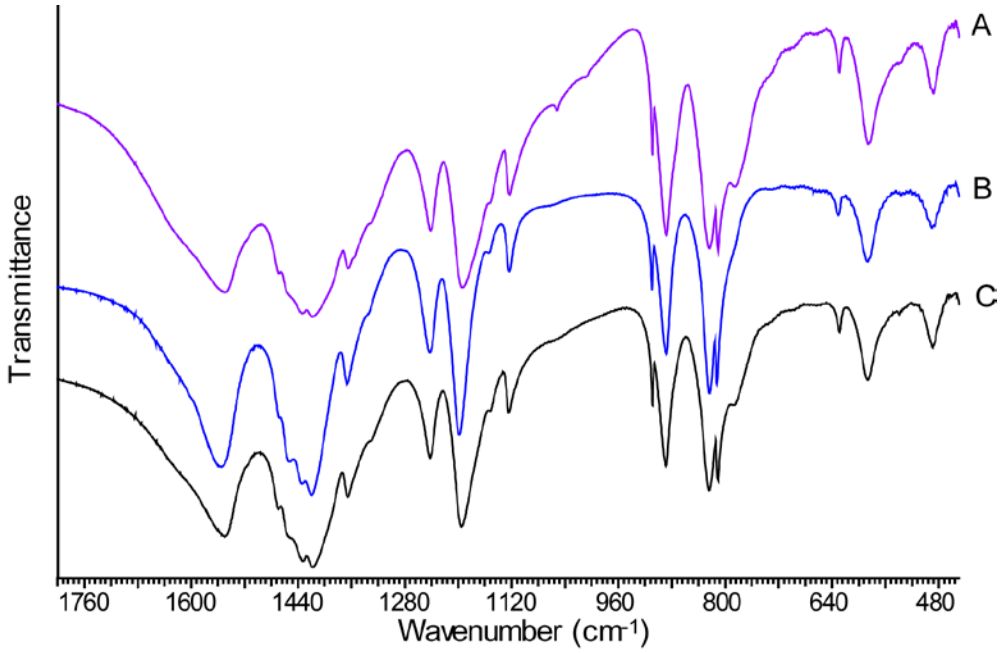

Figure 2.15. Overlay of IR spectra of: a) pristine, b) hydrated, and c) regenerated Co/DODBC.

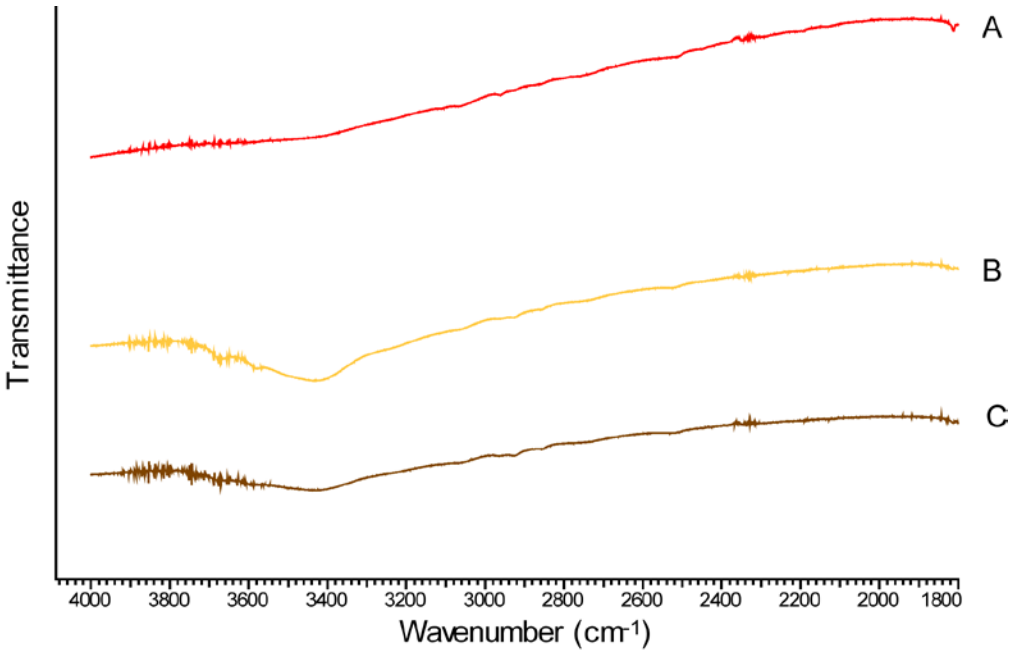

Figure 2.16. Overlay of IR spectra of: a) pristine, b) hydrated, and c) regenerated Mg/DODBC.

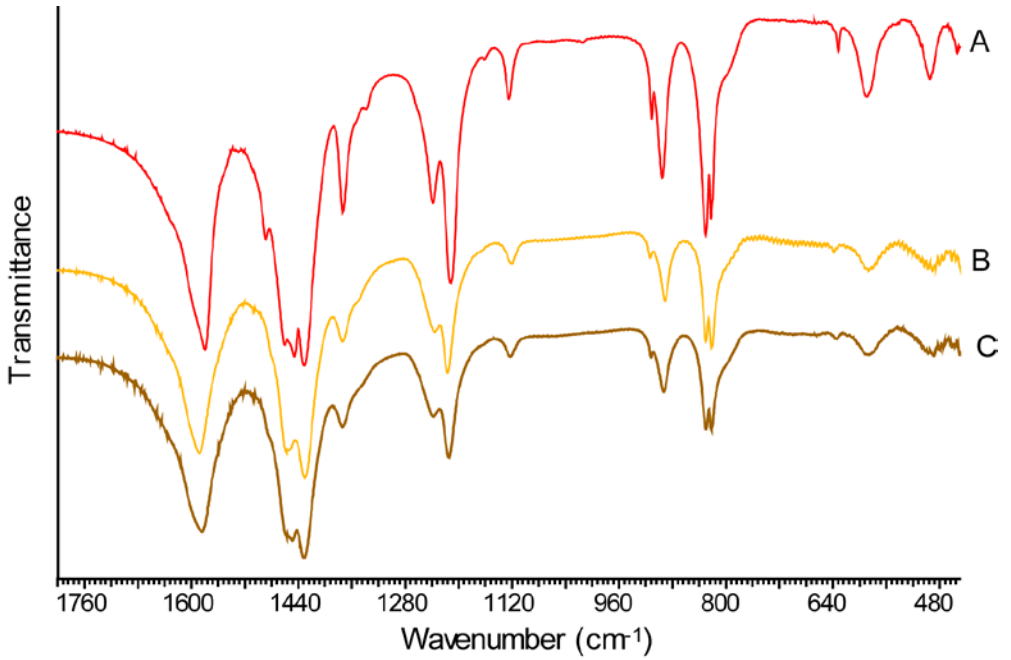

Figure 2.17. Overlay of IR spectra of: a) pristine, b) hydrated, and c) regenerated Mg/DODBC.

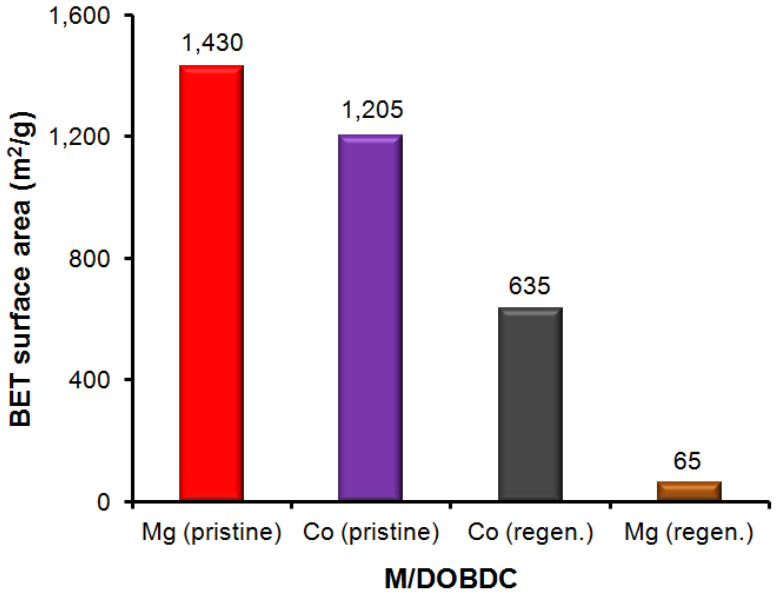

Figure 2.18. BET surface areas of pristine and regenerated Mg/DOBDC and Co/DOBDC.

2.6 Conclusions

In this study the CO_2 capacities of MCPs in the M/DOBDC series of materials were examined at ambient temperature under flow conditions with dry, and humidified gas mixtures of 5/1 N_2/CO_2 deployed as a surrogates for flue gas. Given that CO_2 is much more strongly adsorbed than N_2 at room temperature in physisorbents, CO_2 capture performance of M/DOBDC materials under flow conditions with dry surrogate flue gas was expected to track with the static CO_2 uptakes, and this indeed was confirmed. Although Mg/DOBDC exhibits superior capacity for CO_2 in dry surrogate flue gas, the capacity was drastically diminished after H_2O breakthrough and subsequent regeneration. Under identical protocols, Co/DOBDC retained about 90% of the initial capacity. The capacity of Co/DOBDC further diminished after cyclical hydration and thermal regeneration. These data indicate that although CO_2 capacity under dry conditions is an important criterion for identifying candidate MCPs for adsorption-based CO_2 capture, post-regeneration capacity retention after exposure to humid conditions is a more important factor in choosing candidate MCPs for future development. New materials will

need both superior CO_2 capacity and excellent retention of performance under cyclical operation, in order to minimize costs associated with material replacement and disposal.

2.7 Experimental

2.7.1 Syntheses

2,5-dihydroxy-1,4-benzenedicarboxylic acid (H_4DOBDC) was purchased from Hang Zhou Trylead Chemical Technology Corp., Ltd and used without further purification. All solvents and metal salts were also used as received, without further purification. DMF, NMP and $Zn(NO_3)_2{\cdot}6H_2O$ were obtained from Fisher Scientific. $Ni(NO_3)_2{\cdot}6H_2O$ was obtained from Sigma-Aldrich, $Co(NO_3)_2{\cdot}6H_2O$ was obtained from Acros, and $Mg(OAc)_2{\cdot}4H_2O$ was obtained from Alfa Aesar. House deionized H_2O was used in all syntheses where H_2O was required.

Zn/DOBDC (MOF-74) was synthesized and activated using one-half the scale of a literature preparation.[8] To a 500 mL screw cap jar was added H_4DOBDC (1.25 g, 6.51 mmol), $Zn(NO_3)_2{\cdot}6H_2O$ (5.65 g, 22.0 mmol), 250 mL of DMF and 12.5 mL H_2O. The resulting mixture was homogenized via mechanical stirring with a magnetic stir bar, followed by sonication until dissolution of the solids was complete. Afterwards, the jar was tightly sealed with a Teflon-lined cap and placed into an oven heated at 100 °C. After 20 hours the jar was removed from the oven and the hot mother liquor was decanted and replaced with 200 mL of MeOH. The supernatant was decanted and replaced with 200 mL of MeOH 3 times over 6 days. After the solvent exchange, the material was loaded into a glass ampoule, evacuated at room temperature until the material was dry, then heated at 270 °C under dynamic vacuum for about 14 hours. Afterwards, the material was transferred to a N_2 glove box.

Co/DOBDC was synthesized and activated using a literature procedure.[10] To a 500 mL screw cap jar was added H_4DOBDC (0.48 g, 2.50 mmol), $Co(NO_3)_2{\cdot}6H_2O$ (2.38 g, 8.18 mmol), and 200 mL of 1/1/1 DMF/EtOH/H_2O. The resulting mixture was homogenized via mechanical stirring with a magnetic stir bar, followed by sonication until dissolution of the solids was complete. Afterwards, the jar was tightly sealed with a

Teflon-lined cap and placed into an oven heated at 100 °C. After 24 hours, the jar was removed and allowed to cool to room temperature. The mother liquor was decanted and replaced with 200 mL of MeOH. The supernatant was decanted and replaced with 200 mL of MeOH 4 times over 2 days. After the solvent exchange, the material was loaded into a glass ampoule, evacuated at room temperature until dry, and then heated at 250 °C under dynamic vacuum for 5 hours. Afterwards, the material was transferred to a N_2 glove box.

Ni/DOBDC was prepared using a method slightly modified from the literature prepartion.[10] H_4DOBDC (0.478 g, 2.50 mmol), and $Ni(NO_3)_2 \cdot 6H_2O$ (2.38 g, 8.21 mmol) were placed into an Erlenmeyer flask and dissolved in 200 mL 1/1/1 (v/v/v) DMF/EtOH/H_2O. The resulting mixture was homogenized via mechanical stirring with a magnetic stir bar, followed by sonication until dissolution of the solids was complete. The resulting solution was dispensed into twenty 20 mL vials, with 10 mL of stock solution per vial. The vials were sealed with Teflon-lined caps and placed into an oven heated at 100 °C. After 24 hours, the vials were removed and allowed to cool to room temperature. The mother liquor was decanted from each vial, and replaced with MeOH. A spatula was used to dislodge the material from the vial surface; the resulting suspension from in each vial was transferred to a 500 mL Erlenmeyer flask. The supernatant was decanted and replenished with 200 mL fresh MeOH 4 times over 2 days. After solvent exchange, the material was loaded into a glass ampoule, evacuated at room temperature until dry, and then heated at 250 °C under dynamic vacuum for 5 hours. Afterwards, the material was transferred to a N_2 glove box.

Mg/DOBDC (CPO-27-Mg) was prepared using a modification of the literature method.[15] H_4DOBDC (2.98 g, 15.5 mmol) of was placed into a 500 mL Erlenmeyer flask and suspended in NMP/H_2O (180 mL NMP/ 20 mL H_2O). The mixture was sonicated, mechanically stirred, and then filtered into a 500 mL jar containing $Mg(OAc)_2 \cdot 4H_2O$ (6.44 g, 34.9 mmol) . The mixture was sealed with a Teflon-lined cap, sonicated, and then placed into an oven heated at 120 °C. After 24 hours, the jar was removed from the oven, and the hot mother liquor was immediately decanted, and replaced with approximately 250 mL of MeOH. After most of the material had settled, two additional decant/replenish cycles were performed using fresh MeOH. The supernatant MeOH was

decanted and replenished with fresh MeOH 4 times over 2 days. After solvent exchange, about 3/4 of the as-synthesized material was loaded into a glass ampoule then evacuated at 30 ~ 40 °C for 2 hours in order to dry the material. The ampoule was then heated to 250 °C under dynamic vacuum for approximately 10 hours. Afterwards, the material was transferred to a N_2 glove box.

2.7.2 Gas Sorption

CO_2 sorption isotherms of activated samples of M/DOBDC materials were measured with an Autosorb-1C (volumetric method) outfitted with the micropore option by Quantachrome Instruments (Boynton Beach, Florida, USA) running version 1.55 of the ASWin software package. CO_2 isotherms were measured at 25 °C in the range 1.00 x 10^{-4} atm ≤ P < 1.00 atm using bone dry CO_2 (99.8%).

Static CO_2 uptakes at P = 0.167 atm were determined by fitting a virial-type isotherm[24] to the adsorption branches of CO_2 sorption isotherms measured at 25 °C in the pressure range 1.00 x 10^{-4} atm < P < 1.00 atm. The virial-type isotherm was developed by Czepiriski et al.,[24] and is based on the experimental observation that adsorption isosteres, functions that relate the equilibrium pressure and temperature, at constant amounts of uptake, are dependent only on the amount adsorbed. From this, the authors derived a linear relationship between pressure, temperature and two temperature-independent functions that can be mathematically described by polynomials of uptake. The resulting virial-type isotherm is given by:

$$\ln P = \ln N + \frac{1}{T}\sum_{i=0}^{m} a_i N^i + \sum_{i=0}^{n} b_i N^i$$

where P = CO_2 pressure (atm)

N = CO_2 uptake

T = sample temperature (K)

a_i, b_i = fitting constants

A 7 parameter virial-type isotherm (m = 4, n = 3) was previously fit to CO_2 sorption data collected from 13X molecular sieves.[29] The CO_2 isotherm of 13X molecular sieves displays a similar profile to that of Mg/DOBDC, thus a 7-parameter isotherm was fit against the CO_2 sorption isotherms of M/DOBDC materials. Uptakes at the desired pressure (P = 0.167 atm) were back-calculated using the optimized fitting constants.

2.7.3 Gas Breakthrough Experiments

Breakthrough experiments were performed using bone dry CO_2 (99.8%), ultra high purity N_2 (99.999%), and pre-purified Ar (99.998%). N_2/CO_2 and $N_2/CO_2/H_2O$ breakthrough curves were collected using a gas flow apparatus designed and constructed in-house (Figure S4). Breakthrough curves are normalized for sample mass and time by plotting C/C_0 versus total volume charged per gram. Here, C/C_0 is equivalent to the ratio of the gas response to the average response for Ar during the initial purge period. The total volume charged is the product of time and the sum of the volumetric flow rates of all gases charged into the adsorbent column.

N_2, Ar, and CO_2 gas flow rates were controlled using Aalborg model GFC17 mass flow controllers. A four-inlet solenoid valve manifold system (Bio-Chem Valve Incorporated model 040T412-54-4) was used to isolate each feed gas line from the central column feed line, to prevent back-mixing of gases during purge/breakthrough cycles. N_2 feed pressure was monitored using a Freescale model MPX4250AC6U-ND pressure transducer.

Temperature, pressure, and humidity data logging, along with gas flow rate control were performed using a custom software package written in Lab View. In preparation for breakthrough experiments, M/DOBDC materials (95 mg of material for breakthrough experiments with N_2/CO_2; 20 – 35 mg of material for breakthrough experiments with $N_2/CO_2/H_2O$) were loaded into copper columns (O.D. = 0.6 cm, length = 7.5 cm) in a N_2 glove box. Columns were plugged on each end with glass wool to retain the sample before installation onto the flow-through apparatus. In order to minimize exposure to air, care was taken to purge the apparatus with Ar, then load the column with Ar gas flowing at 12 cm^3/min from the apparatus.

Column effluent composition was monitored using a Hiden Analytical model HPR20 mass spectrometer running version 6.17.0.47 of MASsoft Professional. Multiple ion detection mode was used to obtain time-dependent responses of ions with mass to charge ratios (m/z) of 18 (H_2O^+), 28 (N_2^+), 40 (Ar^+), and (CO_2^+). It should be noted that the CO^+ fragment of CO_2, which has a relative intensity of 11.4% of the parent ion CO_2^+ response, contributes to the response of m/z = 28. To correct for this, the response for m/z = 28 was reduced by 11.4% of the m/z = 44 response.

Humidification of N_2/CO_2 was achieved by directing N_2 into a bubbler containing a saturated solution of NaCl in deionized water. The humidity of the bubbler effluent was monitored using a Honeywell model HIH-4021-003 humidity sensor. The humidity of the bubbler effluent was typically about 79%. The temperature of the humidified gas and the central column pipe were monitored using RTD probes purchased from Omega Engineering, Stamford, CT. Low humidities were achieved by reducing the N_2 gas flow rate and diluting the bubbler effluent with an appropriate amount of Ar to reach the desired humidity. The relative humidity of the mixed stream was calculated from the relative humidity of the column effluent, and the flow rates of diluent gases (see the final part of section 2.7.4). Table 2.1 provides the gas flow rates used in each experiment.

Table 2.1. Flow rates of gases used in breakthrough experiments.

Experiment	**Ar flow rate**	**N_2 flow rate**	**CO_2 flow rate**
Dry N_2/CO_2 breakthrough	12 cm^3/min (purge)	10 cm^3/min	2 cm^3/min
$N_2/CO_2/H_2O$ breakthrough (9% RH)	12 cm^3/min (purge) 8.75 cm^3/min (diluent)	1.25 cm^3/min	2 cm^3/min
$N_2/CO_2/H_2O$ breakthrough (35% RH)	12 cm^3/min (purge) 5 cm^3/min (diluent)	5 cm^3/min	2 cm^3/min
$N_2/CO_2/H_2O$ breakthrough (70% RH)	12 cm^3/min (purge)	10 cm^3/min	2 cm^3/min

Sample regeneration was performed at 150 °C using a custom-built column heater. This temperature was used in the regeneration of Ni/DOBDC in previous work by LeVan et al.[30] During the preliminary phase of our study, a sample of Zn/DOBDC (hydrated at ~70% RH) was first regenerated 150 °C, and the CO_2 capacity was determined. The sample was then regenerated at 270 °C and the CO_2 capacity was determined again. The capacities were not significantly different relative to the capacity of the pristine material, which indicated that 150 °C is a suitable temperature for regenerating Zn/DOBDC. Given the fact that as-synthesized Zn/DOBDC is activated at the highest temperature compared with other members of the M/DOBDC series, 150 °C was also used as the regeneration temperature for all hydrated materials in this study.

Samples were regenerated *in-situ* under Ar flow, with the column heater placed over the sample column. The temperature was ramped from room temperature to 150 °C over 30 minutes and held at 150 °C for 30 minutes. Afterwards, the sample column was allowed to cool to room temperature under Ar flow. In all cases, H_2O desorption was continuously monitored by mass spectrometry.

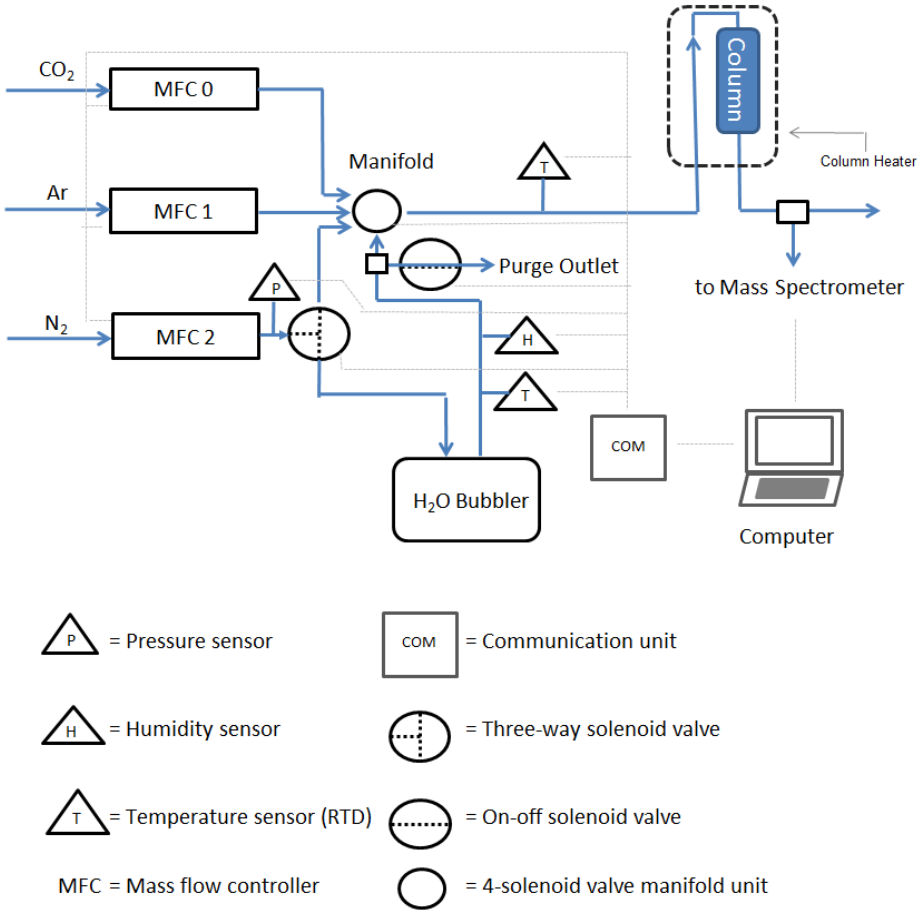

Figure 2.19 Diagram of gas flow apparatus

2.7.4 CO_2 Capacity Determination

Column effluent composition was monitored via multiple ion detection mode or profile scan mode. In either case, the equilibrium point of CO_2 breakthrough curves was estimated by calculating the approximate integral for 30-second time intervals under the breakthrough curves. The approximate derivative of the interval areas was plotted as a function of time. In all cases, the derivative rises to a maximum (corresponding to the inflection point in the approximate integral) before decreasing. The equilibrium point was taken to be the first local minimum after the derivative maximum.

Capacity determinations were initially performed in volumetric units (cm^3 CO_2/g adsorbent), which were referenced to STP (standard temperature and pressure; 0 °C, 1

atm) then subsequently converted into units of wt% (g CO_2/g adsorbent × 100%). In order to assess the CO_2 capacity from the CO_2 breakthrough curve of a given material, a conversion factor was introduced, referred to here as the 'flow factor'. Where,

$$Flow\ factor\ = \frac{Inlet\ CO_2\ flow\ rate}{Average\ CO_2\ response\ at\ Equilibrium}$$

The average CO_2 response at equilibrium was determined by averaging the instrument CO_2 response for the 4 points leading up to, and including, the equilibrium point. A key assumption, was that at equilibrium, the volumetric flow rate of CO_2 in the effluent was essentially equal to the volumetric flow rate of CO_2 in the column inlet and therefore CO_2 response was directly proportional not only to the effluent fractional composition of CO_2, but also to the volumetric flow rate of CO_2. The proportionality constant is the flow factor, and the product of the flow factor and the raw time-dependent CO_2 response generates a time-dependent volumetric flow rate curve, from which CO_2 capacity can be calculated, where:

$$CO_2\ capacity\ (cm^3/g)\ = \frac{V_{CO_2\ Retained}\ - v_{f,CO_2}V_{Void}}{m_{sample}} = \frac{V_{CO_2\ Charged}\ - V_{CO_2\ Detected}\ - v_{f,CO_2}V_{Void}}{m_{sample}}$$

where,

m_{sample} =sample mass

The total volume of CO_2 charged during the experiment ($V_{CO2\ Charged}$) is given by the expression

$$V_{CO_2\ Charged}\ = \dot{v}_{CO_2,inlet}\ \cdot (t_{Eq} - t_0)$$

$$\dot{v}_{CO_2,inlet}\ = \text{inlet volumetric } CO_2 \text{ flow rate } (\text{cm}^3/\text{min})$$

t_{Eq}= time at Equilibrium (min) , t_0 = time at introduction of N_2/CO_2 (min)

The total volume of CO_2 detected during the experiment ($V_{CO2\ Detected}$) corresponds to the area under the time-dependent volumetric CO_2 flow rate curve, which can be approximated using summation of trapezoidal areas, where

$$V_{CO_2\ Detected} = \int_{t_i}^{t_{Eq}} \dot{v}_{CO_2}(t)dt \approx \sum_{i=0}^{Eq} \frac{1}{2}[\dot{v}_{CO_2}(t_{i+1}) + \dot{v}_{CO_2}(t_i)](t_{i+1} - t_i)$$

t_i = time at the *i*th interval

$\dot{v}_{CO_2}(t)$=time-depdent volumetric CO_2 flow rate (cm^3/min)

$\dot{v}_{CO_2}(t) = F_{flow} \cdot R_{CO_2}(t)$

F_{flow} = the flow factor

$R_{CO_2}(t)$ = time-dependent CO_2 response

v_{f,CO_2} = volume fraction of CO_2 in the effluent at t_{Eq}

For dry surrogate flue gas (5/1 N_2/CO_2)

$$v_{f,CO_2} = \frac{\dot{v}_{CO_2}}{\dot{v}_{N_2} + \dot{v}_{CO_2}} = \frac{2\ cm^3/min}{2\ cm^3/min + 10\ cm^3/min} = 0.167$$

The total void volume (V_{Void}) is equal to the void volume within the apparatus ($V_{Apparatus}$), less the volume occupied by the framework of the porous material ($V_{Framework}$). The apparatus void volume was determined by loading a blank column containing only glass wool plugs onto the apparatus, followed by purging the apparatus with Ar, then flushing the apparatus with 5/1 N_2/CO_2. Conversion of the time-dependent Ar response curve to time-dependent volumetric flow rate, and integration of the Ar decay provided an apparatus void volume of approximately 9.65 cm^3. The volume occupied by the framework was approximated by subtracting the total pore volume (V_{Pore}) from the total sample volume (V_{Sample}), where

$$V_{framework} = V_{Sample} - V_{Pore}$$

$$V_{Sample} = \frac{m_{sample}}{\rho_{crystal}}$$

$$V_{Pore} = v_p \cdot m_{sample}$$

Where,

$\rho_{crystal}$ =crystal density (g/cm^3)

v_p = pore volume (cm^3/g) = 0.39 cm^3/g for MOF-74 (Zn/DOBDC)[8]

Therefore,

$$V_{framework} = m_{sample}\left(\frac{1}{\rho_{crystal}} - v_p\right)$$

Crystal densities for desolvated M/DOBDC materials were determined from the published crystallographic data for solvated MOF-74.[8] The unit cell of MOF-74 contains a total of 18 Zn atoms; since the framework is neutral, a total of 9 DOBDC^{4-} units must also be present. The crystal density ($\rho_{crystal}$) is given by

$$\rho_{crystal} = \frac{Z \cdot FW}{VN_A} = \frac{MW}{VN_A}$$

where,

Z = number of formula units per unit cell = 9 for MOF-74 [31]

FW = formula weight (g/mol)

V = unit cell volume (Å^3)

N_A = Avogadro's Number

MW = molecular weight (g/mol)

Assuming that the unit cell volume is essentially the same for all M/DOBDC materials, a general expression for the crystal density of all M/DOBDC materials can be written

$$\rho_{crystal} = \frac{Z \cdot FW}{VN_A} = \frac{MW}{VN_A} = \frac{18M_{AW} + 9L_{MW}}{VN_A} = \frac{18M_{AW} + 1747.17g/mol}{VN_A}$$

Where,

M_{AW} = atomic weight of the appropriate metal (g/mol)

L_{MW} = molecular weight of the $DOBDC^{4-}$ linker units (194.13 g/mol)

Table 2.2. Calculated crystal densities for M/DOBDC materials.

Material	ρ_{cryst} of desolvated material (g/cm^3)
Zn/DOBDC	1.22
Ni/DOBDC	1.17
Co/DOBDC	1.17
Mg/DOBDC	0.911

Pore volume (v_p, in units of cm^3/g) for Ni/DOBDC, Co/DOBDC and Mg/DOBDC was determined using the reported pore volume of Zn/DOBDC (MOF-74). If v_p^* is pore volume expressed in units of void volume per unit mole, then

$$v_p{}^* = v_p \cdot MW = v_p \cdot Z \cdot FW$$

Since void volume per unit mole is equivalent for all M/DOBDC materials, the pore volume in units of cm^3/g for Ni/DOBDC, Co/DOBDC and Mg/DOBDC can be calculated using the pore volume of Zn/DOBDC as a reference, where

$$v_p = \frac{v_p{}^*}{Z \cdot FW} = \frac{v_p{}^{Ref} \cdot Z \cdot FW^{Ref}}{Z \cdot FW} = v_p{}^{Ref} \frac{FW^{Ref}}{FW}$$

Table 2.3. Calculated pore volumes for M/DOBDC materials.

Material	v_p (cm^3/g)
Ni/DOBDC	0.41
Co/DOBDC	0.41
Mg/DOBDC	0.52

Therefore, the full void volume correction is given by

$$V_{Void} = V_{Apparatus} - \left(\frac{1}{\rho_{crystal}} - v_p\right) m_{sample}$$

CO_2 capacities from $N_2/CO_2/H_2O$ breakthrough experiments were determined in the same manner as those obtained from N_2/CO_2 experiments. The only difference was the treatment of the $v_{f,CO2}V_{Void}$ term. For humidified surrogate flue gas, the equilibrium time for CO_2 breakthrough is observed well before equilibrium time for H_2O. Therefore the volume fraction of CO_2 in the total void volume is not straightforward. Here we assumed that at the equilibrium time for CO_2, the apparatus void volume is filled with N_2, CO_2 and H_2O, and the sample void volume is filled with N_2 and CO_2. So the $v_{f,CO2}V_{Void}$ term is instead

$$v_{f,CO_2}V_{Void} = v_{f,CO_2,Apparatus}\ V_{Apparatus} - v_{f,CO_2,Pore}\ V_{Pore}$$

where,

$$v_{f,CO_2,Apparatus} = \frac{\dot{v}_{CO_2}}{\dot{v}_{N_2} + \dot{v}_{H_2O} + \dot{v}_{CO_2}}$$

The volumetric flow rate of H_2O (v_{H2O}) can be determined by performing a total mole balance on bubbler, and expressing the molar flow rate of H_2O as a function of N_2 molar flow rate. Assuming ideal behavior, the volumetric flow rate of H_2O vapor in the bubbler effluent is given by the expression

$$\dot{v}_{H_2O} = \frac{\dot{v}_{N_2}}{\frac{P}{RH' \cdot p^*_{H_2O}(T)} - 1}\frac{P_{N_2}}{P} \xrightarrow{Assuming\ \ P \approx P_{Ave}} \dot{v}_{H_2O} = \frac{\dot{v}_{N_2}}{\frac{P_{Ave}}{RH' \cdot p^*_{H_2O}(T)} - 1}\frac{P_{N_2}}{P_{Ave}}$$

Where,

P_{Ave} = average of the inlet and outlet bubbler pressures

RH' = fractional relative humidity of the bubbler effluent; frac. RH = RH%/100%

$p^*_{H_2O}(T)$ = sat'd vapor pressure of H_2O at temp. T; provided by the Antoine Equation

$$p^*_{H_2O}(T) = 10\text{^}\left(A - \frac{B}{C+T}\right)$$

Where A, B and C are constants (A = 8.10765, B = 1750.286, C = 235.000);[32] for the Antoine equation, T is in units of °C

Also,

$$v_{f,CO_2,Pore} = \frac{\dot{v}_{CO_2}}{\dot{v}_{N_2} + \dot{v}_{CO_2}}$$

For each material, three CO_2 breakthrough curves were collected and the CO_2 capacities were calculated, then averaged.

The relative humidity of the combined bubbler effluent (N_2/H_2O) and CO_2 or CO_2/Ar stream was determined using the definition of relative humidity. All gases were assumed to behave ideally. The fractional relative humidity of the $Ar/N_2/CO_2/H_2O$ stream is given by

$$RH = \frac{y_{H_2O} P_{Total}}{p^*_{H_2O}(T)} = \frac{1}{p^*_{H_2O}(T)}\left(\frac{\dot{n}_{H_2O}}{\dot{n}_{Total}}\right)\left(\frac{\dot{n}_{Total}\, RT}{\dot{V}_{Total}}\right) = \frac{\dot{n}_{H_2O} RT}{\dot{V}_{Total}\ p^*_{H_2O}(T)}$$

Where,

RH = fractional relative humidity of the $Ar/N_2/CO_2/H_2O$ stream

y_{H_2O} = mole fraction of H_2O in the $Ar/N_2/CO_2/H_2O$ stream

P_{Total} = total pressure of the $Ar/N_2/CO_2/H_2O$ stream

$\dot{n}_{H_2O} = molar\ flow\ rate\ of\ H_2O$

$\dot{n}_{Total}$ = total molar flow rate

$\dot{V}_{Total}$ = total volumetric flow rate

The molar flow rate of water from the bubbler can be determined from a mole balance based on N_2, and is given by

$$\dot{n}_{H_2O} = \frac{y_{H_2O}{}'}{1 - y_{H_2O}{}'} \dot{n}_{N_2}$$

Where,

$y_{H_2O}{}'$ = mole fraction of H_2O in the bubbler effluent, which is given by

$$y_{H_2O}{}' = \frac{RH' p^*_{H_2O}(T)}{P'}$$

Where,

P' = pressure at the bubbler outlet

By substitution,

$$RH = \left(\frac{y_{H_2O}{}'}{1 - y_{H_2O}{}'}\right)\left(\frac{RT}{\dot{V}_{Total}\, p^*_{H_2O}(T)}\right)\dot{n}_{N_2}$$

$$= \left(\frac{y_{H_2O}{}'}{1 - y_{H_2O}{}'}\right)\left(\frac{P_{N_2}\dot{V}_{N_2}}{\dot{V}_{Total}\, p^*_{H_2O}(T)}\right)$$

$$= \left(\frac{1}{\frac{1}{y_{H_2O}{}'} - 1}\right)\left(\frac{P_{N_2}\dot{V}_{N_2}}{\dot{V}_{Total}\, p^*_{H_2O}(T)}\right)$$

$$= \left(\frac{1}{\frac{P'}{RH'\, p^*_{H_2O}(T)} - 1}\right)\left(\frac{P_{N_2}\dot{V}_{N_2}}{\dot{V}_{Total}\, p^*_{H_2O}(T)}\right)$$

$$= \frac{P_{N_2}\dot{V}_{N_2}}{\dot{V}_{Total}\left[\frac{P'}{RH'} - p^*_{H_2O}(T)\right]}$$

Assuming $P' \approx P_{Ave}$, where P_{Ave} is the average of inlet and outlet bubbler pressures

$$RH = \frac{P_{N_2}\dot{V}_{N_2}}{\dot{V}_{Total}\left[\frac{P_{Ave}}{RH'} - p^*_{H_2O}(T)\right]}$$

$$= \frac{P_{N_2}\dot{V}_{N_2}}{\left(\dot{V}_{N_2} + \dot{V}_{Ar} + \dot{V}_{CO_2} + \dot{V}_{H_2O}\right)\left[\frac{P_{Ave}}{RH'} - p^*_{H_2O}(T)\right]}$$

Substituting the previous expression for V_{H2O} as a function of V_{N2} leads to the final expression for RH

$$RH = \frac{P_{N_2}\dot{V}_{N_2}}{\left[\dot{V}_{N_2}\left(1 + \frac{1}{\frac{P_{Ave}}{RH' p^*_{H_2O}(T)} - 1}\right) + \dot{V}_{Ar} + \dot{V}_{CO_2}\right]\left[\frac{P_{Ave}}{RH'} - p^*_{H_2O}(T)\right]}$$

Where,

$P_{N_2} =$ feed pressure of N_2 at the bubbler inlet

$\dot{V}_{N_2} =$ volumetric flow rate of N_2 into the bubbler

$\dot{V}_{Ar} =$ volumetric flow rate of Ar into the bubbler

$\dot{V}_{CO_2} =$ volumetric flow rate of CO_2 into the bubbler

2.7.5 IR Spectroscopy

FT-IR spectra of pristine, hydrated and regenerated M/DOBDC materials were obtained via KBr disk. The salt was dried under vacuum at 200 °C for ~ 16 hours, and stored in a N_2 glovebox. Samples of M/DOBDC (1 ~ 2 mg of material) were ground with 450 mg of KBr under N_2 atmosphere. About 220 mg of the mixture was transferred to a die kit and pressed into a pellet. Spectra of the pellets were obtained using a Nicolet Avatar 360 spectrometer pre-purged with N_2. Peak listings are provided below:

Co/DOBDC, pristine: IR 3438 (M), 3103 (M), 3055 (M), 2960 (M), 2926 (M), 2883 (M), 2856 (M), 2816 (M), 2743 (M), 2697 (M), 2477 (M), 2441 (M), 2407 (M), 2175 (W), 2108 (W), 1808 (M), 1550 (VS), 1433 (VS), 1417 (VS), 1364 (S), 1242 (S), 1194 (VS), 1123 (M), 1052 (M), 1010 (W), 909 (M), 888 (S), 824 (S), 810 (S), 785 (M), 629 (W), 586 (M), 488 (W), 446 (W) cm^{-1}.

Co/DOBDC, hydrated: IR 3676 (M), 3589 (M), 3434 (M), 3102 (M), 3058 (M), 2929 (M), 2867 (M), 2743 (M), 2703 (M), 2525 (M), 2483 (M), 2441 (M), 2184 (M), 2112 (M), 1809 (M), 1554 (VS), 1452 (S), 1419 (VS), 1366 (S), 1242 (M), 1198 (S), 1155 (W), 1123 (W), 1063 (VW), 910 (M), 888 (M), 824 (S), 812 (S), 631 (W), 588 (W), 491 (W) cm^{-1}.

Co/DOBDC, regenerated: IR 3438 (M), 3103 (M), 3055 (M), 2968 (M), 2923 (M), 2861 (M), 2754 (M), 2698 (M), 2477 (M), 2437 (M), 2105 (W), 1808 (M), 1550 (S), 1432 (VS), 1418 (VS), 1365 (S), 1242 (S), 1195 (S), 1124 (M), 909 (M), 889 (S), 824 (S), 810 (S), 788 (M), 629 (W), 586 (M), 490 (W) cm^{-1}.

Mg/DOBDC, pristine: IR 3051 (M), 2962 (M), 2860 (M), 2750 (M), 2517 (M), 1812 (M), 1579 (VS), 1488 (S), 1460 (VS), 1446 (VS), 1431 (VS), 1373 (M), 1338 (W), 1238 (M), 1212 (S), 1161 (W), 1124(W), 1013 (VW), 911 (W), 895 (M), 830 (S), 822 (M), 632 (VW), 589 (W), 491 (W), 454 (VW) cm^{-1}.

Mg/DOBDC, hydrated: IR 3748 (M), 3680 (M), 3584 (M), 3435 (M), 3072 (W), 2926 (W), 2856 (W), 1588 (VS), 1457 (VS), 1430 (VS), 1374 (M), 1236 (M), 1216 (M), 1120 (W), 914 (W), 891 (W), 830 (M), 822 (M), 638 (VW), 587 (W), 498 (W) cm^{-1}.

Mg/DOBDC, regenerated: IR 3429 (W), 3052 (W), 2926 (W), 2856 (W), 1584 (S), 1457 (VS), 1448 (VS), 1431 (VS), 1374 (M), 1238 (M), 1212 (M), 1122 (W), 912 (W), 893 (W), 830 (M), 634 (VW), 591 (W), 489 (W) cm^{-1}.

2.8 References

(1) Chui, S. S.-Y.; Lo, S. M.-F.; Charmant, J. P. H.; Orpen, A. G.; Williams, I. D. *Science* **1999**, *283*, 1148-1150.

(2) Kondo, M.; Yoshitomi, T.; Matsuzaka, H.; Kitagawa, S.; Seki, K. **1997**, *36*, 1725-1727.

(3) Li, H.; Eddaoudi, M.; Groy, T. L.; Yaghi, O. M. *J. Am. Chem. Soc.* **1998**, *120*, 8571-8572.

(4) Li, H.; Eddaoudi, M.; O'Keeffe, M.; Yaghi, O. M. *Nature* **1999**, *402*, 276-279.

(5) Millward, A. R.; Yaghi, O. M. *J. Am. Chem. Soc.* **2005**, *127*, 17998-17999.

(6) Bordiga, S.; Regli, L.; Bonino, F.; Groppo, E.; Lamberti, C.; Xiao, B.; Wheatley, P. S.; Morris, R. E.; Zecchina, A. *Phys. Chem. Chem. Phys.* **2007**, *9*, 2676-2685.

(7) Liu, Y.; Kabbour, H.; Brown, C. M.; Neumann, D. A.; Ahn, C. C. *Langmuir* **2008**, *24*, 4772-4777.

(8) Rowsell, J. L. C.; Yaghi, O. M. *J. Am. Chem. Soc.* **2006**, *128*, 1304-1315.

(9) Inglezakis, V. J.; Poulopoulos, S. G. *Adsorption, Ion Exchange and Catalysis: Design of Operations and Environmental Applications*; Elsevier: Amsterdam ; Boston, 2006.

(10) Caskey, S. R.; Wong-Foy, A. G.; Matzger, A. J. *J. Am. Chem. Soc.* **2008**, *130*, 10870-10871.

(11) Rosi, N. L.; Kim, J.; Eddaoudi, M.; Chen, B.; O'Keeffe, M.; Yaghi, O. M. **2005**, *127*, 1504-1518.

(12) Dietzel, P. D. C.; Johnsen, R. E.; Blom, R.; Fjellvåg, H. *Chem.-Eur. J.* **2008**, *14*, 2389-2397.

(13) Dietzel, P. D. C.; Panella, B.; Hirscher, M.; Blom, R.; Fjellvåg, H. *Chem. Comm.* **2006**, 959-961.

(14) Dietzel, P. D. C.; Morita, Y.; Blom, R.; Fjellvåg, H. *Angew. Chem. Int. Ed.* **2005**, *44*, 6354-6358.

(15) Dietzel, P. D. C.; Besikiotis, V.; Blom, R. *J. Mater. Chem.* **2009**, *19*, 7362-7370.

(16) Dietzel, P. D. C.; Georgiev, P. A.; Eckert, J.; Blom, R.; Strässle, T.; Unruh, T. *Chem. Comm.* **2010**, *46*, 4962-4964.

(17) Walton, K. S.; Abney, M. B.; Douglas LeVan, M. **2006**, *91*, 78-84.

(18) Yazaydin, A. Ö.; Snurr, R. Q.; Park, T.-H.; Koh, K.; Liu, J.; LeVan, M. D.; Benin, A. I.; Jakubczak, P.; Lanuza, M.; Galloway, D. B.; Low, J. J.; Willis, R. R. *J. Am. Chem. Soc.* **2009**, *131*, 18198-18199.

(19) Liu, J.; Wang, Y.; Benin, A. I.; Jakubczak, P.; Willis, R. R.; LeVan, M. D. *Langmuir* **2010**, *26*, 14301-14307.

(20) Yazaydin, A. Ö.; Benin, A. I.; Faheem, S. A.; Jakubczak, P.; Low, J. J.; Willis, R. R.; Snurr, R. Q. *Chem. Mater.* **2009**, *21*, 1425-1430.

(21) Liang, Z.; Marshall, M.; Chaffee, A. L. *Energy Fuels* **2009**, *23*, 2785-2789.

(22) Granite, E. J.; Pennline, H. W. *Ind. Eng. Chem. Res.* **2002**, *41*, 5470-5476.

(23) Yang, R. T. *Gas separation by adsorption processes*; Imperial College Press ; distributed by World Scientific: London : Singapore ; River Edge, N.J., 1997.

(24) Czepirski, L.; JagieŁŁo, J. *J. Chem. Eng. Sci.* **1989**, *44*, 797-801.

(25) Britt, D.; Furukawa, H.; Wang, B.; Glover, T. G.; Yaghi, O. M. *Proc. Natl. Acad. Sci.* **2009**, *106*, 20637-20640.

(26) Saturated NaCl was utilized to maintain the humidity below 100%, thus reducing the probability of condensate formation in the gas lines of the apparatus.

(27) Hausdorf, S.; Baitalow, F.; Böhle, T.; Rafaja, D.; Mertens, F. O. R. L. *J. Am. Chem. Soc.* **2010**, *132*, 10978-10981.

(28) Feldblyum, J. I.; Liu, M.; Gidley, D. W.; Matzger, A. J. *J. Am. Chem. Soc.* **2011**, *133*, 18257-18263.

(29) Czepirski, L.; JagieLlo, J. *Chem. Eng. Sci.* **1989**, *44*, 797-801.

(30) Liu, J.; Wang, Y.; Benin, A. I.; Jakubczak, P.; Willis, R. R.; LeVan, M. D. *Langmuir* **2010**, *26*, 14301-14307.

(31) Rosi, N. L.; Kim, J.; Eddaoudi, M.; Chen, B.; O'Keeffe, M.; Yaghi, O. M. *J. Am. Chem. Soc* **2005**, *127*, 1504-1518.

(32) Felder, R. M.; Rousseau, R. W. *Elementary principles of chemical processes*; J. Wiley & Sons: New York, 2000.

Chapter 3

Design, Synthesis and Characterization of a Microporous Coordination Polymer Featuring Proximal Amines

3.1 Introduction

In Chapter 2, the effect of humidity on MCPs of the M/DOBDC series was evaluated, and in all cases was found to be detrimental to CO_2-capture performance after a single exposure. Utilization of any of these materials as CO_2-capture adsorbents for cyclical operations would necessitate the use of a guard bed containing another adsorbent dedicated to trapping H_2O from the flue gas stream. In a pilot plant, or a full-scale industrial operation, this would require a separate regeneration step to periodically remove H_2O from the guard bed, in addition to the periodic removal of CO_2 from the exhausted primary bed, thus leading to increased equipment and operation costs. To avoid these complexities, a CO_2 capture adsorbent should exhibit attributes of excellent stability in addition to superior CO_2 uptake at low partial pressures and ambient temperatures. Given that the M/DOBDC materials are currently regarded as the best MCPs for CO_2 capture, yet clearly not stable enough to meet the task, there remains a strong driving force for the development of new MCPs.

One strategy for improving CO_2-capture performance would be to generate a material with a higher density of coordinatively unsaturated metal sites. The presence of these sites is believed to be responsible for the superior performance of the M/DOBDC materials.[1] However a critical drawback to this approach is the ability of contaminants such as H_2O to bind these sites, and significantly diminish the material performance. As shown in Chapter 2, the M/DOBDC materials completely lose their capacity upon full hydration, even at low relatively humidities. Interestingly, Snurr and co-workers demonstrated that when HKUST-1 is intentionally poisoned with 4 wt% H_2O, which according to the authors[2] corresponds to half all coordinatively unsaturated metal sites

being subsequently occupied by H_2O, it exhibits higher CO_2 uptake in the low pressure region. It is not clear if this phenomenon is unique to HKUST-1 or general to all MCPs with coordinatively unsaturated metals centers, but in either case, the effect was demonstrated with dry CO_2. It is feasible that an MCP pre-treated with H_2O would likely adsorb additional H_2O to the pore surface via hydrogen-bonding under flue gas conditions, thus resulting in diminished capacity for CO_2 over time.

An alternative approach is to post-synthetically modify an MCP that exhibits superior hydrothermal stability with functional groups that have strong affinity for CO_2, thus generating a new material that possesses both of these critical attributes. Post-synthetic modification of MCPs has been used by Cohen[3] and others[4-7] to introduce functional groups that could not otherwise be incorporated into the material. A common approach to deploying post-synthetic modification is to generate an MCP with a linker bearing a reactive functional group. The MCP is then treated with a modifier that reacts with the linker-bound functional group to incorporate the desired functionality into the material. The drawback to this approach is that the presence of the reactive functionalities on the starting linker can interfere with the formation of the MCP, and/or participate in side reactions that generate undesirable impurities. A second approach, illustrated in Figure 3.1, is to utilize an MCP with coordination sites that are occupied by solvent molecules; upon thermal activation, removal of the solvent molecules yields coordinatively unsaturated metal sites, onto which modifiers can be appended.

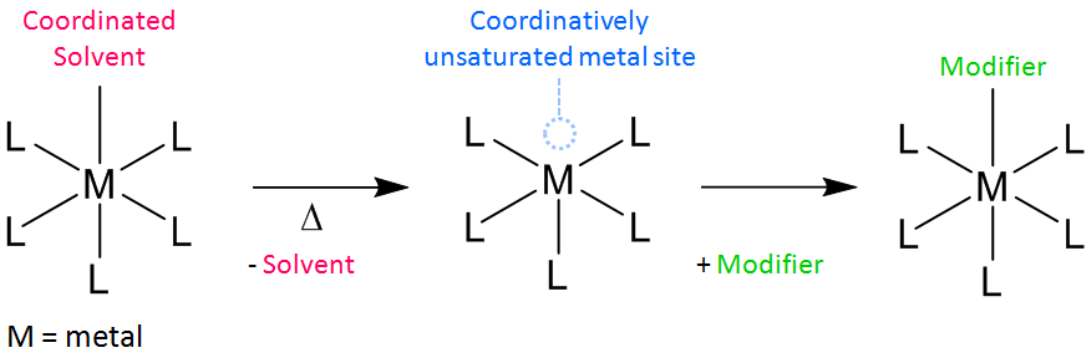

Figure 3.1. Utilization of coordinatively unsaturated metal sites for post-synthetic modification of an MCP.

With regards to CO_2-capture, selection of an MCP with superior hydrothermal stability is a logical starting point, because an ideal CO_2-capture adsorbent should be amenable to cyclical operation in flue gas, which is humid, with minimal degradation. The MCPs of the MIL-100(M) series (where M = Cr,[8,9] Fe,[9] Al[10]) have been demonstrated to possess superior hydrothermal stabilities.[11,12] In particular, MIL-100(Al) is an attractive candidate for CO_2-capture, because it is constructed from a light, abundant metal, the linker is readily available, and unlike the Cr and F analogs, the preparation does not require the use of HF, a highly toxic reagent. The structure is built up from 1,3,5-benzenetricarboxylate linkers that connect trigonal oxo-centered metal clusters (Figure 3.2) to form cages of about 10, 21, and 31 Å in diameter (Figure 3.3). The metal cluster features three AlO_6 octahedra that share an O atom as a common vertex, and are bridged by 1,3,5-benzenetricarboxylate linkers whose O atoms occupy the four equatorial sites of the octahedra. The remaining axial sites of two octahedra are occupied by coordinating solvent molecules such as H_2O; these sites become coordinatively unsaturated upon thermal activation, and can be utilized for post-synthetic modification. An axial site on a third AlO_6 octahedron is occupied by a charge balancing OH^-.

Given that the modifier should exhibit high affinity for CO_2, amines are logical candidates for this role. Studies by Long and co-workers have shown post-synthetically modifying the MCP Cu-BTTri (BTTri = benzene-1,3,5-tris(triazolate)) with ethylenediamine[6] and N,N'-dimethylethylenediamine[7] lead to enhanced CO_2 uptakes in the low partial pressure (0.1 atm) regime. Cu-BTTri features open metal sites, which after modification with ethylenediamine or N,N'-dimethylethylenediamine are presumably occupied by one coordinated amine, leaving the free amine to interact with CO_2 in the pore. The authors explain that the enhanced CO_2 sorption behavior is a result of the free amine attacking CO_2 to produce a carbamate or carbamic acid. However, the currently accepted mechanism of amine-based CO_2 capture engages two amines per CO_2; therefore isolated amines cannot participate in any chemical interaction with CO_2, and improved uptakes are likely due to enhanced polarization of CO_2.

The ideal amine should have a branched structure, wherein one amine can coordinate to available open metal sites, and at least two free amines in relatively close proximity are available for reacting with CO_2. The alkylamine tris(2-aminoethyl)amine

(tren, Figure 3.4) meets this criterion, thus modification of MIL-100(Al) with tren was conceived as a route to generating a new MCP with good stability and high affinity for CO_2.

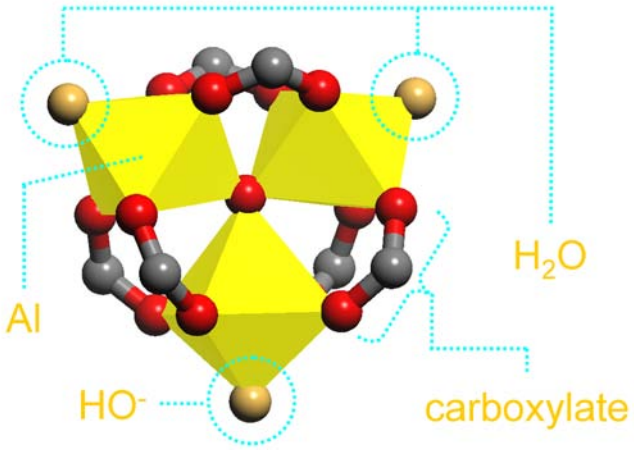

Figure 3.2. Trigonal Al_3O cluster in MIL-100(Al). Note that removal of coordinated H_2O generates coordinatively unsaturated metal sites.

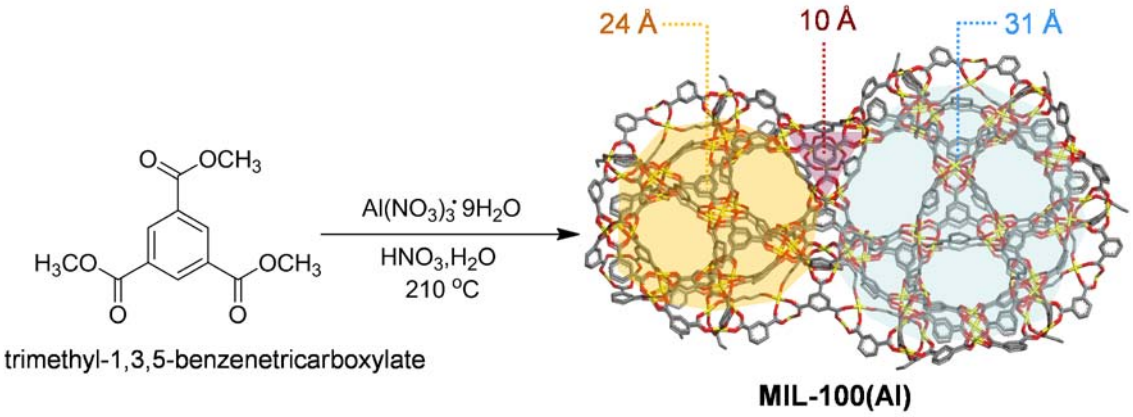

Figure 3.3. Synthesis and structure of MIL-100(Al) with cages sizes shown.

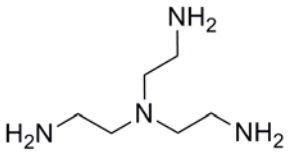

Figure 3.4 Tris(2-aminoethyl)amine, tren.

3.2 Tren@MIL-100(Al)

In order to generate the target amine-modified MCP, MIL-100(Al) was synthesized and activated, then treated with a refluxing solution of toluene and excess tren (see Experimental), followed by washing in hexanes. Powder X-ray diffraction (Figure 3.5) confirms the retention of the MIL-100 structure after treatment with tren. Thermogravimetric analysis of a control sample indicated that solvent loss was essentially completed by 150 °C, thus evacuation of the as-synthesized material was performed at this temperature to afford tren-modified MIL-100(Al), referred to hereafter as tren@MIL-100(Al). Incorporation of tren was verified by IR spectroscopy; an overlay of the spectra of MIL-100(Al) and tren@MIL-100(Al) in the 4000 cm^{-1} to 2400 cm^{-1} region (Figure 3.6) reveals three new peaks between 3317 cm^{-1} and 3145 cm^{-1}, corresponding to N-H stretches, and a new band at 2945 cm^{-1}, corresponding to the aliphatic C-H stretches associated with tren.

Digestion of the tren@MIL-100(Al) sample in $NaOH/D_2O$ and subsequent ^1H NMR spectral analysis also confirmed the incorporation of tren, as evidenced by overlays of ^1H NMR spectra of tren, the control, and digested tren@MIL-100(Al) (Figure 3.7). A sample of 1,3,5-benzenetricarboxylic acid was also digested in $NaOH/D_2O$, and the aryl region of the 1H NMR spectrum of the sample was compared to that of the control, and digested tren@MIL-100(Al) (Figure 3.8), thus confirming the identity of the linker. The absence of obscuring peaks in the control permits straightforward determination of tren loading. The ratio of the peak integrals for the methylene protons of tren and those of the aryl protons for the linker 1,3,5-benzenetricarboxylate were used to determine the molar ratio between tren and the linker, which was found to be 0.98 tren per linker; based on the empirical formula for the desolvated MIL-100(Al) (see Experimental section), this corresponds to, on average, about 2 trens per metal cluster.

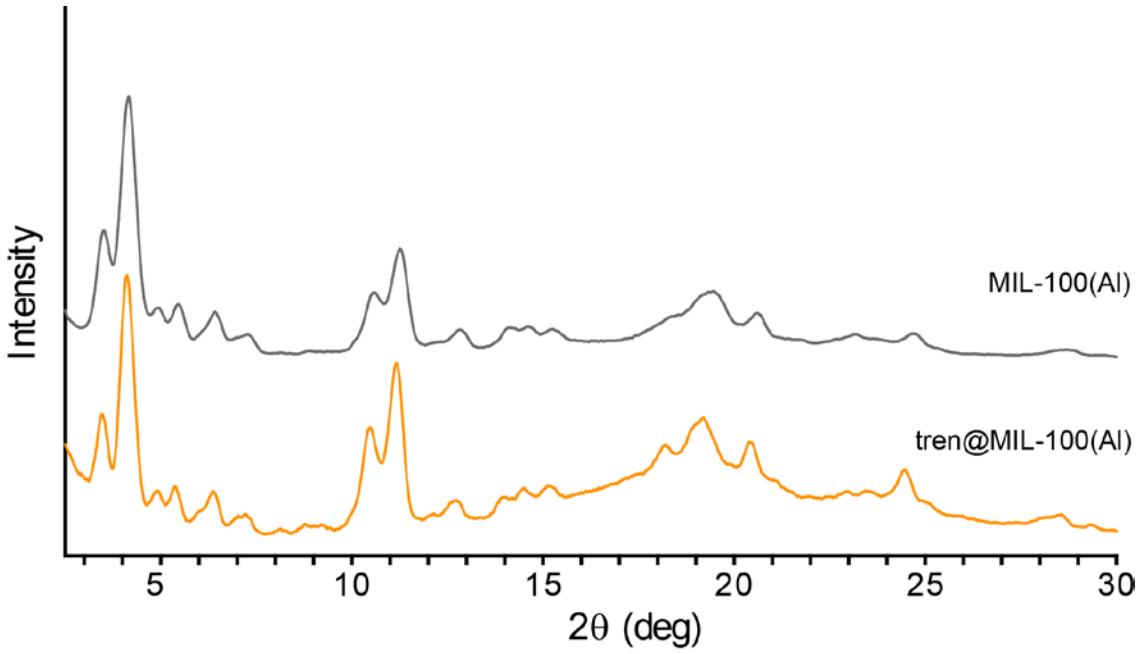

Figure 3.5. Powder X-ray diffraction patterns of MIL-100(Al) and tren@MIL-100(Al).

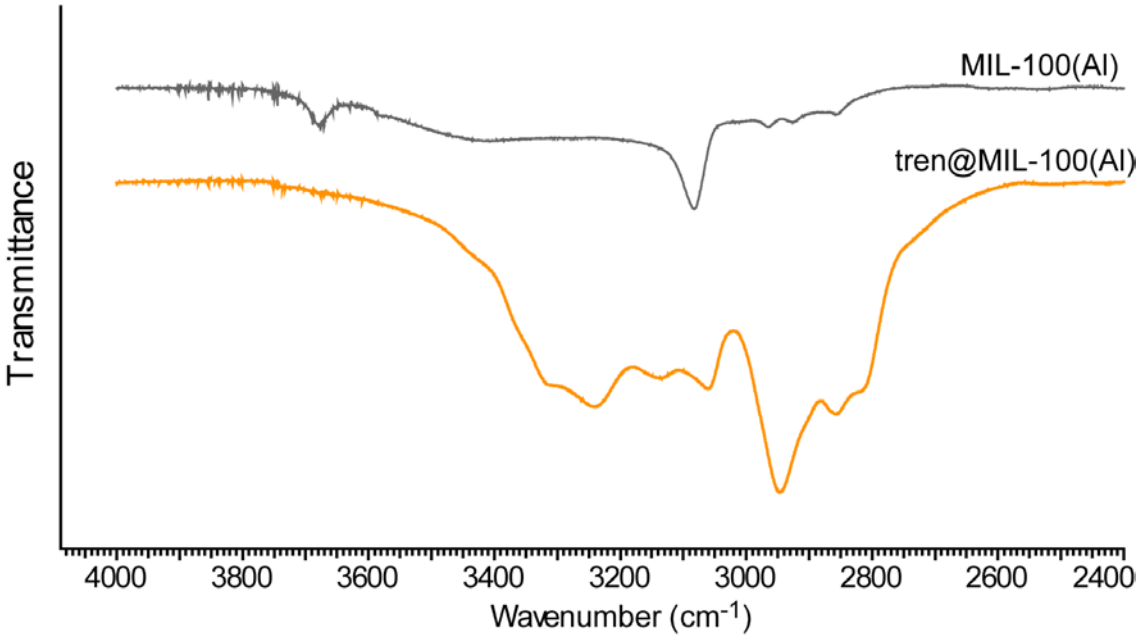

Figure 3.6. IR spectra of a) activated MIL-100(Al), b) activated tren@MIL-100(Al).

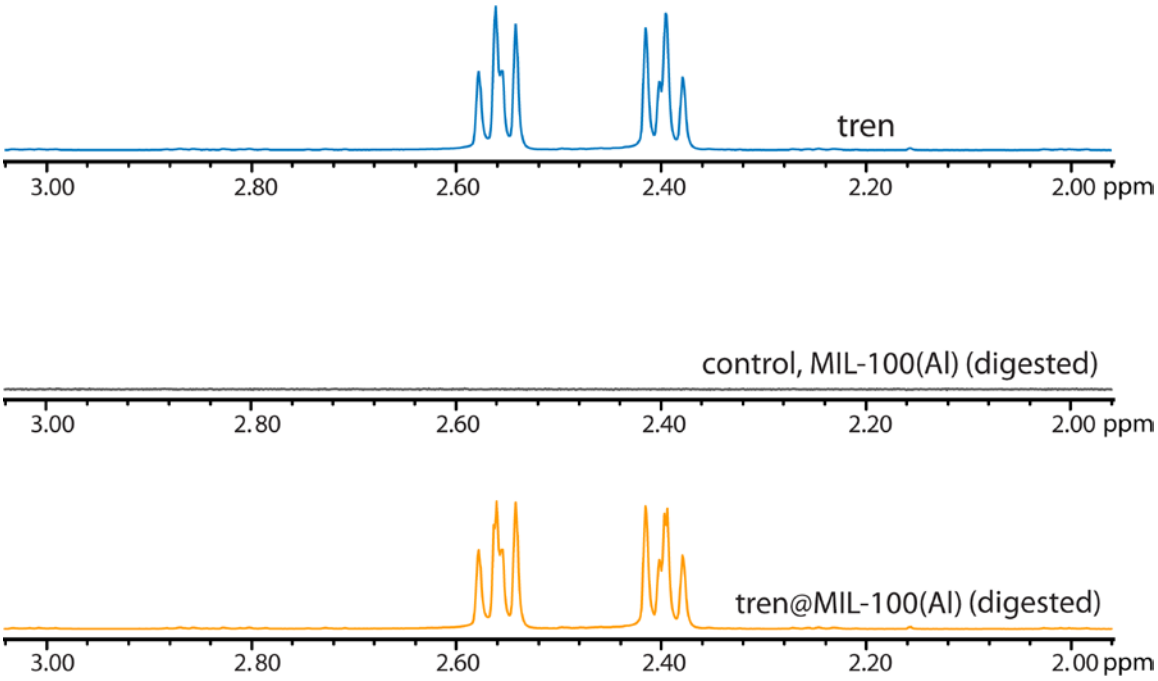

Figure 3.7. ^{1}H NMR spectra of tren, MIL-100(Al) (control), and tren@MIL-100(Al) in $NaOH/D_2O$.

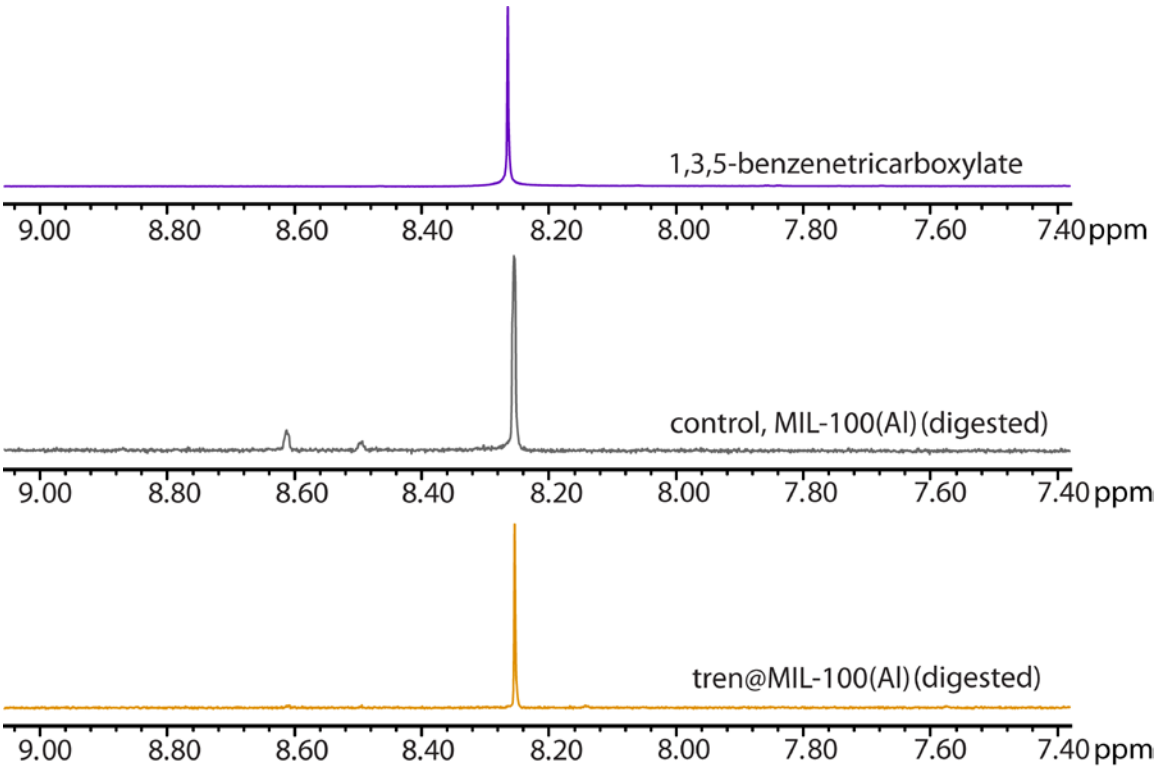

Figure 3.8. ^{1}H NMR spectra of 1,3,5-benzenetricarboxylate, MIL-100(Al) (control), and tren@MIL-100(Al) in NaOH/D_2O.

In order to investigate the potential for tren@MIL-100(Al) to serve as an adsorbent for CO_2-capture, CO_2 sorption isotherms of pristine MIL-100(Al) and tren@MIL-100(Al) were measured at 25 °C. As shown in Figure 3.9, the uptakes in the low pressure region are significantly higher in tren@MIL-100(Al) indicating strong interaction with CO_2. The CO_2-capture performance of the material was also investigated under flow-through conditions; dry 5/1 N_2/CO_2 gas breakthrough experiments were performed on a packed column of the material, and CO_2 capacity was determined to be 9 wt% CO_2. Such performance represents a nearly 6-fold improvement in performance over the unmodified MIL-100(Al) under the same conditions. In fact, tren@MIL-100(Al) competes with the M/DOBDC materials, surpassing Zn/DOBDC in CO_2-capture performance (Figure 3.10).

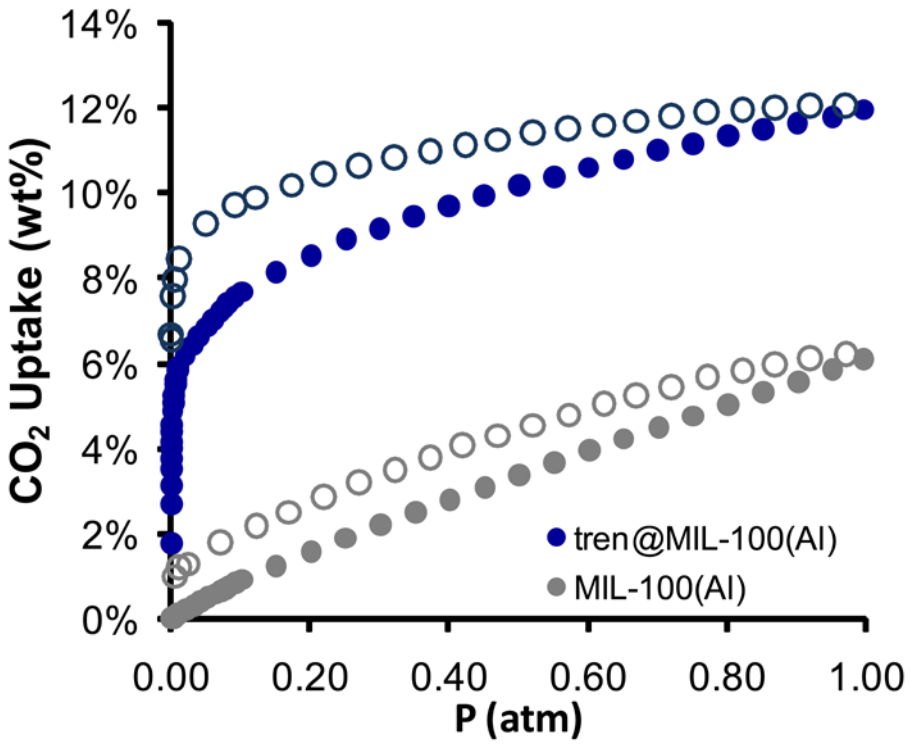

Figure 3.9. CO_2 sorption isotherms for MIL-100(Al), and tren@MIL-100(Al) measured at 25 °C. Filled and open markers represent adsorption and desorption points, respectively.

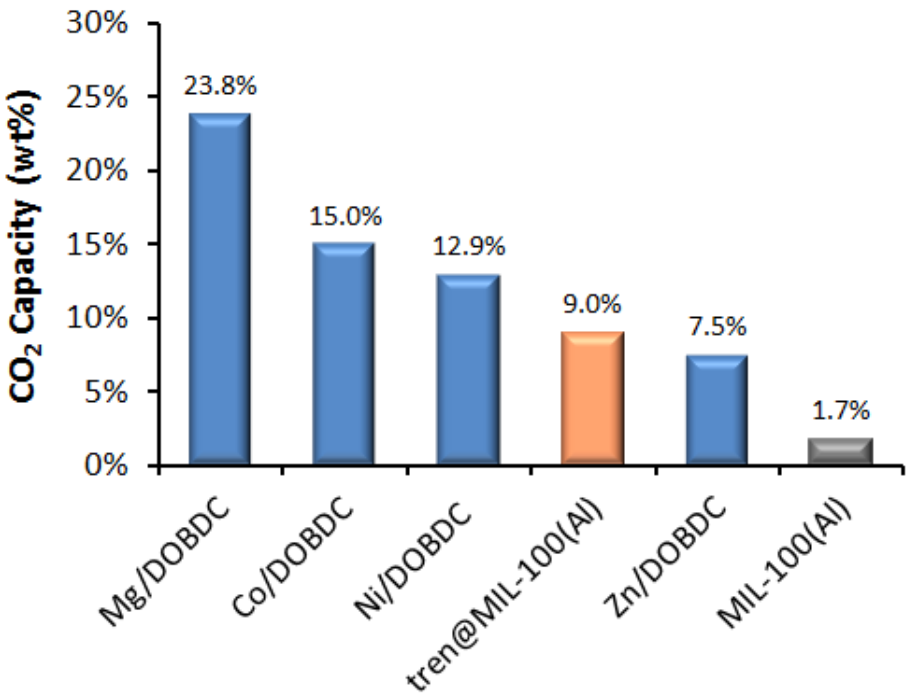

Figure 3.10. Comparison between CO_2 capacities of MIL-100(Al), tren@MIL-100(Al) and M/DOBDC materials in 5/1 N_2/CO_2 at ambient temperature.

To study the recyclability of tren@MIL-100(Al), regeneration of the material was attempted at ambient temperature with flowing Ar, but only 3.8 wt% of the CO_2 was removed. Thermal desorption at 85 °C, 100 °C, and 135 °C, was performed resulting in release of additional CO_2, but the full capacity could not be recovered. In fact over several cycles of N_2/CO_2 breakthrough and subsequent thermal desorption, the capacity of the material actually diminished (Figure 3.11). The IR spectrum of the spent material after CO_2 breakthrough was compared with that of the pristine material (Figure 3.12), and exhibited the N-H stretches associated with tren, indicating that the material had retained the amine during cyclical operation. The mechanism of capacity degradation is not clear at this point, but a physisorptive-based mechanism seems unlikely. For a physisorptive process, the adsorbate loading drastically diminishes as the temperature of the adsorbent is increased. Thus even a strong physisorbent will retain less adsorbate after regeneration at higher temperatures, resulting in a higher capacity in the subsequent gas sorption step. This is not observed with tren@MIL-100(Al), since the capacity diminishes over time.

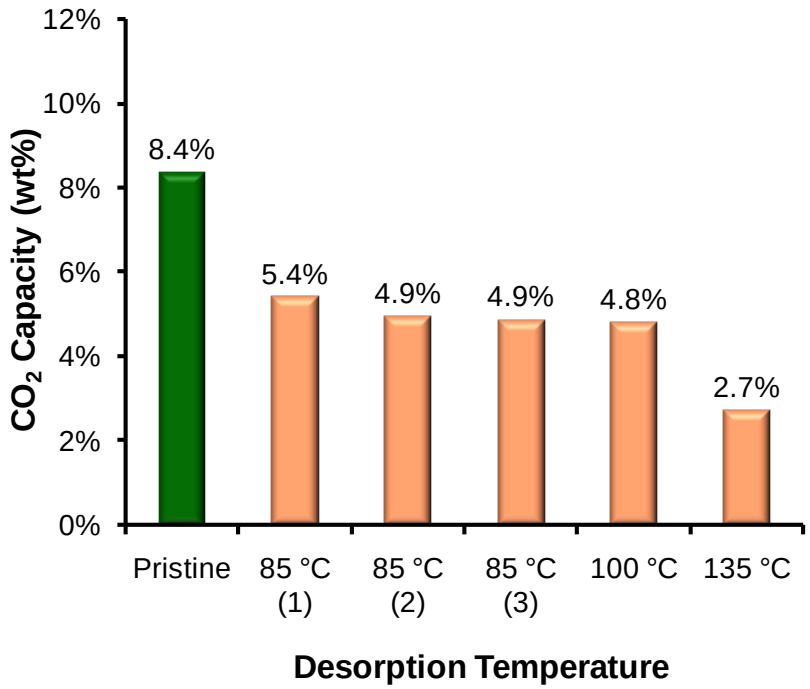

Figure 3.11. Capacities for a sample of tren@MIL-100(Al) as a function of desorption temperature, prior to the subsequent CO_2 breakthrough.

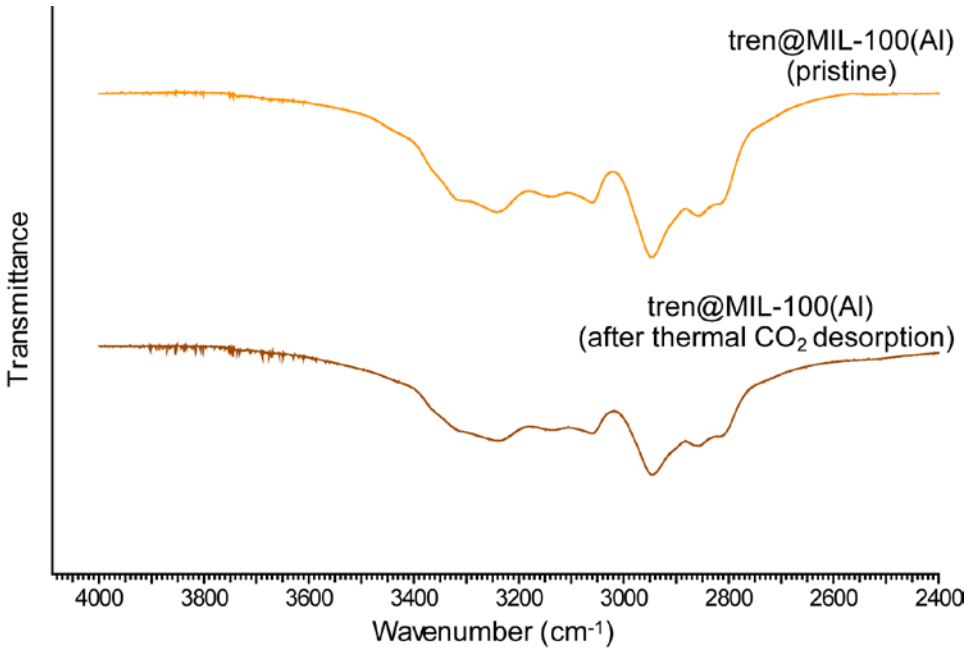

Figure 3.12. IR spectra of pristine tren@MIL-100(Al), and tren@MIL-100(Al) after several cycles of CO_2 breakthrough and thermal desorption.

The performance of tren@MIL-100(Al) was also investigated under humid conditions. A packed column of the material was treated with humidified N_2 at about 71% RH until H_2O breakthrough was observed to ensure that the entire bed was hydrated. The material was then exposed to humidified 5/1 N_2/CO_2, and the CO_2 capacity was determined from the corresponding breakthrough curve. The material exhibited a capacity of 3.7 wt%. This value is clearly far lower than the capacity of the pristine material under dry conditions; however, it represents an improvement over the M/DOBDC materials, which do not exhibit any capacity for CO_2 after hydration.

3.3 Conclusions

Post-synthetic modification, a powerful tool for imparting existing MCPs with enhanced functionality, was utilized to generate a new material designed for CO_2-capture. The MCP MIL-100(Al) was modified with a branched amine, tren, resulting in a new MCP, tren@MIL-100, with an exceptionally high CO_2-capacity of 8.4 wt% in dry 5/1 N_2/CO_2, thus competing with M/DOBDC materials. The performance of the material was found to degrade under cyclical operation under dry conditions. Retention of tren was confirmed by IR spectroscopy, and the performance degradation is potentially due to the formation of a highly stable adduct between the material and CO_2. Further examination of this phenomenon may be critical to determining the optimal activation protocol. The performance of tren@MIL-100(Al) was also examined under humid conditions (N_2/CO_2, 71% RH), and the capacity (3.7 wt%) was diminished when compared with that of the pristine material under dry conditions. Although the performance was diminished, the fact that the material retains capacity for CO_2 is in stark contrast to the M/DOBDC materials, which exhibit no capacity for CO_2 when fully hydrated under these conditions. Data obtained thus far in this study, demonstrates that amine-modification of hydrothermally stable MCPs is an advantageous route to producing high-performance materials for capture-dioxide capture.

3.4 Experimental

3.4.1 Syntheses

Unless otherwise noted, all reagents were used as received. 1,3,5-benzenetricarboxylic acid was purchased from TCI. $Al(NO_3)_3 \cdot 9H_2O$ was purchased from Aldrich. Hydrochloric acid, N,N-dimethylformamide (DMF), methanol and hexanes were purchased from Fisher. Toluene was purchased from Fisher, and dried over a column of activated alumina before use. Tris(2-aminoethyl)amine (tren), was purchased from Acros. House deionized H_2O was used.

Although commercially available, trimethyl-1,3,5-benzenetricarboxylate can be readily synthesized via esterification of 1,3,5-benzenetricarboxylic acid.[13]

MIL-100(Al) was synthesized via modification of a literature preparation.[10] To a 45-mL Teflon cup, was added $Al(NO_3)_3 \cdot 9H_2O$ (1.64 g, 4.37 mmol), trimethyl-1,3,5-benzenetricarboxylate (0.74 g, 2.94 mmol), and H_2O (20 mL). The resulting suspension was vigorously stirred and 1M aqueous HCl (5.5 mL) was added. The resulting suspension was sealed inside of a Parr vessel, then placed into an oven pre-heated at 210 °C for 3.5 hours, and then removed and allowed to cool to room temperature. The resulting suspension was centrifuged; after decanting the supernatant, the solid product was washed and centrifuged in H_2O (3 × 25 mL), with decantation of the supernatant between each wash. The solid was then suspended in DMF, and transferred to a Teflon-lined parr vessel, and was heated at 150 °C for 4 hours. After cooling to room temperature, the material was washed and centrifuged in H_2O (3 × 25 mL), with decantation of the supernatant between each wash. Afterwards, the solid material was suspended in 25 mL of 1/1 CH_3OH/H_2O, and transferred to a Teflon-lined parr vessel, and heated at 100 °C for 12 hours. The sample was removed from the oven, and allowed to cool to room temperature. The resulting suspension was centrifuged, and the supernatant was decanted. The solid product was washed in CH_3OH, and centrifuged. After decantation of the supernatant, the solid product was dried under vacuum at room temperature for approximately 6 hours. The resulting powder was loaded into a glass ampoule, which was evacuated and heated to 220 °C for approximately 16 hours. After

cooling, the material was transferred to a N_2 glovebox, for storage and subsequent analysis. The powder X-ray diffraction pattern was consistent with the MIL-100 structure. Surface area of the activated material was determined by applying the BET adsorption model to the N_2 sorption isotherm measured at 77 K, and was 1980 m^2/g; Ferey and co-workers report a surface area of 2100 m^2/g.[10]

Tren@MIL-100(Al) was synthesized by charging a 50-mL oven-dried N_2-purged round-bottom schlenk flask, equipped with an oven-dried stir bar, with anhydrous toluene (10 mL) and tris(2-aminoethyl)amine (1.25 mL, 1.28 g, 8.76 mmol). N_2 was bubbled through the resulting solution for 10 ~ 15 minutes, then activated MIL-100(Al) (0.44 g, 0.82 mmol) was added to the solution under flow N_2, and the resulting mixture was heated to reflux for ~ 12 hours. After cooling, the resulting suspension was diluted with hexanes and centrifuged. The solid product was washed/centrifuged with hexanes (3 × 20 mL), with decantation of the supernatant between washings. The solid was dried under vacuum at room temperature, then loaded into a glass ampoule and evacuated at 150 °C for ~ 14 hours. After cooling, the sample was transferred to a N_2 glovebox for storage.

3.4.2 Amine Content Determination

Samples of tren, 1,3,5-benzenetricarboxylic acid, tren@MIL-100(Al), and the control (reactivated MIL-100(Al) previously treated with refluxing toluene) were digested in a solution of NaOH (4 wt%) in D_2O. ^1H NMR spectra of the digested samples were obtained on a Varian MR400. Spectra of tren and 1,3,5-benzenetricarboxylate were used to guide the peak assignments, and integration for digested tren@MIL-100(Al).

The linker contains aryl protons, which are known to have relaxation rates that differ from those aliphatic protons found in species such as tren. Consequently, if the spectrometer relaxation delay time is too short, the intensity of the signal derived from the aryl protons will be lower, thus giving rise to erroneous peak integrals. To address this, the ^1H NMR spectrum was obtained for a mixture of 1,3,5-benzenetricarboxylic (2.4 mg, 0.12 mmol) and tren (1.7μL, 0.11 mmol) dissolved in 2.0 mL of NaOH (4 wt%) in D_2O. The peak integrals were calculated as a function of the incrementally increased relaxation delay time (0.5 sec, 5 sec, 10 sec, and 15 sec) until minimal change was

observed. Virtually no change was observed in the peak integrations obtained at 10 sec and 15 sec, thus a relaxation delay time of 10 sec was utilized for the digested sample of tren@MIL-100(Al).

A sample of tren@MIL-100(Al) (2 mg) was digested in a solution of NaOH (4 wt%) in D_2O (2.0 mL). Quantification of tren loading was based on the stoichiometric relation that for every molecule of 1,3,5-benzenetricarboxylate, there are 3 aryl protons, and for every molecule of tren there are 12 methylene protons. For tren, the methylene protons were identified by two quartets with an integration ratio of 1/1; the integral for the quartet located between 2.38 ppm and 2.42 ppm was assigned an integral of 6.00, which served as the basis for subsequent integrals in the spectrum. The molar ratio of tren to linker in the digested tren@MIL-100(Al) sample is equal to the ratio of total integral of methylene protons/12 and the total integral of the aromatic 1,3,5-benzenetricarboxylate protons/3. Given the empirical formula for MIL-100(Al) is $Al_3O(OH)(BTC)_3$, the formula for tren@MIL-100(Al) must be $Al_3O(OH)(BTC)_2(tren)_x$, where x is the number of tren molecules per formula unit. For the digested sample of tren@MIL-100(Al), the ratio of tren to BTC was determined to be 0.98/1, therefore $x \approx 2$.

3.4.3 Powder X-ray Diffraction

Samples of material were coated in mineral oil, then loaded onto a Nylon loop and mounted onto a Rigaku R-axis Spider diffractometer. Images were collected in transmission mode with χ set at 45°, φ rotating at 10°/min and ω oscillating between 80° and 140° at 1 °/min. Background-subtraction and integration of the resulting images was performed in the AreaMax (version 2.3.8., Rigaku 2008) software package.

3.4.4 Gas Sorption

Gas sorption isotherms were measured with an Autosorb-1C (volumetric method) outfitted with the micropore option by Quantachrome Instruments (Boynton Beach, Florida, USA) running version 1.55 of the ASWin software package. CO_2 isotherms were

measured at 298 K in the range 1.00 x 10^{-4} atm ≤ P < 1.00 atm using bone dry CO_2. N_2 isotherms were measured at 77 K in the range 1.00 x 10^{-5} atm ≤ P/P_0 < 1.00 atm using ultra-high purity N_2 (99.999%).

3.4.5 Gas Breakthrough Experiments

N_2/CO_2 and $N_2/CO_2/H_2O$ breakthrough curves were acquired using a gas-flow apparatus designed and constructed in-house. Flow rates of N_2 (ultra-high purity, 99.999%), Ar (pre-purified, 99.998%), and CO_2 (bone dry) were controlled using Aalborg model GFC17 mass flow controllers. Samples of MIL-100 materials were loaded into columns under N_2, then installed onto the gas-flow apparatus with Ar flowing. For N_2/CO_2 breakthrough experiments, 95 ~ 100 mg of material was used; for $N_2/CO_2/H_2O$ breakthrough experiments ~ 50 mg samples were used. Each sample column was first purged with Ar, then treated with dry or humid N_2/CO_2; column effluent was analyzed using a Hiden Analytical model HPR20 mass spectrometer. See the experimental section of Chapter 2 for details regarding the determination of capacities from CO_2 breakthrough curves.

3.4.6 IR Spectroscopy

FT-IR spectra of activated MIL-100(Al), pristine and spent tren@MIL-100(Al) materials were obtained by via KBr disk. The salt was dried under vacuum at 200 °C for ~ 16 hours, and stored in a N_2 glovebox. Samples of material (~1 mg) were ground with 500 mg of KBr under N_2 atmosphere. About 150 mg of the mixture was transferred to a die kit and pressed into a pellet. Spectra of the pellets were obtained using a Nicolet Avatar 360 spectrometer pre-purged with N_2. Peak listings are provided below:

MIL-100(Al): IR 3670 (VW), 3082 (W), 2965 (VW), 2923 (VW), 2856 (VW), 1673 (S), 1626 (S), 1579 (M), 1551 (M), 1466 (S), 1402 (VS), 1345 (M), 1203 (VW), 1118 (VW),

1029 (VW), 945 (VW), 837 (W), 788 (M), 770 (S), 724 (S), 692 (M), 559 (M), 485 (M), 419 (M) cm^{-1}.

tren@MIL-100(Al): IR 3318 (W), 3242 (W), 3145 (W), 3062 (W), 2946 (M), 2856 (W), 2820 (W), 1674 (VS), 1646 (S), 1592 (S), 1465 (VS), 1403 (VS), 1353 (M), 1192 (VW), 1115 (VW), 1042 (W), 938 (VW), 770 (S), 731 (S), 687 (S), 537 (M), 484 (W), 422 (M) cm^{-1}.

3.5 References

(1) Yazaydin, A. Ö.; Snurr, R. Q.; Park, T.-H.; Koh, K.; Liu, J.; LeVan, M. D.; Benin, A. I.; Jakubczak, P.; Lanuza, M.; Galloway, D. B.; Low, J. J.; Willis, R. R. *J. Am. Chem. Soc.* **2009**, *131*, 18198-18199.

(2) Yazaydin, A. Ö.; Benin, A. I.; Faheem, S. A.; Jakubczak, P.; Low, J. J.; Willis, R. R.; Snurr, R. Q. *Chem. Mater.* **2009**, *21*, 1425-1430.

(3) Cohen, S. M. *Chem. Rev.* **2012**, *112*, 970-1000.

(4) Hwang, Y. K.; Hong, D.-Y.; Chang, J.-S.; Jhung, S. H.; Seo, Y.-K.; Kim, J.; Vimont, A.; Daturi, M.; Serre, C.; Férey, G. *Angew. Chem. Int. Ed.* **2008**, *47*, 4144-4148.

(5) Morris, W.; Doonan, C. J.; Furukawa, H.; Banerjee, R.; Yaghi, O. M. *J. Am. Chem. Soc.* **2008**, *130*, 12626-12627.

(6) Demessence, A.; D'Alessandro, D. M.; Foo, M. L.; Long, J. R. *J. Am. Chem. Soc.* **2009**, *131*, 8784-8786.

(7) McDonald, T. M.; D'Alessandro, D. M.; Krishna, R.; Long, J. R. *Chem. Sci.* **2011**, *2*, 2022-2028.

(8) Férey, G.; Serre, C.; Mellot-Draznieks, C.; Millange, F.; Surblé, S.; Dutour, J.; Margiolaki, I. *Angewandte Chemie* **2004**, *116*, 6456-6461.

(9) Llewellyn, P. L.; Bourrelly, S.; Serre, C.; Vimont, A.; Daturi, M.; Hamon, L.; De Weireld, G.; Chang, J.-S.; Hong, D.-Y.; Kyu Hwang, Y.; Hwa Jhung, S.; FeÌ□rey, G. r. *Langmuir* **2008**, *24*, 7245-7250.

(10) Volkringer, C.; Popov, D.; Loiseau, T.; FeÌrey, G. r.; Burghammer, M.; Riekel, C.; Haouas, M.; Taulelle, F. *Chem. Mater.* **2009**, *21*, 5695-5697.

(11) Seo, Y.-K.; Yoon, J. W.; Lee, J. S.; Hwang, Y. K.; Jun, C.-H.; Chang, J.-S.; Wuttke, S.; Bazin, P.; Vimont, A.; Daturi, M.; Bourrelly, S.; Llewellyn, P. L.; Horcajada, P.; Serre, C.; Férey, G. *Adv. Mater.* **2011**, *24*, 806-810.

(12) Jeremias, F.; Khutia, A.; Henninger, S. K.; Janiak, C. *J. Mater. Chem.* **2012**.

(13) Castaldi, M. P.; Gibson, S. E.; Rudd, M.; White, A. J. P. *Chem.- Eur. J.* **2006**, *12*, 138-148.

Chapter 4

Synthesis and Characterization of a Microporous Coordination Polymer Derived From a Beta-Diketonate Linker

4.1 Introduction

As demonstrated in Chapters 3, post-synthetic modification can be utilized to generate new materials with enhanced performance. Although the challenge of optimizing regeneration conditions remains, the post-synthetic modification of a hydrothermally stable MCP with proximal alkylamines appears to be a viable approach to generating MCPs with exceptionally high CO_2 uptake and superior structural stability in the presence of moisture. MCPs such as the MIL-100 materials,[1,2] MIL-101(Cr)[3] and UiO-66[4] have been shown to reversibly adsorb and desorb H_2O, with retention of structure and porosity. An underlying commonality in these materials is favorable combination of the hard basicity of the carboxylate and the hard acidity of highly charged cations such as Cr^{3+} and Zr^{4+}. This appears to be an effective approach in attaining MCPs with enhanced stability; however, a limitation to this approach is that it excludes soft metal cations, and thus narrows the scope of possible MCPs that would otherwise be attained.

The development of non-carboxylate linkers has been explored as an alternative route to generating MCPs of enhanced stability. Non-carboxylate MCPs have been synthesized from imidazolates;[5,6] in particular Zn(imidazolate)$_2$ (also referred to as ZIF-8) has been touted as being chemically robust.[5] However, there have been studies indicating that this material undergoes structural change after exposure to H_2O.[7,8] In addition, the non-linear coordination geometry of the imidazole unit inhibits facile design and synthesis and new linkers. The stability of MCPs synthesized from tetrazolates,[9,10] and triazolates[11] have also been studied via PXRD, but as previously shown in Chapter 2, this alone is not a good indicator of retention of sorption performance.

Interestingly ligands of the β-diketonate class have seen relatively little attention with regards to MCP synthesis. Crystalline coordination polymers have been synthesized with linkers that utilize beta-diketonate functionalities as kinetically inert linkages attached to more labile benzonitrile,[12] nitrile,[13] and pyridyl units.[14-18] The lability of these neutral N-donor coordinating functionalities presumably allows enough reversible metal-ligand binding to obtain materials that are crystalline, while also incorporating kinetically inert β-diketonate unit. However gas sorption data for these systems have yet to be reported, possibly because of the presence of charge-balancing counter-ions residing in the pores, or structural collapse, which in either case would impart the materials with low porosity, or non-porosity. An approach to mitigate these potential occurrences is to use ligand/metal combinations that result in a net neutral charge on the coordination polymer. In addition, linkers utilizing neutral N donor ligands as coordinating functionalities have been known to yield materials of low structural integrity,[19] and are typically avoided at the outset of any attempt to make rationally conceived coordination polymers that exhibit porosity by gas sorption.

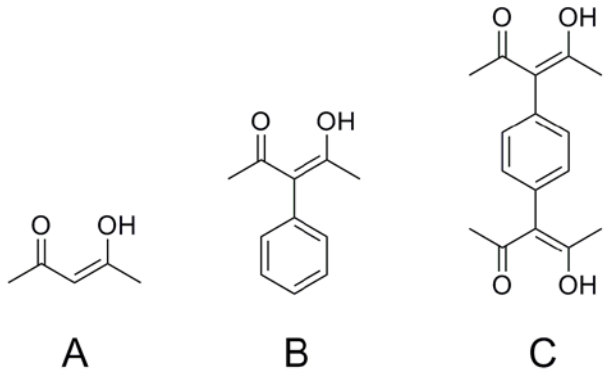

Figure 4.1. β-diketone moieties: a) Acetylacetone, b) 3-phenylacetylacetone (Ph-acac), c) Ditopic linker H_2BAB (BAB = 1,4-bis(3'-acetylacetonylate)benzene)

Utilization of linkers that rely exclusively on β-diketonates as chelating coordinating functionalities may offer a route to structurally and chemically stable MCPs with relatively high porosity. It has been previously been suggested that the utilization of linkers based exclusively on chelating ligands could yield coordination polymers with exceptional chemical stability.[20] Utilization of acetylacetone (Figure 4.1) presents an

appealing route to testing this hypothesis, due to the relatively high stability of its metal complexes in aqueous media.[21,22]

An added advantage of the chelating coordination mode is that only a single metal atom is needed to generate a secondary building unit. With regards to MCPs, a secondary building unit[19] can be conceptualized as the geometric unit spatially defined by the coordination functionality of the linker and its bonds with the metal(s). The chelating coordination mode is in stark contrast to the bridging coordination mode typically found in many carboxylate MCPs, wherein the carboxylates straddle two or more metal atoms in clusters such as the $Cr_3O(CO_2)_6X_3$ cluster found in MIL-101(Cr) and the $Zr_6O_8(CO_2)_{12}$ found in UiO-66 (Figure 4.2).

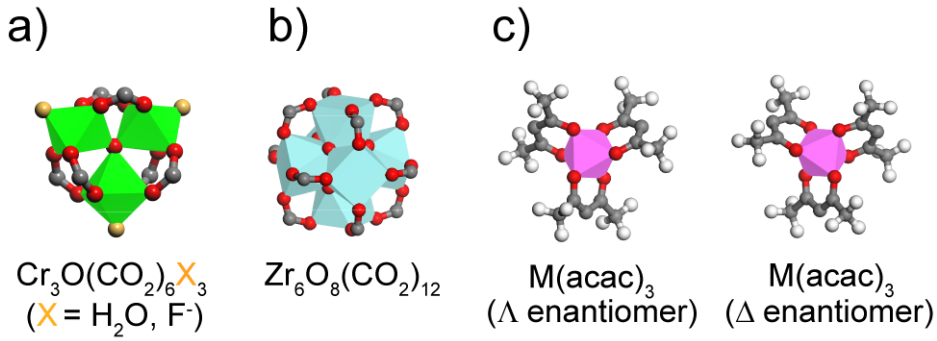

Figure 4.2. Metal clusters in the MCPs of a) MIL-100 and b) UiO-66 that feature the carboxylate coordination functionalities in bridging coordination mode. This is in contrast with c), where the chelating coordination mode, found in octahedral metal complexes of acetylacetonate, utilizes only a single metal atom to generate a secondary building unit.

A computational study by Schnobrich et al.[23] showed that reduction in the weight of the secondary building unit is beneficial in improving MCP surface area, which is typically measured in the gravimetric units of m^2/g. Although the pursuit of high surface area is not an effective approach to designing MCPs for CO_2-capture, the lesson from this study is that the mass contribution of the secondary building unit should be minimized for sorption applications where mass is a basis for measuring performance. Because gravimetric CO_2 capacity (g CO_2/g sorbent) is the typical measure of CO_2-capture

performance, a reduction in the mass of the secondary building unit via concomitant decrease in the contribution of the metal atoms is beneficial.

With regards to the acetylacetonate unit, 1D[24-26] and 2D[25] coordination polymers have been reported, but at present the aforementioned design principles have yet to be executed to generate MCPs, with porosity evidenced by gas sorption, from linkers exclusively bearing acetylacetonate as the coordination functionality, thus prompting the present study.

It has previously been demonstrated by Robson and co-workers that the use of rigid, multitopic organic ligands can be used to generate coordination polymers with exceptional porosity, as evidenced by X-ray diffraction.[27,28] Although this approach does not guarantee that the resulting materials will exhibit porosity by gas sorption, it has served as a useful starting point for the synthesis of a myriad of MCPs.[29-31] Adhering to this approach, a simple and rigid linear linker bearing acetylacetonyl functionalities was sought; thus H_2BAB (BAB = 1,4-bis(3'-acetylacetonylate)benzene) (Figure 4.1) was deemed a suitable candidate for initial efforts towards acetylacetonate MCPs.

One can envision the combination of linear ditopic molecules (i.e., BAB^{2-}) bearing chelating coordination functionalities (i.e., acetylacetonate units) binding with divalent metal ions to form chains of linear coordination polymers which likely would packed in a manner that would prevent permanent porosity. However the combination of the aforementioned linkers with trivalent metal ions, can be expected to form chiral octahedral subunits, which serve as trigonal nodes. In the case where all linkers connect one Δ subunit to one Λ subunit, the result is a porous 2D 'honeycomb' network of hexagonal pores (Figure 4.3). These 2D sheets may stack in any number of configurations, some of which may occlude porosity. However, careful determination of the material synthesis conditions has been effective in mitigating this possibility.[32] Given that the octahedral tris(acetylacetonate) complex of Al is known,[33-35] and that Al has the advantage of being relatively light and abundant, it is an excellent candidate metal for initial efforts towards acetylacetonate MCPs.

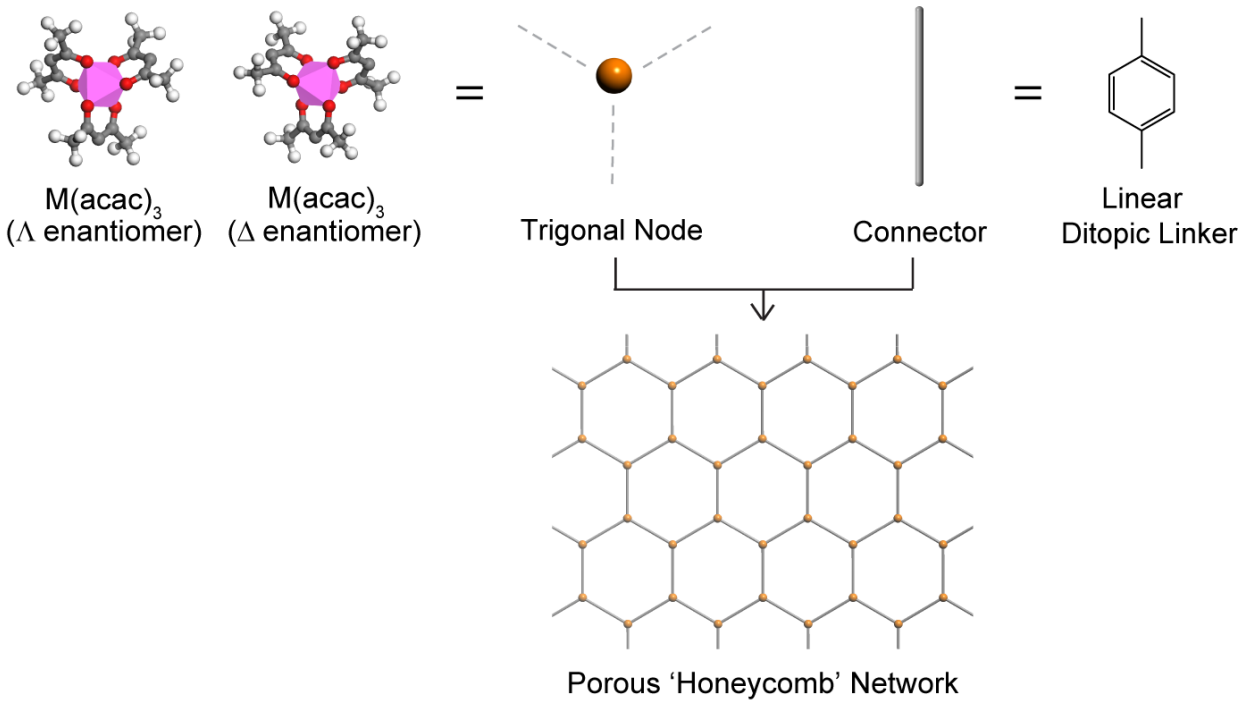

Figure 4.3. Assembly of trigonal nodes with a linear ditopic connectors giving rise to a honeycomb network of pores.

4.2 Al/BAB

The reaction conditions of the monomeric compound $Al(Ph\text{-}acac)_3$[18] were utilized as a starting point for determining conditions under which the ditopic linker would form the desired porous material. Reaction of the linker H_2BAB with Al^{3+} under basic conditions at ambient temperature, as used in the preparation of the monomeric analog, yielded a material which did exhibit porosity by gas sorption. It was hypothesized that raising the reaction temperature would improve the solubility of the linker, allowing for facile deprotonation and subsequent coordination to the Al^{3+} cations. When the linker was heated at 85 °C with excess base in presence of Al^{3+}, a new material was obtained, and hereafter is referred to as Al/BAB. The material exhibited porosity by N_2 sorption (Figure 4.4), with sharp uptake in the low relative pressure region, indicative of microporosity. The porosity of Al/BAB was also probed by CO_2 sorption at 25 °C, and the material demonstrated an uptake of 1.4 wt% at about 0.16 atm.

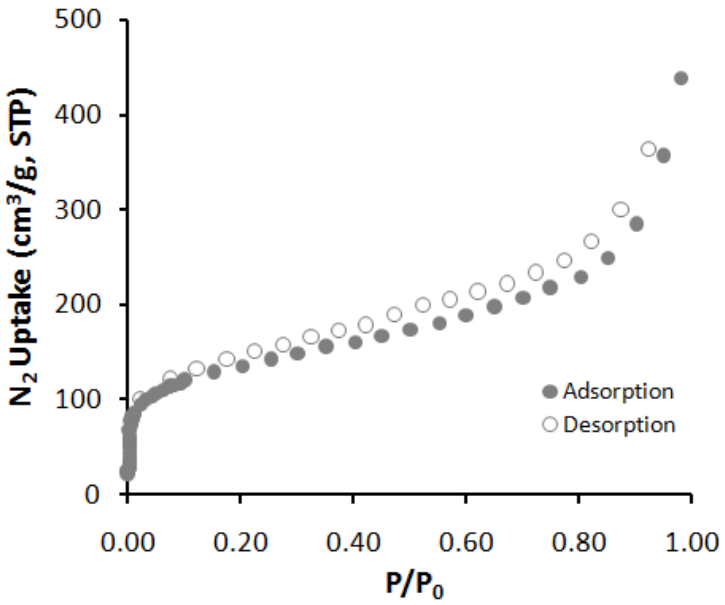

Figure 4.4. N_2 sorption isotherm for Al/BAB at 77 K.

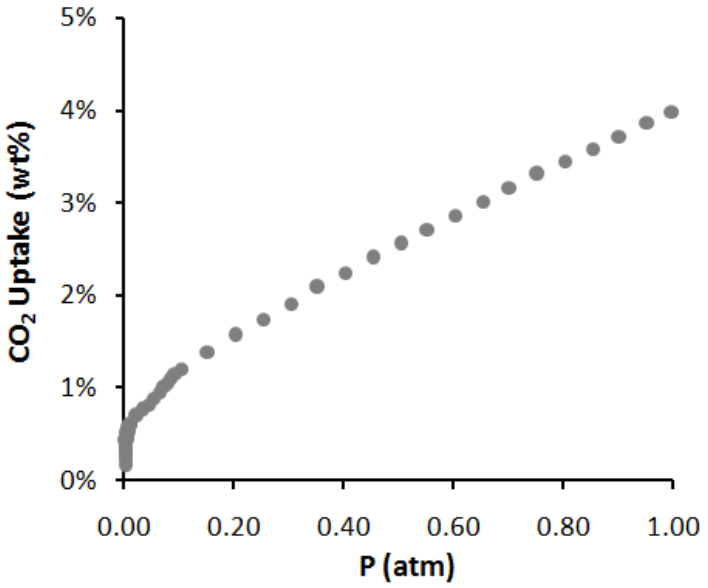

Figure 4.5. CO_2 sorption isotherm for Al/BAB at 25 °C.

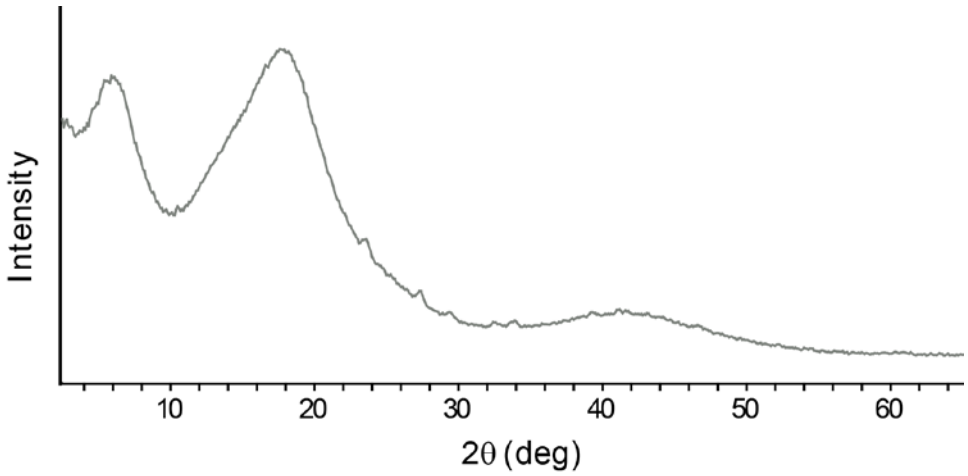

Figure 4.6. Powder X-ray diffraction pattern of Al/BAB.

Powder X-ray diffraction was performed on a sample of Al/BAB, and as shown in Figure 4.6, the broad features are indicative of poor long-range order, thus preventing structural analysis using X-ray crystallography, and necessitating the of additional characterization methods to obtain structural insight into the material.

Infrared spectral analysis confirms the incorporation of the linker, as evidenced by a peak centered at 3028 cm^{-1}, which corresponds to the aryl C-H stretch. A shift in the linker band centered at 1600 cm^{-1} to 1590 cm^{-1} in Al/BAB (Figure 4.7), is also observed. Given that the aryl ring exhibits only very weak IR absorption in the range of 1479 cm^{-1} and 1815 cm^{-1},[36] the very strong absorption observed at 1600 cm^{-1} and 1590 cm^{-1} in H_2BAB and Al/BAB, respectively, and is attributable to the acetylacetonate moiety. The metal complex $Al(acac)_3$ is reported to have a very strong band centered at values ranging from 1585 to 1599 cm^{-1};[35-37] the band observed here is well in-line with these data. Furthermore, on the basis of isotopic labeling[38] and computation studies,[35,37] the CO stretch contributes significantly to the character of this band. Because chelation of the acac moiety is accomplished through coordination of the CO groups, the band is expected to shift significantly after the acac units bind with metal. In particular, the shifted band is expected to be lower in wavenumber when compared with the un-complexed ligand, due to the donation of electron density from the ligand to the metal, thereby weakening the CO bond (this of course, is in the absence of π-backbonding, where ligands donate

electron density into transition metal p or d-orbitals, but Al^{3+} cannot participate in this type of metal-ligand chemistry, because it has no d-electrons to donate). To provide further evidence of coordination, the IR spectrum of $Al(Ph\text{-}acac)_3$, which serves as a monomeric model complex, was compared with that of the product material. Similar to $Al(acac)_3$, the model compound also contains a very strong absorption, centered at 1589 cm^{-1} (Figure 4.8). Assignments have been made for the aryl contributions to IR absorption bands in this compound, and all are under 1500 cm^{-1}[139]; and similar with $Al(acac)_3$, this band is attributable to CO and CC vibrational modes associated with the acac moiety. The IR spectrum of Al/BAB is therefore consistent with the coordination of the acac moiety to Al.

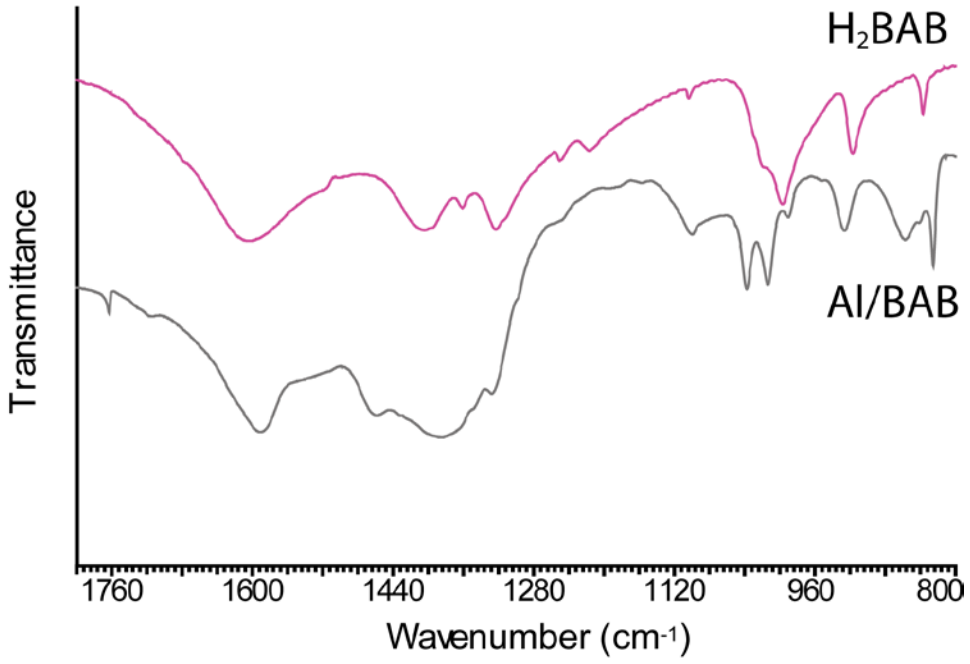

Figure 4.7. IR spectra of H_2BAB and Al/BAB.

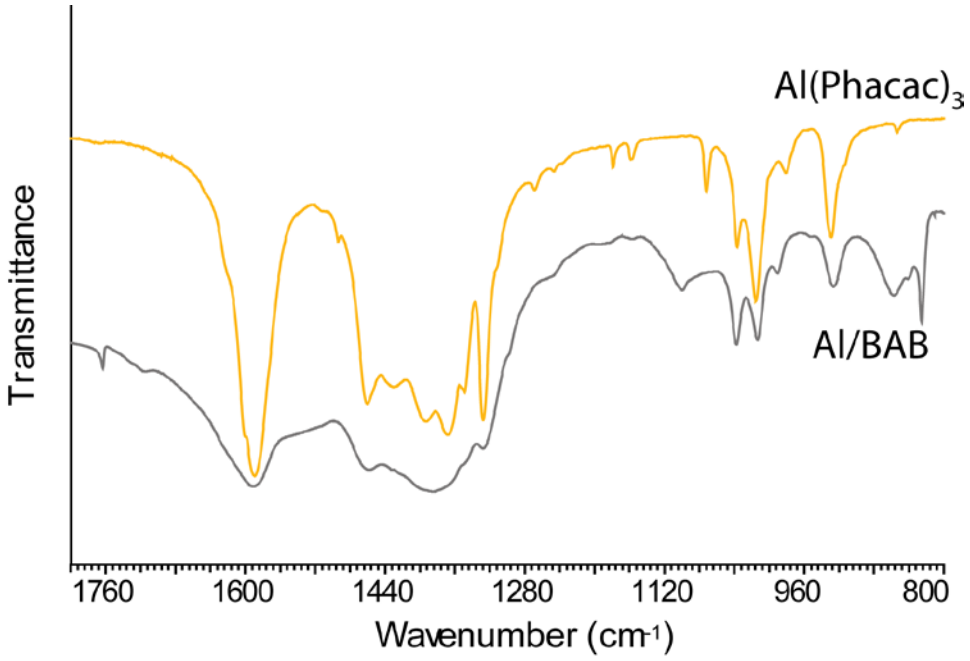

Figure 4.8. IR spectra of Al(Ph-acac)$_3$ and Al/BAB.

To confirm the expected Al loading, a sample of Al/BAB was digested and analyzed via ICP-OES. For an octahedral coordination unit formed between Al and chelating BAB^{2-} units, with a linkage two Al atoms per BAB^{2-}, the stoichiometric relationship is 1/1.5 Empirically, Al/BAB can be expressed by the formula $Al_2(BAB)_3$. Therefore the expected Al content is 6 wt% (g Al/g MCP). ICP- OES data revealed that the digested sample of Al/BAB contained 7 wt% Al, which is well-matched with the expected amount. Data analysis of the IR spectra and ICP-OES metal content are consistent with the expected mononuclear coordination units of Al^{3+} cations linked by BAB^{2-} ligands to form an MCP.

4.3 Conclusions

The synthesis of a microporous coordination polymer based exclusively on beta-diketonate chemistry was accomplished by a rationale design approach. Here a ditopic linker (BAB^{2-}) was selected to serve as a linear connector, and a trivalent metal (Al^{3+}) was chosen to act as a trigonal node. Combination of these two building units under conditions similar to those previously known to provide the desired secondary building unit, yielded a new material, Al/BAB. Although the material exhibits poor long-range order, IR spectral analysis of the material and the model compound $Al(Ph\text{-}acac)_3$, coupled with metal content analysis via ICP-OES, confirm the expected metal/ligand stoichiometry of 2/3, which is consistent with octahedra of Al atoms linked via ditopic BAB^{2-} linkers. A study utilizing solid state Al NMR would be insightful, in determining if the coordination environment around the metal in Al/BAB, is consistent with that of the model compound. Future assessment of the hydrothermal stability will provide additional insight into the potential for using beta-diketonate MCPs as lightweight scaffolds for anchoring functional groups such as amines, to generate materials with exceptional CO_2-capture performance.

4.4 Experimental

4.4.1 Syntheses

CuI and 1,4-diiodobenzene were purchased from Acros. Acetylacetone was purchased from Aldrich. K_2CO_3, L-proline, DMSO, ethylacetate, petroleum ether and dichloromethane were purchased from Fisher. All reagents were used as received.

3'-Phenylacetylacetone (Ph-acac),[40] and the corresponding model compound $Al(Ph\text{-}acac)_3$[18] were synthesized by literature preparations.

H_2BAB (BAB = 1,4-bis(3'-acetylacetonylate)benzene) was synthesized by modification of the literature preparation for Ph-acac.[40] To a 3-neck 1L round-bottom flask equipped with a stir bar was added DMSO (140 ml) and acetylacetone (5 mL, 5 g, 100 mmol). The resulting solution was purged with N_2 for ~ 40 min, then 1,4-

diiodobenzene (5.6 g, 17 mmol), and K_2CO_3 powder (4.6 g, 33 mmol) were added. The mixture was purged for an additional 10 ~ 15 min, then a solid mixture of L-proline (0.4 g, 3.4 mmol), and CuI (0.32 g, 1.7 mmol) was added, the resulting mixture was heated to 60 °C, and monitored by TLC. 18/3/1 petroleum ether/dichloromethane/ethyl acetate was determined to be the optimal eluant based on previous TLC trials. The successive addition of more acetylacetone, base, catalyst, and L-proline was necessary to drive the mono-substituted product to the desired compound. When the consumption of diiodobenzene and the monocoupled product was completed, as observed by TLC, the reaction was allowed to cool to room temperature, then quenched with 2M HCl until the mixture was slightly acidic ($6 < pH < 7$). The mixture was extracted with ethylacetate (3 × 300 mL); the organic portions were combined and washed with ~ 500 mL H_2O, followed by ~ 500 mL brine. Afterwards the volatiles were removed via rotary evaporation. Silica and ethylacetate were added to the residue, and the volatiles were removed via rotary evaporation; the resulting powder was chromatographed on a silica gel column with 18/3/1 PE/DCM/EA is the eluant, to afford H_2BAB ($r_f \approx 0.2$); the ^{1}H NMR spectrum was consistent with published data.[41]

Al/BAB was prepared by loading H_2BAB (50 mg, 0.18 mmol), $KHCO_3$ (80 mg, 0.8 mmol), and CH_3OH (0.65 mL) into a 23-mL Teflon cup. The mixture was stirred for ~ 20 minutes, then a solution of $Al(NO_3)\cdot 9H_2O$ (60 mg, 0.16 mmol) in CH_3OH (0.35 mL) was added. The resulting suspension was sealed in a parr vessel, and heated to 85 °C for 3 hours. After the sample had cooled to room temperature, the resulting solid was washed in CH_3OH. The material was evacuated at 50 °C for 12 hours, before subsequent analysis.

4.4.2 Gas sorption

Gas sorption isotherms were measured with an Autosorb-1C (volumetric method) outfitted with the micropore option by Quantachrome Instruments (Boynton Beach, Florida, USA) running version 1.55 of the ASWin software package. N_2 isotherm was measured at 77 K in the range 1.00×10^{-5} atm $\leq P/P_0 < 1.00$ atm using ultra-high purity

N_2 (99.999%). CO_2 isotherm was measured at 298 K in the range 1.00 x 10^{-4} atm ≤ P < 1.00 atm using bone dry CO_2.

4.4.3 IR Spectroscopy

FT-IR spectra of activated H_2BAB, Al(Ph-acac)$_3$, and Al/BAB pristine were obtained by via KBr disk. The salt was dried under vacuum at 200 °C for ~ 16 hours, and stored in a N_2 glovebox. Samples of material (~2 mg) were ground with 250 mg of KBr under N_2 atmosphere. About 150 mg of the mixture was transferred to a die kit and pressed into a pellet. Spectra of the pellets were obtained using a Nicolet Avatar 360 spectrometer pre-purged with N_2. Peak listings are provided below:

H_2BAB: IR 3077 (M), 3029 (M), 2972 (M), 2925 (M), 2575 (M), 2281 (W), 1921 (W), 1810 (W), 1603 (VS), 1521 (S), 1404 (VS), 1361 (S), 1323 (VS), 1251 (S), 1217 (M), 1103 (M), 997 (S), 917 (S), 837 (M), 665 (W), 589 (M), 520 (W), 431 (W) cm^{-1}.

Al/BAB: IR 3510 (S), 3024 (S), 2972 (M), 2930 (M), 2836 (M), 2796 (M), 2739 (M), 2534 (M), 2505 (M), 2430 (M), 2397 (M), 2068 (M), 1763 (M), 1717 (S), 1590 (VS), 1458 (VS), 1384 (VS), 1328 (S), 1099 (M), 1038 (M), 990 (W), 927 (M), 857 (M), 825 (M), 756 (W), 738 (W), 706 (M), 631 (M), 511 (M) cm^{-1}.

Al(Ph-acac)$_3$: IR 3211 (W), 3144 (W), 3074 (W), 3053 (W), 3024 (W), 2976 (W), 2929 (W), 1956 (W), 1888 (W), 1825 (W), 1773 (W), 1589 (VS), 1460 (S), 1430 (S), 1393 (S), 1368 (S), 1349 (S), 1328 (S), 1269 (W), 1247 (W), 1179 (W), 1159 (W), 1071 (W), 1037 (M), 1015 (M), 981 (W), 929 (M), 854 (VW), 782 (W), 770 (W), 716 (M), 706 (M), 680 (W), 623 (W), 606 (M), 534 (W), 498 (S), 448 (W), 431 (W) cm^{-1}.

4.5 References

(1) Jeremias, F.; Khutia, A.; Henninger, S. K.; Janiak, C. *J. Mater. Chem.* **2012**.

(2) Seo, Y.-K.; Yoon, J. W.; Lee, J. S.; Hwang, Y. K.; Jun, C.-H.; Chang, J.-S.; Wuttke, S.; Bazin, P.; Vimont, A.; Daturi, M.; Bourrelly, S.; Llewellyn, P. L.; Horcajada, P.; Serre, C.; Férey, G. *Adv. Mater.* **2011**, *24*, 806-810.

(3) Hong, D.-Y.; Hwang, Y. K.; Serre, C.; Férey, G.; Chang, J.-S. **2009**, *19*, 1537-1552.

(4) Cavka, J. H.; Jakobsen, S.; Olsbye, U.; Guillou, N.; Lamberti, C.; Bordiga, S.; Lillerud, K. P. **2008**, *130*, 13850-13851.

(5) Park, K. S.; Ni, Z.; Côté, A. P.; Choi, J. Y.; Huang, R.; Uribe-Romo, F. J.; Chae, H. K.; O'Keeffe, M.; Yaghi, O. M. *Proc. Natl. Acad. Sci.* **2006**, *103*, 10186-10191.

(6) Huang, X.-C.; Lin, Y.-Y.; Zhang, J.-P.; Chen, X.-M. *Angew. Chem. Int. Ed.* **2006**, *45*, 1557-1559.

(7) Küsgens, P.; Rose, M.; Senkovska, I.; Fröde, H.; Henschel, A.; Siegle, S.; Kaskel, S. **2009**, *120*, 325-330.

(8) Cychosz, K. A.; Matzger, A. J. *Langmuir* **2010**, *26*, 17198-17202.

(9) Dincă, M.; Yu, A. F.; Long, J. R. *J. Am. Chem. Soc.* **2006**, *128*, 17153-17153.

(10) Dincă, M.; Yu, A. F.; Long, J. R. *J. Am. Chem. Soc.* **2006**, *128*, 8904-8913.

(11) Demessence, A.; D'Alessandro, D. M.; Foo, M. L.; Long, J. R. *J. Am. Chem. Soc.* **2009**, *131*, 8784-8786.

(12) Carlucci, L.; Ciani, G.; Maggini, S.; Proserpio, D. M.; Visconti, M. *Chem.-Eur. J.* **2010**, *16*, 12328-12341.

(13) Kondracka, M.; Englert, U. *Inorg. Chem.* **2008**, *47*, 10246-10257.

(14) Chen, B.; Fronczek, F. R.; Maverick, A. W. *Chem. Commun.* **2003**, 2166-2167.

(15) Chen, B.; Fronczek, F. R.; Maverick, A. W. *Inorg. Chem.* **2004**, *43*, 8209-8211.

(16) Li, D.-J.; Mo, L.-Q.; Wang, Q.-M. *Inorg. Chem. Commun.* **2011**, *14*, 1128-1131.

(17) Vreshch, V. D.; Chernega, A. N.; Howard, J. A. K.; Sieler, J.; Domasevitch, K. V. *Dalton Trans.* **2003**, 1707-1711.

(18) Vreshch, V. D.; Lysenko, A. B.; Chernega, A. N.; Howard, J. A. K.; Krautscheid, H.; Sieler, J.; Domasevitch, K. V. *Dalton. Trans.* **2004**, 2899-2903.

(19) Yaghi, O. M.; O'Keeffe, M.; Ockwig, N. W.; Chae, H. K.; Eddaoudi, M.; Kim, J. *Science* **2003**, *423*, 705-714.

(20) Robson, R. *Dalton Trans.* **2008**, 5113-5131.

(21) Martell, A. E.; Smith, R. M. *Critical stability constants*; Plenum Press: New York, 1974.

(22) Barraclough, C.; Martin, R.; Stewart, I. *Aust. J. Chem.* **1969**, *22*, 891-904.

(23) Schnobrich, J. K.; Koh, K.; Sura, K. N.; Matzger, A. J. *Langmuir* **2010**, *26*, 5808-5814.

(24) Oh, J. S.; Bailar Jr, J. C. *J. Inorg. Nucl. Chem.* **1962**, *24*, 1225-1234.

(25) Burrows, A. D.; Cassar, K.; Mahon, M. F.; Rigby, S. P.; Warren, J. E. *CrystEngComm* **2008**, *10*, 1474-1479.

(26) Aromi, G.; Gamez, P.; Reedijk, J. *Coord. Chem. Rev.* **2008**, *252*, 964-989.

(27) Hoskins, B. F.; Robson, R. *J. Am. Chem. Soc.* **1990**, *112*, 1546-1554.

(28) Hoskins, B. F.; Robson, R. *J. Am. Chem. Soc.* **1989**, *111*, 5962-5964.

(29) Eddaoudi, M.; Kim, J.; Rosi, N.; Vodak, D.; Wachter, J.; O'Keeffe, M.; Yaghi, O. M. *Science* **2002**, *295*, 469-472.

(30) Li, H.; Eddaoudi, M.; O'Keeffe, M.; Yaghi, O. M. *Nature* **1999**, *402*, 276-279.

(31) Rowsell, J. L. C.; Yaghi, O. M. *Micro. Mesoporous Mater.* **2004**, *73*, 3-14.

(32) Côté, A. P.; Benin, A. I.; Ockwig, N. W.; O'Keeffe, M.; Matzger, A. J.; Yaghi, O. M. **2005**, *310*, 1166-1170.

(33) Shirodker, M.; Borker, V.; Nather, C.; Bensch, W. *Ind. J. Chem. A* **2010**, *49*, 1607.

(34) Sabolović, J.; Mrak, ź.; Koštrun, S.; Janeković, A. *Inorg. Chem.* **2004**, *43*, 8479-8489.

(35) Diaz-Acosta, I.; Baker, J.; Cordes, W.; Pulay, P. *Phys. Chem. A* **2000**, *105*, 238-244.

(36) Spectral Database for Organic Compounds. http://riodb01.ibase.aist.go.jp/sdbs/cgi-bin/direct_frame_top.cgi (accessed May 2012)

(37) Slabzhennikov, S.; Ryabchenko, O.; Kuarton, L. *Russ. J. Coord. Chem.* **2006**, *32*, 545-551.

(38) Pinchas, S.; Silver, B. L.; Laulicht, I. *J. Chem. Phys.* **1967**, *46*, 1506-1510.

(39) Murakami, Y.; Nakamura, K.; Uchida, H.; Kanaoka, Y. *Inorg. Chim. Acta* **1968**, *2*, 133-138.

(40) Jiang, Y.; Wu, N.; Wu, H.; He, M. *Synlett* **2005**, *2005*, 2731,2734.

(41) Lambert, J.; Liu, Z. *J. Chem. Crystallogr.* **2007**, *37*, 629-639.

Chapter 5

Conclusions and Future Directions

5.1 Summary

Since the foundational work of Robson and co-workers,[1-3] where it was demonstrated that rationally preconceived coordination polymers could be materialized and structurally characterized, the rapid development of a new subset of microporous materials has built upon those early contributions. These materials, MCPs, owing to their tunable structural characteristics, have been investigated for a myriad of applications,[4-12] including CO_2-capture.[9,13-16] In particular, MCPs of the M/DOBDC series, which were previously shown to exhibit superior CO_2 uptakes under dry static conditions,[13,16] were studied in Chapter 2 of this dissertation to examine the effect of humidity on their performance under flow conditions. It was discovered that Mg/DOBDC experienced significant degradation in performance after a single cycle of hydration and thermal regeneration, while Co/DOBDC exhibited superior retention of CO_2 capacity.

Chapter 2 highlighted the need to incorporate both superior H_2O-stability and CO_2 capacity into adsorbents designed for CO_2-capture; consequently, there remains a strong driving force for the development of new MCPs. In Chapter 3, post-synthetic modification was deployed to design and synthesize a new MCP, wherein MIL-100(Al), which has previously been shown to exhibit superior hydrothermal stability,[17] was utilized as a scaffold onto which was appended a modifier that features proximal amines. Proximity of a least two amines is believed to be an important prerequisite for the chemical reaction with CO_2. The new material, tren@MIL-100(Al) exhibited significantly higher CO_2-capture performance compared with unmodified MIL-100(Al), and even outperformed Zn/DOBDC. Even when fully hydrated, the material also exhibits capacity for CO_2, marking a significant improvement over the M/DOBDC materials.

However the full regeneration of the material is a remaining challenge, in addition to the elucidation of the interaction between CO_2 and tren@MIL-100(Al).

The work in Chapter 3 demonstrates that post-synthetic modification is a powerful tool for generating MCPs with enhanced performance. Utilization of this approach with a scaffold based on lightweight secondary building units could conceivably be used to generate MCPs with exceptional CO_2-capture performance, because gravimetric capacity (g CO_2/g adsorbent) is a common unit of assessing adsorbent CO_2-capture performance. Reducing the mass contribution of the metal is an approach to achieving this.[18] Towards this goal, the β-diketonate coordination functionality acetylacetonate was identified as a suitable candidate for initial studies, due to the fact that it forms highly stable metal complexes[19,20] and binds with trivalent metals such as Al^{3+} to form octahedral complexes that feature only a single metal atom. Conceptually these octahedral complexes can serve as trigonal motifs, in concert with linear spacer units such as a 1,4-di-substituted benzene ring, to form a porous 2D network. The design approach guided the selective combination of Al^{3+} and H_2BAB to yield the material Al/BAB, which was found to be porous by gas sorption. Infrared spectral analysis confirmed the incorporation of the linker, and ICP-OES confirms the expected metal/linker stoichiometry.

5.2 Future Work: Characterization of the Adsorption Behavior of CO_2 in tren@MIL-100(Al)

As previously discussed, the material tren@MIL-100(Al) exhibited remarkably strong affinity for CO_2, as evidenced by the inability to fully regenerate the CO_2-sorbed material at temperatures comparable to that of aqueous MEA systems (aqueous amine solutions are typically heated to ~120 °C),[21,22] and the successive decline in capacity after increased regeneration temperature. These data are consistent with chemisorptive behavior, but a spectroscopic study that confirms this hypothesis, and identifies the species that is being formed would be useful in determining the optimal activation conditions. From a utilitarian standpoint, a logical direction of further study is to synthetically tailor an amine that results in facile regeneration of the material, while

maintaining superior capture performance. Loading such an amine into a hydrothermally stable scaffold such as MIL-100(Al) or MIL-101(Cr) can be expected to further increase the viability of MCPs for carbon dioxide capture. Potential displacement of the amine by competitive binding of contaminants such as H_2O is another potential area of further investigation, in addition to the long-term stability of the amine over cyclical usage.

Although alkylamines have been extensively utilized in porous silicas,[23-34] this approach is still in the early stages of being explored with MCPs.[35-38] The advantage of utilizing MCPs include relatively high surface, allowing for facile diffusion of gaseous species into the structure, an immense structural diversity offering a wide array of options for tailoring the optimal the amine-MCP combination, and unique pore surface features such as coordinatively unsaturated metal centers, which allow the amine to be anchored through coordinate bonds, as opposed to alkylsilicate linkages in porous silicas, which are susceptible[39] to hydrolysis. The utilization of hydrothermally-stable MCPs that are derived from inexpensive starting materials, and contain coordinatively unsaturated metal centers as sites, onto which tailored amines can be introduced, may be a successful approach to generating new MCPs that can enhance the economic-viability of adsorption-based carbon dioxide capture.

5.3 Further Development of Acetylacetonate MCPs; Improving Structural Order

As previously discussed in Chapter 4, the poor structural order present in Al/BAB inhibited the determination of the material structure by X-ray crystallographic methods. Instead, several additional characterization techniques were collectively deployed to gain additional structural insight; however, finer structural details such as pore aperture geometry, pore accessibility, absence/presence of interpenetration, are typically acquired from crystal structures or models thereof. Establishing the synthetic conditions that yield highly crystalline acetylacetonylate (hereafter, acac) MCPs, would allow a greater amount of structural information to be accessed, thereby facilitating the elucidation of structure-property correlations, and the design of future acac MCPs tailored for applications such as CO_2 capture. Given these considerations, a sustained effort was made towards generating the first crystalline MCP based on coordination units with

exclusive utilization of the acac moiety as a coordinating functionality. Herein, highlights of this effort are provided.

As presented in Chapter 4, the linear linker H_2BAB served as a useful starting point for preliminary trials into generating acac MCPs, and likewise was deployed in initial efforts to generate highly crystalline members within this material class. It was postulated that the utilization of acac complexes as metal sources would facilitate reversible exchange between the acac linker and the metal. Reversible metal-ligand exchange is believed to be an important prerequisite for the formation of crystalline coordination polymers.[2,40] Given this consideration, acac complexes of divalent metals were the focus of crystallization experiments; these complexes feature stability constants that are comparatively lower than those of trivalent acac complexes,[19] thereby making them more amenable to facile ligand exchange. In particular, the compound $Ni(acac)_2$ exhibits dynamic behavior, in which it can reversibly interconvert between two forms: A 'red' form, where Ni, in a square planar coordination environment, is chelated by two co-planar acac ligands,[41] and a trimeric 'green' form,[41] wherein the acac units are oriented in three dimensions about three Ni atoms[42] (Figure 5.1). Conceptually, in the case of the square planar form, replacing the H atoms bound to the central carbon in the OC-CH-CO unit, with 1,4- phenylene units that link together acac units of adjacent complexes, would give rise to a linear coordination polymer; however, in the case of the trimeric form, such linkages could give rise to an MCP with a 3D structure.

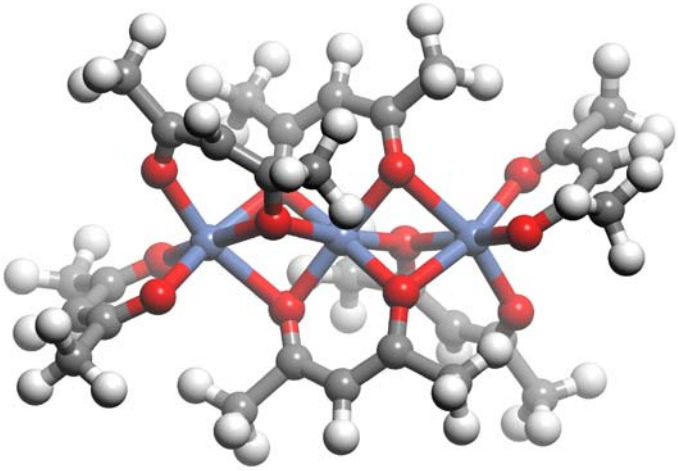

Figure 5.1. Structure of trimeric $Ni(acac)_2$. Spheres represent atoms, and their colors designate the corresponding elements: Blue, Ni; Red, O; Black, C; White, H.

Given the labile behavior of $Ni(acac)_2$, the compound was selected as a metal source for the attempted generation of a crystalline acac MCP. Given the high miscibility of acac complexes in halogenated solvents, chloroform was chosen as an initial reaction medium. Dissolution of H_2BAB with $Ni(acac)_2$ in chloroform at ambient temperature, within minutes, lead to the precipitation of a pink powder that was found to exhibit crystallinity by X-ray diffraction. In an attempt to optimize the crystallization conditions via modification of the solvent system, high-throughput screening was deployed with mixtures of halogenated solvents (ex. CH_2Cl_2, $CHCl_3$, $CHBr_3$) and alkanes or aromatics, but failed to yield single crystals. In addition, when the material porosity was examined by N_2 sorption at 77 K, the material was found to be non-porous.

In the pursuit of achieving both porosity as evidenced by gas sorption, and crystallinity, it was hypothesized that a linker of higher topicity would be beneficial for generating an MCP from divalent metals. In particular, the combination of a tritopic acac linker, wherein the acac units chelate in a square planar fashion with a divalent can be expected to yield a material featuring 2D arrays of hexagonal pores. Towards this goal, the tritopic linker H_3TAB (TAB = 1,3,5-tris(3'-acetylacetonylate)benzene)) was synthesized by the route shown in Figure 5.2.

Upon heating a mixture of H_3TAB and Ni(acac)$_2$ in isooctance at 185 °C, a green material was obtained, with a powder x-ray diffraction pattern (Figure 5.3) that was distinct from that of the starting materials. N_2 sorption at 77 K (Figure 5.4) revealed that the material was porous, and the BET surface area was determined to be 450 m^2/g. Attempts to optimize the crystallization conditions were hampered by the difficulty in building up large quantities of the linker H_3TAB. This was primarily due to the inexplicably low yield (10 ~ 20%) of the reduction of trimethyl-1,3,5-tricarboxylate to the corresponding alcohol; a typical literature yield of 78%[43] is reported for this reaction.

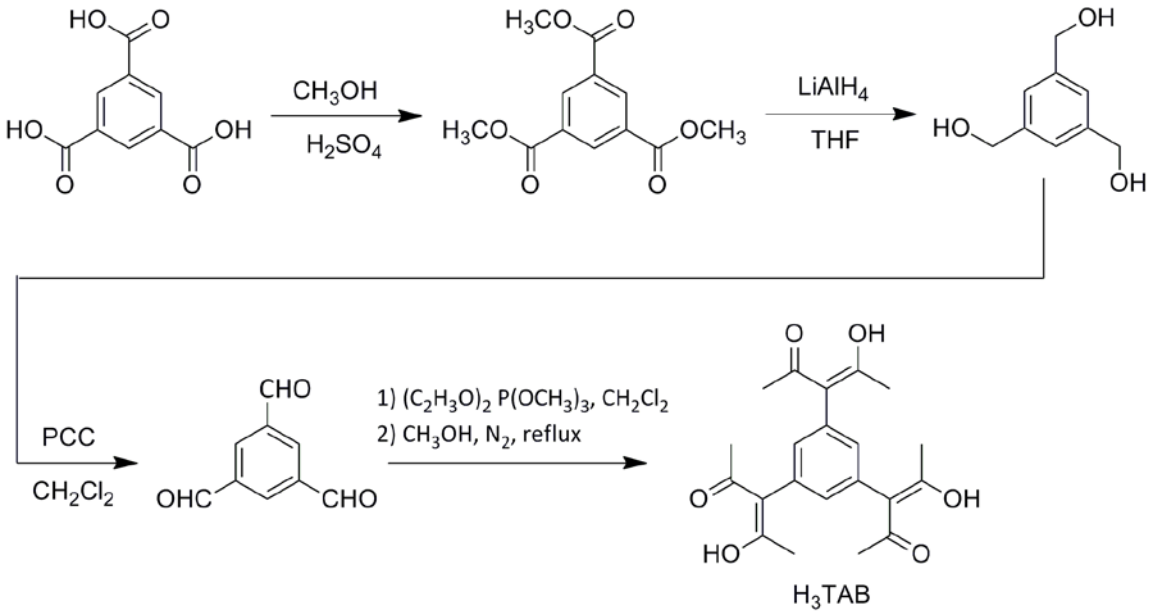

Figure 5.2. Synthetic route to the tritopic acac linker H_3TAB.

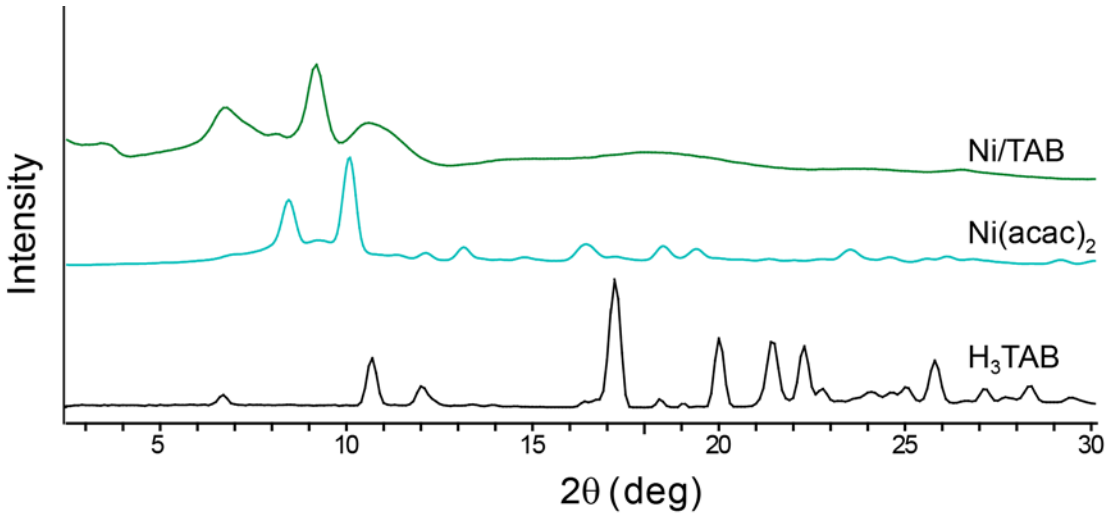

Figure 5.3. Powder X-ray diffraction pattern of Ni/TAB.

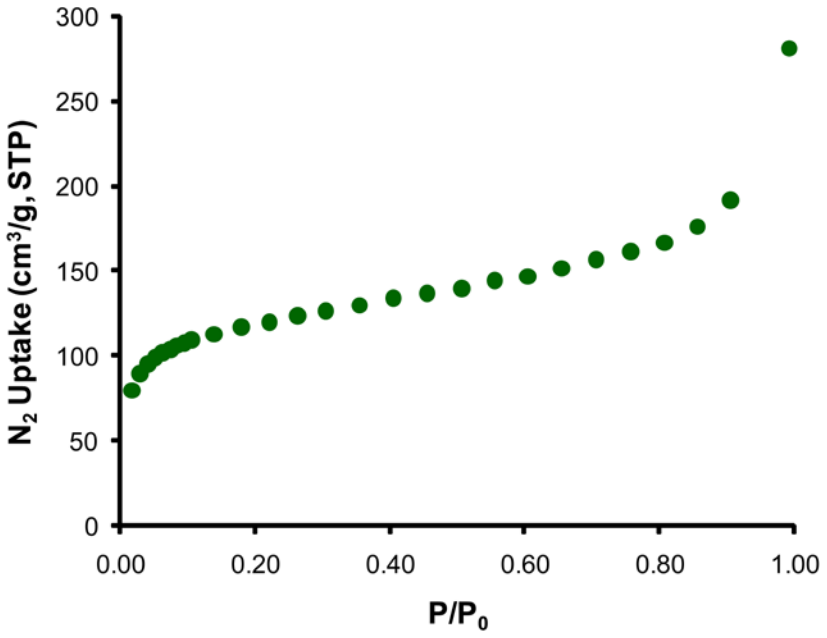

Figure 5.4. N_2 sorption isotherm for Ni/TAB at 77 K.

Striving for an assortment of organic linkers featuring the acac unit, the tetratopic linker H_4TAPM (TAPM = tetrakis(3'-acetylacetonylate-1,4-phenylene)methane) was sought. The combination of this linker with divalent metals favoring a square planar geometry (notably Cu) can be expected to give rise to an MCP with diamondoid

structure, although structural robustness may be compromised if there is deviation of co-planarity of the acac units. In addition, combination of the tetratopic linker with a trivalent metal that forms octahedral coordination units, can also be expected to give rise to an MCP. Successful synthesis of the tetratopic linker was carried out as shown in Figure 5.5. Large-scale production of H_4TAPM proved arduous, owing to the difficulty in running a large-scale lithium-halogen exchange for generating the tetra-aldehyde, followed by the low yield (~10%) of the conversion of the aldehyde to the corresponding acac linker.

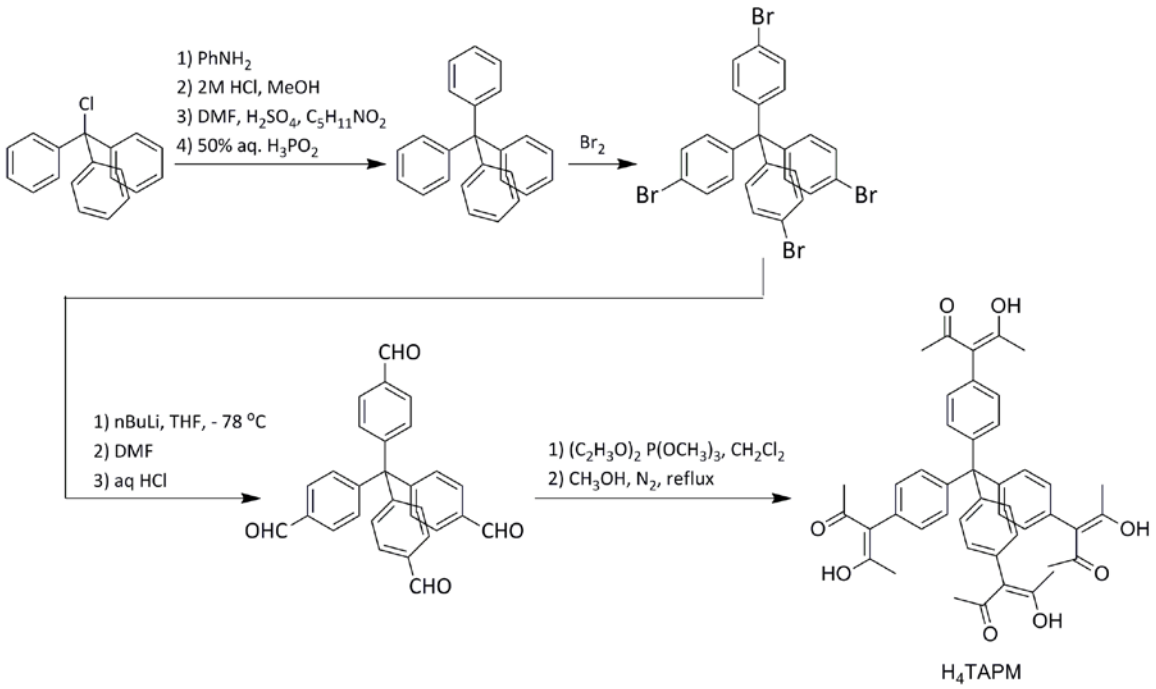

Figure 5.5. Synthetic route to the tetratopic acac linker H_4TAPM.

Several attempts were made to synthesize the linker by an alternate approach (Figure 5.6), where TIPM (tetrakis(iodo-1,4-phenylene)methane) was treated with acac in the CuI/L-proline catalyst system utilized by Jiang et al[44] in the arylation of acac (also utilized here in the synthesis of H_2BAB, see Chapter 4); however, all attempts to couple acac with TIPM failed as evidenced by the lack of consumption of the starting material by TLC. The low solubility of TIPM in DMSO may be the reason for the failed coupling; utilization of a sulfoxide solvent of with increased aliphatic character, such as tetramethylene sulfoxide, may improve the miscibility just enough to facilitate

dissolution at the elevated temperature in which the reaction is conducted, and thereby allow the desired coupling to be performed.

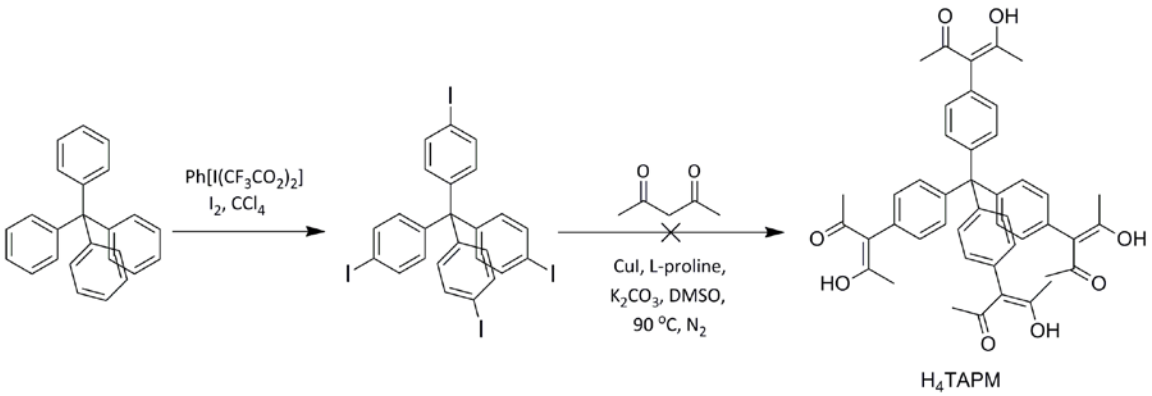

Figure 5.6. Failed synthetic route to H_4TAPM, via attempted CuI/L-proline catalyzed coupling of acac with the iodinated arene.

Future forays into the development acac MCPs would greatly benefit from optimization of the aforementioned linker syntheses. Large-scale production of these linkers will allow for rigorous high-throughput screening of solvent systems and reaction temperatures; these efforts may lead to the discovery of conditions that are amenable to the generation of acac MCPs with improved structural ordering. This endeavor may yield samples of high enough quality for the application of crystallographic structure determination techniques, thus providing insight into local structural features such as the accessibility of coordinatively unsaturated metal centers, pore aperture dimensions, and linker orientation, information that may otherwise be difficult to ascertain, and would be useful in the subsequent design of linkers and MCPs.

Currently the production of new MCPs is dominated by the routine utilization of the carboxylate unit as a coordination functionality. Although this moiety has engendered a subset of coordination polymers with unique structural features and unprecedented properties, there awaits yet another dimension of MCPs. Given the rich structural diversity within the field of acac metal complexes,[45-51] and the glaring underutilization of this ligand in linker conception, it is clear that an entirely new subset of MCPs remains to be explored. These MCPs, accessible through the acac moiety, and with properties and characteristics yet to be determined, may prove to be just as unique and fascinating as those of the carboxylate subset that currently define the field.

5.4 References

(1) Hoskins, B. F.; Robson, R. *J. Am. Chem. Soc.* **1989**, *111*, 5962-5964.

(2) Hoskins, B. F.; Robson, R. *J. Am. Chem. Soc.* **1990**, *112*, 1546-1554.

(3) Robson, R. *Dalton Trans.* **2008**, 5113-5131.

(4) Collins, D. J.; Zhou, H.-C. *J. Mater. Chem.* **2007**, *17*, 3154-3160.

(5) Dincă, M.; Long, J. R. *Angew. Chem. Int. Ed.* **2008**, *47*, 6766-6779.

(6) Hu, Y. H.; Zhang, L. *Adv. Mater.* **2010**, *22*, E117-E130.

(7) Lin, X.; Jia, J.; Hubberstey, P.; Schröder, M.; Champness, N. R. *CrystEngComm* **2007**, *9*, 438-448.

(8) Britt, D.; Tranchemontagne, D.; Yaghi, O. M. *Proc. Natl. Acad. Sci.* **2008**, *105*, 11623-11627.

(9) Dietzel, P. D. C.; Besikiotis, V.; Blom, R. *J. Mater. Chem.* **2009**, *19*, 7362-7370.

(10) Eddaoudi, M.; Kim, J.; Rosi, N.; Vodak, D.; Wachter, J.; O'Keeffe, M.; Yaghi, O. M. *Science* **2002**, *295*, 469-472.

(11) Ma, S.; Zhou, H.-C. *Chem. Comm.* **2010**, *46*, 44-53.

(12) Wu, H.; Zhou, W.; Yildirim, T. *J. Am. Chem. Soc.* **2009**, *131*, 4995-5000.

(13) Caskey, S. R.; Wong-Foy, A. G.; Matzger, A. J. *J. Am. Chem. Soc.* **2008**, *130*, 10870-10871.

(14) Choi, S.; Drese, J. H.; Jones, C. W. *ChemSusChem* **2009**, *2*, 796-854.

(15) D'Alessandro, D. M.; Smit, B.; Long, J. R. *Angew. Chem. Int. Ed.* **2010**, *49*, 6058-6082.

(16) Yazaydin, A. Ö.; Snurr, R. Q.; Park, T.-H.; Koh, K.; Liu, J.; LeVan, M. D.; Benin, A. I.; Jakubczak, P.; Lanuza, M.; Galloway, D. B.; Low, J. J.; Willis, R. R. *J. Am. Chem. Soc.* **2009**, *131*, 18198-18199.

(17) Jeremias, F.; Khutia, A.; Henninger, S. K.; Janiak, C. *J. Mater. Chem.* **2012**.

(18) Schnobrich, J. K.; Koh, K.; Sura, K. N.; Matzger, A. J. *Langmuir* **2010**, *26*, 5808-5814.

(19) Martell, A. E.; Smith, R. M. *Critical stability constants*; Plenum Press: New York, 1974.

(20) Barraclough, C.; Martin, R.; Stewart, I. *Aust. J. Chem.* **1969**, *22*, 891-904.

(21) Rochelle, G. T. *Science* **2009**, *325*, 1652-1654.

(22) Puxty, G.; Rowland, R.; Allport, A.; Yang, Q.; Bown, M.; Burns, R.; Maeder, M.; Attalla, M. **2009**, *43*, 6427-6433.

(23) Leal, O.; Bolívar, C.; Ovalles, C.; García, J. J.; Espidel, Y. *Inorg. Chim. Acta* **1995**, *240*, 183-189.

(24) Franchi, R. S.; Harlick, P. J. E.; Sayari, A. *Ind. Eng. Chem. Res.* **2005**, *44*, 8007-8013.

(25) Harlick, P. J. E.; Sayari, A. *Ind. Eng. Chem. Res.* **2006**, *45*, 3248-3255.

(26) Serna-Guerrero, R.; Da'na, E.; Sayari, A. *Ind. Eng. Chem. Res.* **2008**, *47*, 9406-9412.

(27) Zeleňák, V.; Badaničová, M.; Halamová, D.; Čejka, J.; Zukal, A.; Murafa, N.; Goerigk, G. *Chem. Eng. J.* **2008**, *144*, 336-342.

(28) Belmabkhout, Y.; Sayari, A. *Energy Fuels* **2010**, *24*, 5273-5280.

(29) Bhagiyalakshmi, M.; Park, S. D.; Cha, W. S.; Jang, H. T. *Appl. Surf. Sci.* **2010**, *256*, 6660-6666.

(30) Liu, S.-H.; Wu, C.-H.; Lee, H.-K.; Liu, S.-B. *Top. Catal.* **2010**, *53*, 210-217.

(31) Serna-Guerrero, R.; Belmabkhout, Y.; Sayari, A. *Adsorption* **2010**, *16*, 567-575.

(32) Serna-Guerrero, R.; Belmabkhout, Y.; Sayari, A. *Chem. Eng. Sci.* **2010**, *65*, 4166-4172.

(33) Yang, Y.; Li, H.; Chen, S.; Zhao, Y.; Li, Q. *Langmuir* **2010**, *26*, 13897-13902.

(34) Zhang, Z.; Ma, X.; Wang, D.; Song, C.; Wang, Y. *AIChE J.* **2011**, 1 - 7.

(35) Hwang, Y. K.; Hong, D.-Y.; Chang, J.-S.; Jhung, S. H.; Seo, Y.-K.; Kim, J.; Vimont, A.; Daturi, M.; Serre, C.; Férey, G. *Angew. Chem. Int. Ed.* **2008**, *47*, 4144-4148.

(36) Demessence, A.; D'Alessandro, D. M.; Foo, M. L.; Long, J. R. *J. Am. Chem. Soc.* **2009**, *131*, 8784-8786.

(37) McDonald, T. M.; D'Alessandro, D. M.; Krishna, R.; Long, J. R. *Chem. Sci.* **2011**, *2*, 2022-2028.

(38) McDonald, T. M.; Lee, W. R.; Mason, J. A.; Wiers, B. M.; Hong, C. S.; Long, J. R. *J. Am. Chem. Soc.* **2012**, *134*, 7056-7065.

(39) Asenath Smith, E.; Chen, W. *Langmuir* **2008**, *24*, 12405-12409.

(40) Rowsell, J. L. C.; Yaghi, O. M. *Micro. Mesoporous Mater.* **2004**, *73*, 3-14.

(41) Fackler, J. P.; Cotton, F. A. *J. Am. Chem. Soc.* **1961**, *83*, 3775-3778.

(42) Hursthouse, M. B.; Laffey, M. A.; Moore, P. T.; New, D. B.; Raithby, P. R.; Thornton, P. *Dalton Trans.* **1982**, 307-312.

(43) Kaur, N.; Delcros, J.-G.; Imran, J.; Khaled, A.; Chehtane, M.; Tschammer, N.; Martin, B.; Phanstiel, O. *J. Med. Chem.* **2008**, *51*, 1393-1401.

(44) Jiang, Y.; Wu, N.; Wu, H.; He, M. *Synlett* **2005**, *2005*, 2731,2734.

(45) Cotton, F. A.; Elder, R. C. *J. Am. Chem. Soc.* **1964**, *86*, 2294-2295.

(46) Roof, R. *Acta. Crystallogr.* **1956**, *9*, 781-786.

(47) Vreshch, V. D.; Yang, J.-H.; Zhang, H.; Filatov, A. S.; Dikarev, E. V. *Inorg. Chem.* **2010**, *49*, 8430-8434.

(48) Shibata, S.; Onuma, S.; Iwase, A.; Inoue, H. *Inorg. Chim. Acta* **1977**, *25*, 33-39.

(49) Shibata, S.; Onuma, S.; Inoue, H. *Inorg. Chem.* **1985**, *24*, 1723-1725.

(50) Bennett, M. J.; Cotton, F. A.; Eiss, R. *Acta. Cryst. B* **1968**, *24*, 904-913.

(51) Shirodker, M.; Borker, V.; Nather, C.; Bensch, W. *Ind. J. Chem. A* **2010**, *49*, 1607.